CORONARY ARTERY DISEASE PROGRESSION AND CALCIFICATION IN METABOLIC SYNDROME

Mikaela Lee McKenney

Submitted to the faculty of the University Graduate School
in partial fulfillment of the requirements
for the degree
Doctor of Philosophy
in the Department of Cellular & Integrative Physiology,
Indiana University

November 2014

Accepted by the Graduate Faculty, Indiana University, in partial fulfillment of the requirements for the degree of Doctor of Philosophy.

_____

Michael S. Sturek, Ph.D., Chair

_____

Carmella Evans-Molina, M.D., Ph.D.

Doctoral Committee

_____

Sharon M. Moe, M.D.

August 19, 2014

_____

Johnathan D. Tune, Ph.D.

DEDICATION

To my loving and unselfish parents, Erin and Julie, thank you for teaching me self-motivation, showing me how to be a strong leader, and reminding me to always keep a kind heart. I am forever grateful to you both.

To my sister, Kasey, thank you for being proud of me and for always supporting me. This world is so big; I cannot wait to see what you do in it.

To my unwavering partner in life, Alex, thank you for your unconditional love. Your patience, understanding, and consistent support have undoubtedly led to my success. I am so excited to “do life” with you. And to our bright-eyed and bushy-tailed fur-baby, Charly, thank you for bringing sunshine to stormy days.

To my extended family, my future family, and all of my friends, thank you for caring and for loving me. I am so fortunate to have you in my life.

This compilation of hard work is dedicated to all of you.

ACKNOWLEDGEMENTS

To my advisor, Mike Sturek, thank you for believing in me, trusting me, and challenging me. Your daily enthusiasm and strong leadership have guided me through this journey. Your “glass is half full” outlook on life has been extremely inspirational to me. Thank you for being a great mentor, a strong role model, and a friend.

To my committee members, Dr. Carmella Evans-Molina, Dr. Sharon M. Moe, and Dr. Johnathan D. Tune, thank you for your invaluable guidance and contributions to my thesis research.

To my work family, past and present: Mouhamad Alloosh, Jim Byrd, Brandy Sparks, Kyle Schultz, Josh Sturek, Jay Patel, Neal Ramchandani, Stacey Dineen, John Martin, Becky Bruning, and Ayeeshik Kole. It’s truly been a pleasure to work with you all. I wouldn’t trade in this large, talented team for anything else. Thank you for making me laugh each day and for contributing greatly to my thesis research. To Meredith Owen, Jill Noblet, Adam Goodwill, Daniel Sassoon, Abass Conteh, and Heather O’Leary, thank you for your friendships, encouragement, and scientific input.

To the IUSM Department of Cellular & Integrative Physiology, thank you for providing a collaborative and supportive environment for graduate students.

This research was supported by the Indiana CTSI Predoctoral TL1 Training Fellowship (TR000162), the Cardiometabolic Disease Research Foundation, and the National Institute of Health (HL062552).

Mikaela Lee McKenney

CORONARY ARTERY DISEASE PROGRESSION AND CALCIFICATION IN METABOLIC SYNDROME

For years, the leading killer of Americans has been coronary artery disease (CAD), which has a strong correlation to the U.S. obesity epidemic. Obesity, along with the presence of other risk factors including hyperglycemia, hypercholesterolemia, dyslipidemia, and high blood pressure, comprise of the diagnosis of metabolic syndrome (MetS). The presentation of multiple MetS risk factors increases a patients risk for adverse cardiovascular events. CAD is a complex progressive disease. We utilized the superb model of CAD and MetS, the Ossabaw miniature swine, to investigate underlying mechanisms of CAD progression. We studied the influence of coronary epicardial adipose tissue (cEAT) and coronary smooth muscle cell (CSM) intracellular Ca^{2+} regulation on CAD progression. By surgical excision of cEAT from MetS Ossabaw, we observed an attenuation of CAD progression. This finding provides evidence for a link between local cEAT and CAD progression. Intracellular Ca^{2+} is a tightly regulated messenger in CSM that initiates contraction, translation, proliferation and migration. When regulation is lost, CSM dedifferentiate from their mature, contractile phenotype found in the healthy vascular wall to a synthetic, proliferative phenotype. Synthetic CSM are found in intimal plaque of CAD patients. We investigated the changes in intracellular Ca^{2+} signaling in

enzymatically isolated CSM from Ossabaw swine with varying stages of CAD using the fluorescent Ca^{2+} indicator, fura-2. This time course study revealed heightened Ca^{2+} signaling in early CAD followed by a significant drop off in late stage calcified plaque. Coronary artery calcification (CAC) is a result of dedifferentiation into an osteogenic CSM that secretes hydroxyapatite in the extracellular matrix. CAC is clinically detected by computed tomography (CT). Microcalcifications have been linked to plaque instability/rupture and cannot be detected by CT. We used ^{18}F-NaF positron emission tomography (PET) to detect CAC in Ossabaw swine with early stage CAD shown by mild neointimal thickening. This study validated ^{18}F-NaF PET as a diagnostic tool for early, molecular CAC at a stage prior to lesions detectable by CT. This is the first report showing non-invasive PET resolution of CAC and CSMC Ca^{2+} dysfunction at an early stage previously only characterized by invasive cellular Ca^{2+} imaging.

Michael S. Sturek, Ph.D., Chair

TABLE OF CONTENTS

LIST OF TABLES

.

LIST OF FIGURES

LIST OF ABBREVIATIONS

CAC - coronary artery calcium
Ca_c - cytosolic calcium
CAD - coronary artery disease
Ca_{SR} - sarcoplasmic reticulum calcium
cCSM - contractile coronary smooth muscle
cEAT - coronary epicardial adipose tissue
CSM - coronary smooth muscle
CFX - circumflex artery
CKD -chronic kidney disease
CT - computed tomography
DCE - dynamic contrast enhanced
EAT - epicardial adipose tissue
ECG - electrocardiogram
EEL - external elastic lamina
F - French (length)
^{18}F-FDG - fluorine-fluorodexoyglucose
^{18}F-NaF - fluorine-sodium fluoride
GMCS - global molecular calcium score
H&E - hematoxylin and eosin
HDL - high density lipoprotein
HU - Houndsfield Unit
IEL - internal elastic lamina
IVUS -intravascular ultrasound
LAD - left anterior descending artery
LDL - low density lipoprotein
LO - left ostium
LV - left ventricle
mEAT - myocardial epicardial adipose tissue
MetS - metabolic syndrome
NC - necrotic core
NX - sodium calcium exchanger
oCSM - osteogenic coronary smooth muscle
PET - positron emission tomography
PMCA - plasma membrane calcium ATPase
PVAT - perivascular adipose tissue
Q-CTA - quantitative computed tomography angiography
RCA - right coronary artery
RO - right ostium
ROI - region of interest
Runx2 - runt-related transcription factor 2
sCSM - synthetic coronary smooth muscle
SERCA - sarco- endoplasmic reticulum calcium ATPase
SM-MHC - smooth muscle myosin heavy chain
SR - sarcoplasmic reticulum
TRPC - transient receptor potential cation channel
TC - total cholesterol
TG - triglycerides
VGCC - voltage-gated calcium channel
VVG - Verhoff-Van Gieson

CHAPTER 1: INTRODUCTION

The American Obesity Epidemic

Merriam-Webster defines an epidemic as “an outbreak of disease that spreads quickly and affects many individuals at the same time”. With the sustained rise in obesity trends in the United States (Fig. 1.1), it is fair to say this is an American epidemic. The latest report from the Centers for Disease Control and Prevention revealed that more than one-third of American adults (34.9%) are obese (1).

While the American sedentary lifestyle undoubtedly plays a role in this epidemic, the *homo sapiens'* “thrifty genotype” is also contributing to the cause. This “thrifty genotype”, first described in a classical review by Neel (2), is synonymous to a propensity to obesity. In his recent review, O’Rourke tells the story of the early South Pacific Polynesian people who battled through an energy-intensive lifestyle with limited food supplies. These events evolutionarily shaped the metabolism of these people so that in order to survive one must store large amounts of consumed calories in the form of adipose in just a short period of time (3). This adaptation allowed them to survive periods of famine. Fast forward our “thrifty genotype” to modern day where we have an overabundance of food and a lack of energy-intensive labor, both of which are fueling this American obesity epidemic. O’Rouke refers to this lifestyle as an “obesogenic” environment.

The Metabolic Syndrome

This “obesogenic” environment has fueled a parallel catastrophic diagnosis for Americans – the metabolic syndrome (MetS). As defined in humans by the National Heart, Lung, and Blood Institute and the American Heart Association, MetS is a diagnosis of 3 or more of the following 5 risk factors: fasting plasma glucose ≥100 mg/dL, high density lipoprotein (HDL) cholesterol <40 mg/dL in men or <50 mg/dL in women, triglycerides ≥150 mg/dL, waist circumference ≥102 cm in men or ≥88 cm in women, and systolic blood pressure ≥130 mmHg or diastolic blood pressure ≥85 mmHg (4). What is now recognized as MetS was originally characterized by Reaven in 1988 as resistance to insulin-stimulated glucose uptake and hyperinsulinemia. Reaven made the statement that this cluster of risk factors plays a “significant role in the genesis of coronary artery disease (CAD) in the American population as a whole” (5). When a person presents with multiple MetS risk factors, their chances for adverse or even fatal cardiovascular problems are far greater than if presenting one risk factor alone (6) (Fig. 1.2, adapted from (6)).

Coronary Artery Disease

MetS increases an individual’s risk of developing CAD at least 2-fold (7) and CAD is estimated to be a diagnosis for >1 in every 3 American adults (4). CAD accounts for 1 in every 4 U.S. deaths, totaling to about 380,000 people and making it the leading cause of fatality in America (8). Health care services,

medications, and lost productivity for this disease alone cost the United States $108.9 billion every year (9).

Macrovascular CAD is thickening of the artery wall due to an inflammatory response as a result of lipid accumulation. These conduit vessels are responsible for supplying oxygen-rich blood to the hard working muscle of the heart. There are three main coronary arteries: the left anterior descending (LAD) and left circumflex (CFX) that stem from the left ostium; and the right coronary artery (RCA) that stems from the right ostium (Fig. 1.3A&B). In the setting of CAD, when blood flow is limited due to plaque buildup, the lack of oxygen delivery to the cardiac muscle results in ischemia. In chronic and/or severe cases, when ischemia exceeds the critical threshold of myocardial oxygen demand, acute myocardial infarction (MI) can lead to fatality. MI can occur as a result of coronary plaque rupture do to plaque instability. Unsettling evidence shows that non-flow limiting lesions (typically <75% luminal narrowing), and therefore clinically insignificant lesions, are more likely to rupture due to their thin fibrous cap structure (10). These thin fibrous cap lesions are most common in hyperlipidemic patients with high dyslipidemia (10), both of which are risk factors for MetS (4;11).

Coronary Epicardial Adipose Tissue

Along with the conventional risk factors of MetS, coronary epicardial adipose tissue (cEAT) is also guilty of contributing to the progression of CAD. The volume of cEAT (Fig. 1.3C) has been deemed an independent risk factor for

CAD by the Framingham heart study (12;13). While this fat depot is naturally occurring, it grows with chronic obesity (14). This cEAT has been directly correlated with CAD and the MetS risk factors by computer tomography (CT) (14;15) and echocardiography (16). Total epicardial adipose tissue (EAT) has been positively correlated with total cholesterol and low-density lipoprotein (17), both of which are MetS risk factors.

More specifically, CAD lesions have been found predominately in regions of coronary arteries covered with cEAT (14;15;18;19). The basis of the hypothesis that cEAT contributes locally and detrimentally to CAD progression stems from pathophysiological evidence of increased proinflammatory, redox, endothelial cell, and angiogenic genes in the fat depot adjacent to known regions of CAD from patients undergoing coronary bypass (20). Prior to our recent pilot study (21), there has been no experimental evidence provided directly linking the role of the presence of cEAT in CAD progression. Furthermore, cEAT (22) and its associated inflammatory secretions (23) have been associated with another complication of CAD, vascular calcification.

Vascular Calcification

Vascular calcification can occur in either the intima or media of the vascular wall (Fig. 1.4A&B) and is made up of calcium in the form of hydroxyapatite (24). As its name suggests, medial calcification occurs in the media. Patients with renal failure, diabetes, aging, and osteoporosis are at risk

for medial calcification. This pathology leads to arterial stiffening and consequently hypertension and left ventricular hypertrophy (25).

For the purpose of this thesis work, the interest lies with intimal vascular calcification specifically. Intimal calcification occurs only within atherosclerotic lesions and has been seen in histological samples as early as type IV lesions (26). Patients with dyslipidemia, hypercholesterolemia, hypertension, diabetes and obesity are at high risk for intimal calcifications (25). It is important to note, a patient with these risk factors would be diagnosed with MetS. The ultimate complication from intimal calcification is altered plaque stability and potential for rupture (25;27-29).

In the past, it was thought that only advanced plaque in elderly CAD patients contained calcified lesions as result of a passive process (24). It is now known, however, that hydroxyapatite crystals can form as early as our third decade of life (26) and that calcification is an active and tightly regulated process (30). Of CAD patients who are classified as having intermediate risk by the Framingham Heart Study, 58% of women and 64% of men had coronary artery calcification (CAC) (4). Those with CAC have 4-10 times greater risk for a cardiovascular event (27). Specifically, CAC has been associated with plaque instability and rupture (28), further increasing mortality risk.

Currently, computed tomography (CT) is used to non-invasively diagnose patients with CAC (31). Unfortunately, recent evidence shows that calcium deposition is occurring in the coronary arteries at a much early stage of CAD than that which CT can measure (26;32). Therefore, it is necessary to pursue an

alternative imaging technique that can measure microcalcifications. Positron emission tomography (PET) can detect molecular activity and calcium metabolism using the classic bone tracer ^{18}F-NaF (33;34). Just as dental fluoride binds to hydroxyapatite in tooth enamel (Fig. 1.4C), ^{18}F-NaF will bind directly to hydroxyapatite on the surface of bone (Fig. 1.4D(a)). The biggest strength of PET imaging is that is provides metabolic information. Areas of increased mineral metabolism and bone turnover will reveal increased ^{18}F-NaF uptake on PET images (Fig. 1.4D(a)). While this molecular-level of activity can be observed with PET, simultaneous CT scans reveal no evidence of increased calcium deposition (Fig. 1.4D(b&c)) (35). Not only in bone, but research in both humans and swine has revealed increased ^{18}F-NaF uptake in the soft tissues of the coronary arteries in the absence of any evidence of CAC by CT imaging (36;37). Recently, ^{18}F-NaF uptake has also been recognized as the first non-invasive method to identify high-risk patients for coronary plaque rupture (38). As stated by Beheshti et al., “molecular calcification as assessed by ^{18}F-NaF likely will provide highly relevant information to our understanding of this common disorder before structural (macrocalcification) is detectable by standard CT techniques.” (36)

Ossabaw Miniature Swine Model

Our laboratory has characterized the Ossabaw miniature swine as a superb model of human MetS and mascrovascular CAD (39-44). The Ossabaw swine’s “thrifty genotype” allows them to store excess fat, which enabled them to survive during food shortages in their natural habitat off the coast of Georgia

(40). The pigs can fluctuate from a lean phenotype in a famine period (Fig. 1.5A) to a more obese phenotype in a feasting period (Fig. 1.5B). In captivity, when fed an excess-calorie atherogenic diet, Ossabaw develop all characteristics of MetS: insulin resistance, hyperglycemia, dyslipidemia, central obesity, and hypertension (45;46) (Fig. 1.5B).

Swine have strikingly similar cardiovascular anatomy and physiology to humans (Fig. 1.3B) (40;47) . Along with MetS, Ossabaw develop mature (Fig. 1.5C&D) and diffuse atheroma (40;42) including the advanced stage of intimal calcification (Fig. 1.5E) making them an ideal model of human CAD in the setting of MetS (42;43). This model is suitable for interventional and *in vivo* large animal studies, as well as for *ex vivo* and *in vitro* studies of cellular mechanisms (40).

Coronary Smooth Muscle Cells

The walls of the coronary arteries are comprised of three distinct sections: adventitia, media, and intima (Fig. 1.3D&E). Boundaries between these sections are identified by the internal and external elastic laminae. The collagen-rich adventitia is separated from the media by the external elastic lamina. This medial layer is made up of quiescent coronary smooth muscle cells (CSM). These cells are of a contractile phenotype and do not replicate and migrate. The media and intima are separated by the internal elastic lamina. The intima of a healthy individual will be composed of only a thin, single layer of endothelial cells (barely visible in Figures 1.3D and 1.5C), which contribute substantially in regulating vasoreactivity. A CAD patient’s intimal layer will have damage to the endothelial

monolayer, which is a major trigger for encroachment of proliferative and migratory CSM (synthetic, sCSM), and a high presence of inflammatory cells such as monocytes, foam cells, and macrophages (48;49).

CSM play a key role in the progression of CAD. Cytosolic Ca^{2+} signaling drives contraction of mature, differentiated CSM. Tight regulation of cytosolic Ca^{2+} is crucial for maintenance of a healthy coronary wall and coronary blood flow. Several Ca^{2+} transporters including channels, pumps, and exchangers are responsible for this role (Fig. 1.6). Dysregulation of intracellular Ca^{2+} signaling is correlated with phenotypic modulation of CSM and dedifferentiation to a synthetic phenotype, sCSM (50). This plasticity allows CSM to adapt to changes in the local environment, i.e. elevated plasma low density lipoprotein (LDL) levels (50). Dedifferentiated sCSM are the cells that proliferate and migrate from the media to the arterial lumen where atherosclerotic plaque buildup of the intima occurs.

It has been unveiled that sCSM will further modulate into an osteogenic phenotype (oCSM). This is supported by studies of smooth muscle phenotype switching to a state of “bone-like” gene expression, i.e. runt-related transcription factor 2 (RUNX2), and a loss of contractile proteins, i.e. smooth muscle myosin heavy chain (SM-MHC) (30;51).

The Sturek laboratory has extensively studied CSM Ca^{2+} regulation in the setting of CAD (46). The plasma membrane Ca^{2+} ATPase (PMCA), a Ca^{2+} extrusion mechanism, appears to be the first impaired in early-stage CAD (52) along with a decrease in Na^{+}-Ca^{2+} exchanger (NX) coupling (52). Ca^{2+} can also accumulate in the cytosol after being released from intracellular cellular stores

through ryanodine receptors (RyR). CSM may compensate for these changes by increasing sarco/endoplasmic reticulum Ca^{2+} ATPase (SERCA) expression, thereby increasing Ca^{2+} buffering by the sarcoplasmic reticulum (SR), the primary intracellular Ca^{2+} store (53). However, there are conflicting data showing SERCA dysfunction in MetS Ossabaw (42) and atherosclerotic rabbits (54). Voltage-gated Ca channels (VGCC), a Ca^{2+} influx mechanism, are downregulated in diabetic and dyslipidemic Yucatan swine (53;55). These data seemingly conflict with data from the Tune laboratory that show increased VGCC expression and current in MetS Ossabaw CSM (56); however, the discrepancy may be explained by the differing “diabetic milieu” in the studies. Another mode of Ca^{2+} influx, transient receptor potential canonical (TRPC1) expression has been correlated with CAD progression and CSM phenotype switching in humans (57). TRPC1 is also increased in MetS Ossabaw (44). In his 2011 *Journal of Applied Physiology* review of CSM Ca^{2+} regulation in disease and exercise, Sturek states: “This apparent discrepancy strongly reinforces the concept that the time course and severity of disease are crucial to interpretation of findings on Ca^{2+} regulation mechanisms.” (46).

The American obesity epidemic and its comorbidities (MetS and CAD) are the motivation for the following described research. Their implications on cardiovascular health were studied on cellular, tissue, and whole animal levels in order to better understand this fatal disease on a translational scale. This written body of work includes three independent studies that encompass the entirety of these introductory pages.

Investigative Aims and Major Hypotheses

1. Coronary epicardial adipose tissue contributes directly to CAD in Ossabaw swine and progression of CAD will be attenuated upon surgical removal of the local fat depot.
2. ^{18}F-NaF uptake in the coronaries of MetS Ossabaw with early stage atherosclerosis will be higher than that of lean Ossabaw and ^{18}F-NaF uptake can be detected at a stage prior to that measurable by CT.
3. CSM Ca^{2+} signaling and function are increased in “early” CAD, but significantly decreased in “later” stages of CAD progression. More specifically, fluctuation in VGCC activity plays a role in oCSM dedifferentiation and CAD progression to CAC.

Figure Legends & Figures

Figure 1.1. Obesity trends among U.S. Adults. The American Obesity Epidemic is displayed across all 50 states with Indiana and the rest of the Midwest ranking among those with the highest occurrence of obesity in adults (58)**.** This trend has evolved over the past 25 years and does not seem to be tapering off according to recent reports (1).

Figure 1.2. An increased number of metabolic syndrome risk factors presented by a patient increases that patient's risk for cardiovascular events. Relative to a patient presenting no metabolic syndrome (MetS) risk factors, a patient presenting only 2 risk factors will more than double their risk for a cardiovascular event. However, this patient is not clinically diagnosed with MetS because they do not present with 3 or more of the risk factors. A clinically diagnosed MetS patient has a more than 3-fold increase in risk of cardiovascular event relative to a none-presenting patient. Figure adapted from (6).

Figure 1.3. Coronary artery anatomy and wall structure. A. Schematic representation of the heart and major epicardial coronary arteries. The aortic root is the origin of both the left ostium (LO) and right ostium (RO). From here, coronary arteries will supply oxygen-rich blood to the hard-working cardiac muscle of the ventricles. The LO leads to the left main which immediately branches into two of the main conduit coronary arteries, the left anterior

descending (LAD) and the circumflex (CFX) arteries. The LAD supplies to the septal, apical, and anterior portions of the left ventricle (LV) while the CFX supplies to the base and posterior portions. The RO leads to the right coronary artery (RCA) which supplies blood to the entire right ventricle. Coronary epicardial adipose tissue (cEAT) lies on top of these conduit vessels and its volume increases with MetS and obesity. **B.** The aortic trunk with conduits and branches dissected from the myocardium of an Ossabaw miniature swine. **C.** A transversely dissected portion of the LAD from a MetS Ossabaw reveals the lumen of the artery with cEAT still intact. cEAT accumulates on the epicardial surface of the heart and increasingly encases the coronary vessels as coronary artery disease progresses. (59) **D.** Histology of a proximal coronary artery segment from a lean Ossabaw swine with the elastin stain, Verhoff-Van Gieson (VVG). The collagen-rich adventitia (A) is separated from the media (M) by the external elastic lamina (EEL), which appears dark brown due to VVG staining. The media (M) is comprised of contractile coronary smooth muscle cells (CSM). The lumen (L) and media (M) are separated by an internal elastic lamina (IEL). Just on the luminal side of the internal elastic lamina is a thin layer of endothelial cells and a small number of synthetic CSM (sCSM) in healthy humans (48) and lean pigs. **E.** Histopathology of proximal coronary artery from a MetS Ossabaw swine stained with VVG reveals a significantly thickened intima (I) which is comprised of sCSM and inflammatory cells. Note the lumen area is reduced and a necrotic core (NC) containing calcifications (Ca) lies in the 3 o’clock orientation.

Figure 1.4. Coronary artery disease progresses to a high-risk stage of calcium deposition within the atherosclerotic lesions. Vascular calcification has two distinct pathologies (25): **A.** medial calcification is designated by hydroxyapatite deposition within the medial layer of the artery wall. This pathology is extremely common in chronic kidney disease patients and is classified by vessel stiffness and hypertension. **B.** intimal or atherosclerotic calcification is designated by hydroxyapatite deposition within the intimal layer of atherosclerotic lesions in patients with coronary artery disease (CAD). Intimal calcification is associated with MetS and increases the risk for plaque instability and rupture leading to adverse cardiovascular events. With strong evidence that calcification occurs early in CAD and at a level below the detectable threshold of computed tomography (CT), researchers have turned to positron emission tomography (PET) with the efforts of detecting calcification at the molecular level using the long-known bone tracer, ^{18}F-NaF. **C.** Fluoride (large blue circle) binds directly to hydroxyapatite by replacing the hydroxyl group (small white and blue circles). Calcium (red) is a major component of this bone mineral that is produced by osteogenic CSM (oCSM) within the arterial wall. (60). **D(a).** In this PET coronal image, ^{18}F-NaF uptake can be seen in the bone tissues (black). This patient as a focal area of bone metabolism and calcium acitivty as indicated by increased ^{18}F-NaF uptake at the site of a rib fracture (yellow arrow). **D(b).** A transaxial view of a simultaneous CT scan shows its high spatial resolution and vivid anatomical structures. **D(c).** A hybrid image is constructed by overlaying the co-registered PET and CT scans to combine the high sensitivity of PET with

the high spatial resolution of CT. The metabolic activity seen on the PET scan is completely absent from the CT images. (35)

Figure 1.5. Ossabaw swine fed an excess-calorie atherogenic diet develop obesity, metabolic syndrome, and coronary artery disease. Lean Ossabaw miniature swine **(A)** bodyweight will plateau, while Ossabaw fed an atherogenic diet **(B)** will continue to gain weight and present all risk factors of metabolic syndrome (MetS) (45). **C.** Proximal coronary artery histopathology with Masson's trichrome staining reveals normal arterial wall structure and composition in lean Ossabaw. The collagen-rich (blue) adventitia (A) surrounds the medial layer (M) of the artery which is composed of contractile coronary smooth muscle cells (CSM) (red). A non-obstructed lumen (L) is also observed. **D.** Masson's trichrome staining of proximal coronary artery from Mets Ossabaw with CAD reveals increased collagen (blue) deposition within the medial layer (M) of the arterial wall. Within the newly formed intimal layer (I), the CSM organization (red) has completely changed due to the transition of contractile cells to the synthetic phenotype which proliferates and migrates towards the lumen (L) and contributes to further collagen deposition (blue). **E.** Identical to human CAD pathology, MetS Ossabaw with later stage CAD will develop intimal calcification due to the transition of CSM to an osteogenic phenotype. The oCSM will deposit calcium in the form of hydroxyapatite into the extracellular matrix. Alizarin red staining of proximal coronary artery from MetS Ossabaw reveals a large calcified structure

(Ca, solid arrow) and spotty, microcalcifications (Ca, dashed arrow) within the atherosclerotic intimal lesion (I).

Figure 1.6. Several transporters including channels, pumps, and exchangers are responsible for regulation of intracellular Ca^{2+} signaling in coronary smooth muscle cells. Due to the high efficacy and potency of Ca^{2+} as a messenger in coronary smooth muscle cells (CSM), it is tightly regulated and kept at low levels in the cytosol (Ca_C) (~100 nM). Intracellular stores such as the sarcoplasmic reticulum will hold large capacities of Ca^{2+} (Ca_{SR}) which can be released to signal events such as contraction, transcription, proliferation, and migration. Two of the influx mechanisms that sit on the plasma membrane are the L-type voltage gated Ca^{2+} channel (VGCC) and the transient receptor potential canonical channel (TRPC). When Ca^{2+} comes into the cell it must be extruded back to the extracellular space or buffered into the internal stores. Two extrusion mechanisms also on the plasma membrane are the Na^{+}-Ca^{2+} exchanger (NCX) and the plasma membrane Ca^{2+} ATPase (PMCA). Elevated Ca_C can also be buffered into the sarcoplasmic reticulum store by a similar pump that sits on the sarcoplasmic reticulum membrane, the sarco/endoplasmic reticulum Ca^{2+} ATPase (SERCA). Ca_{SR} can be released via release channels on the sarcoplasmic reticulum membrane called the ryanodine receptor (RyR). The interplay of these Ca^{2+} transporters is critical in the health and function of CSM. Loss of this tight regulation will lead to CSM dedifferentiation and progression of coronary artery disease.

Figure 1.1

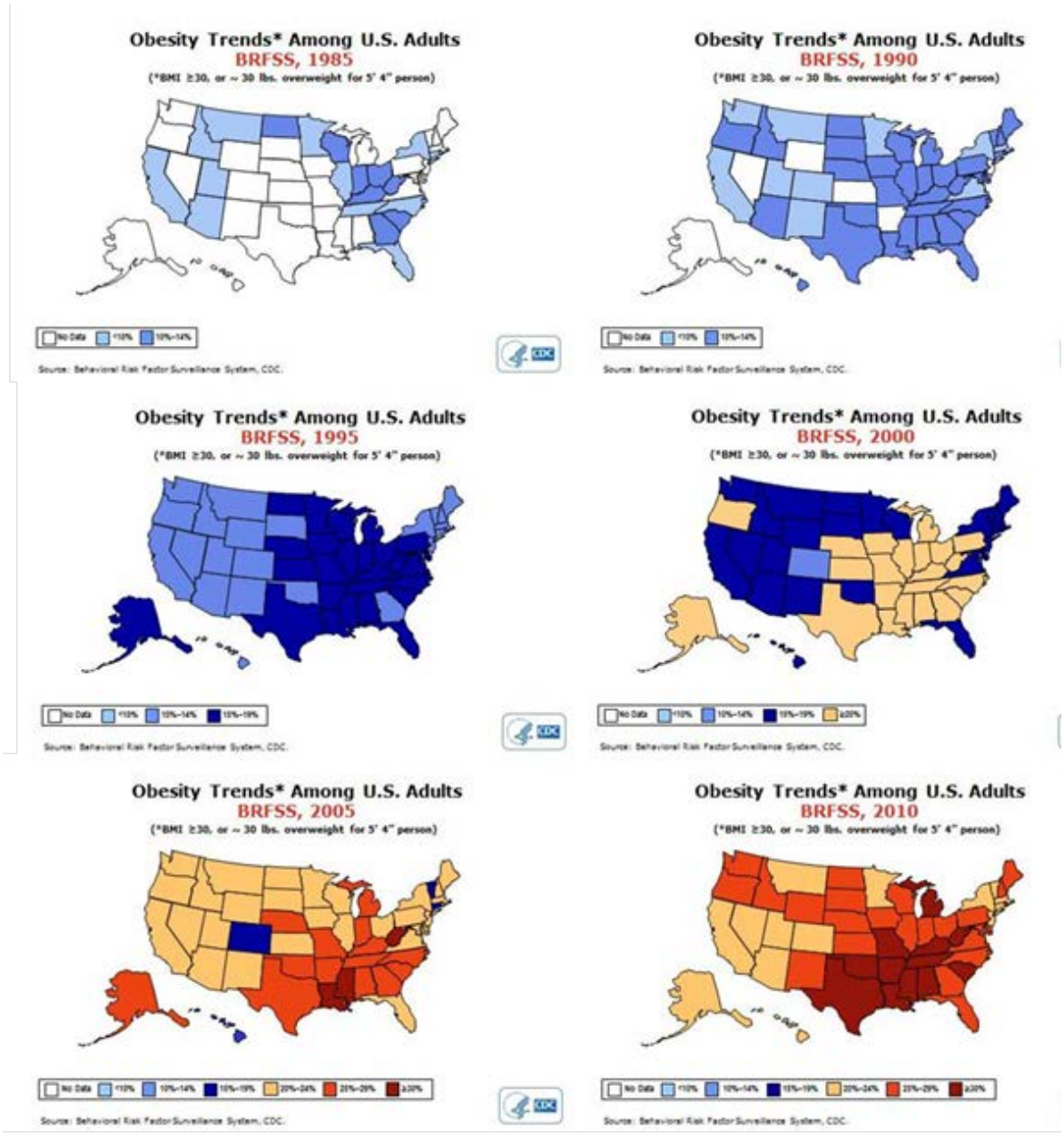
Obesity Trends* Among U.S. Adults
BRFSS, 1985
(*BMI ≥30, or ~ 30 lbs. overweight for 5' 4" person)
Source: Behavioral Risk Factor Surveillance System, CDC.
Obesity Trends* Among U.S. Adults
BRFSS, 1990
(*BMI ≥30, or ~ 30 lbs. overweight for 5' 4" person)
Source: Behavioral Risk Factor Surveillance System, CDC.
Obesity Trends* Among U.S. Adults
BRFSS, 1995
(*BMI ≥30, or ~ 30 lbs. overweight for 5' 4" person)
Source: Behavioral Risk Factor Surveillance System, CDC.
Obesity Trends* Among U.S. Adults
BRFSS, 2000
(*BMI ≥30, or ~ 30 lbs. overweight for 5' 4" person)
Source: Behavioral Risk Factor Surveillance System, CDC.
Obesity Trends* Among U.S. Adults
BRFSS, 2005
(*BMI ≥30, or ~ 30 lbs. overweight for 5' 4" person)
Source: Behavioral Risk Factor Surveillance System, CDC.
Obesity Trends* Among U.S. Adults
BRFSS, 2010
(*BMI ≥30, or ~ 30 lbs. overweight for 5' 4" person)
Source: Behavioral Risk Factor Surveillance System, CDC.

Figure 1.2

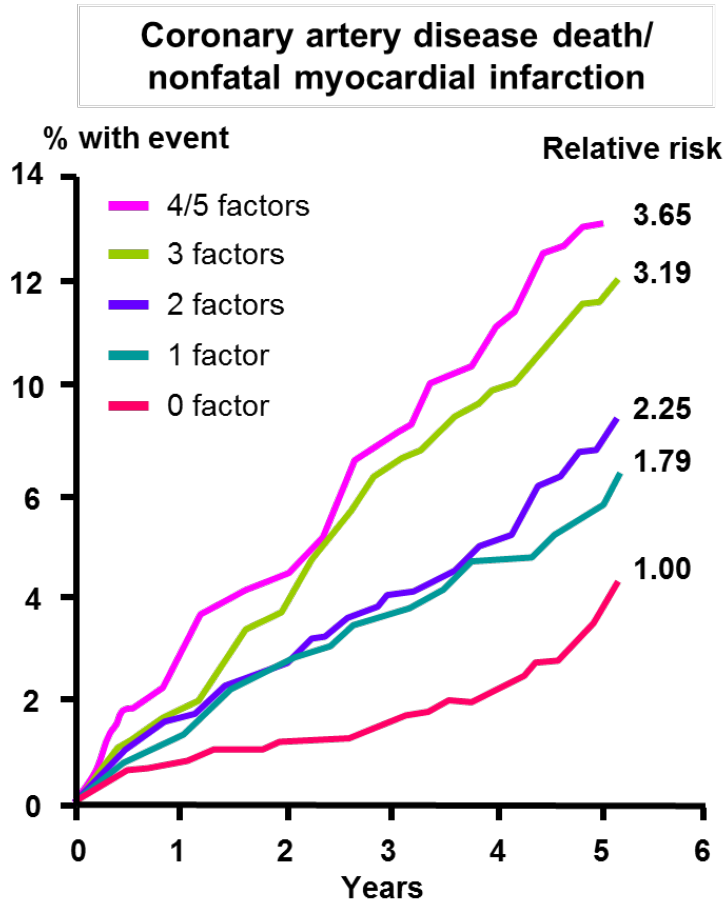
Coronary artery disease death/
nonfatal myocardial infarction
% with event
Relative risk
14
12
10
6
4
2
0
4/5 factors
3 factors
2 factors
1 factor
0 factor
3.65
3.19
2.25
1.79
1.00
0
1
2
3
4
5
6
Years

Figure 1.3

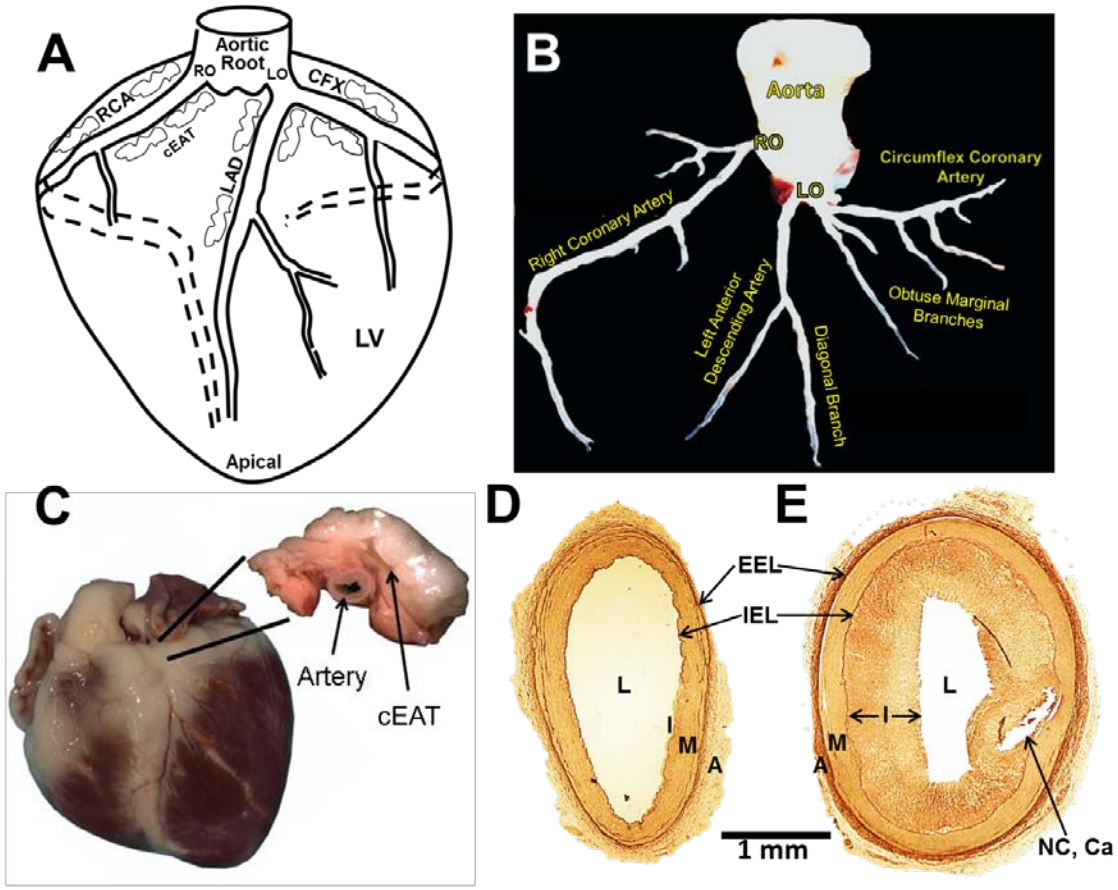
A
Aortic Root
RO
LO
RCA
CFX
cEAT
LAD
LV
Apical
B
Aorta
RO
LO
Circumflex Coronary Artery
Right Coronary Artery
Left Anterior Descending Artery
Diagonal Branch
Obtuse Marginal Branches
C
Artery
cEAT
D
E
EEL
IEL
L
I
M
A
1 mm
NC, Ca

Figure 1.4

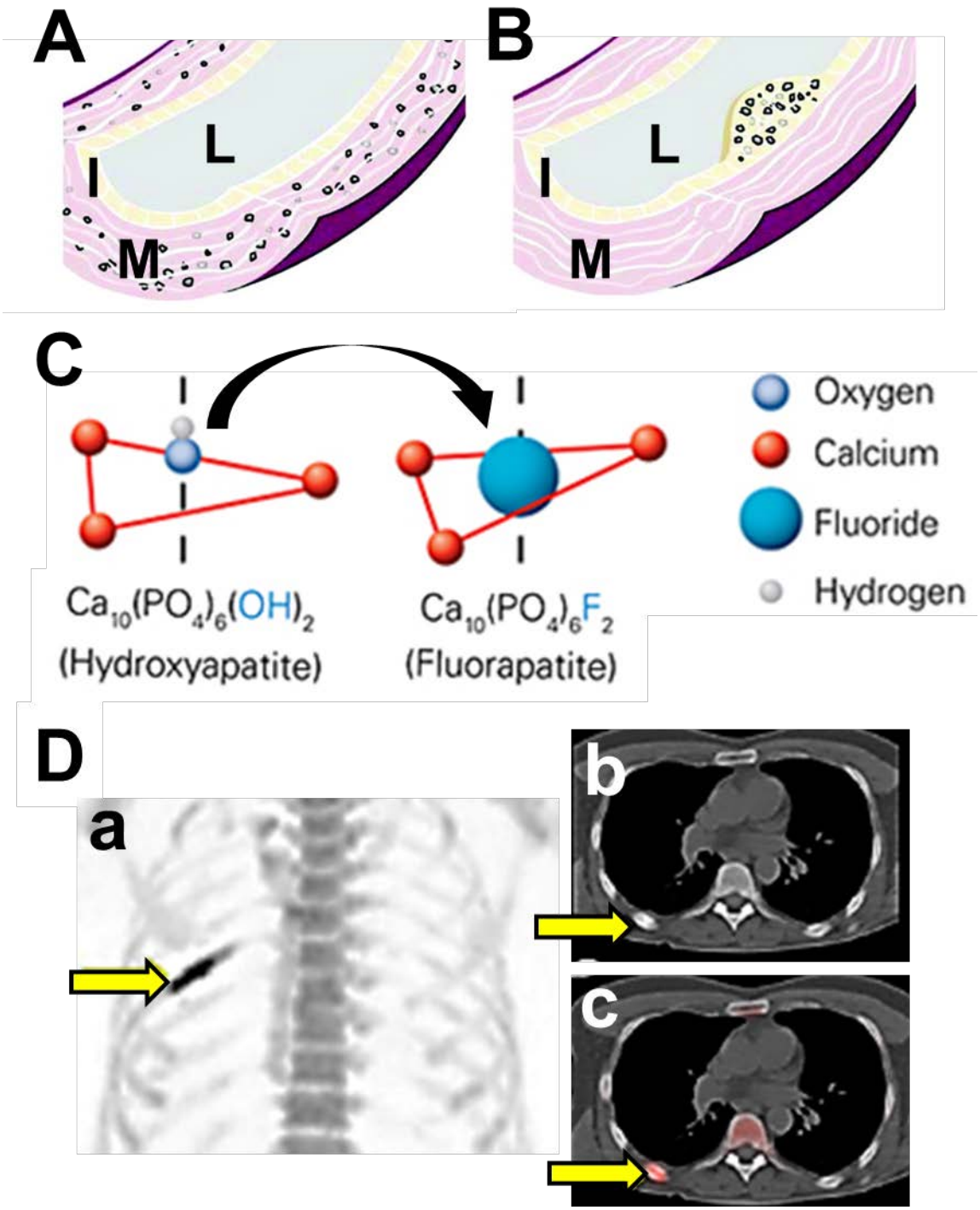
A
L
I
M
B
L
I
M
C
Oxygen
Calcium
Fluoride
Hydrogen
$Ca_{10}(PO_4)_6(OH)_2$
(Hydroxyapatite)
$Ca_{10}(PO_4)_6F_2$
(Fluorapatite)
D
a
b
c

Figure 1.5

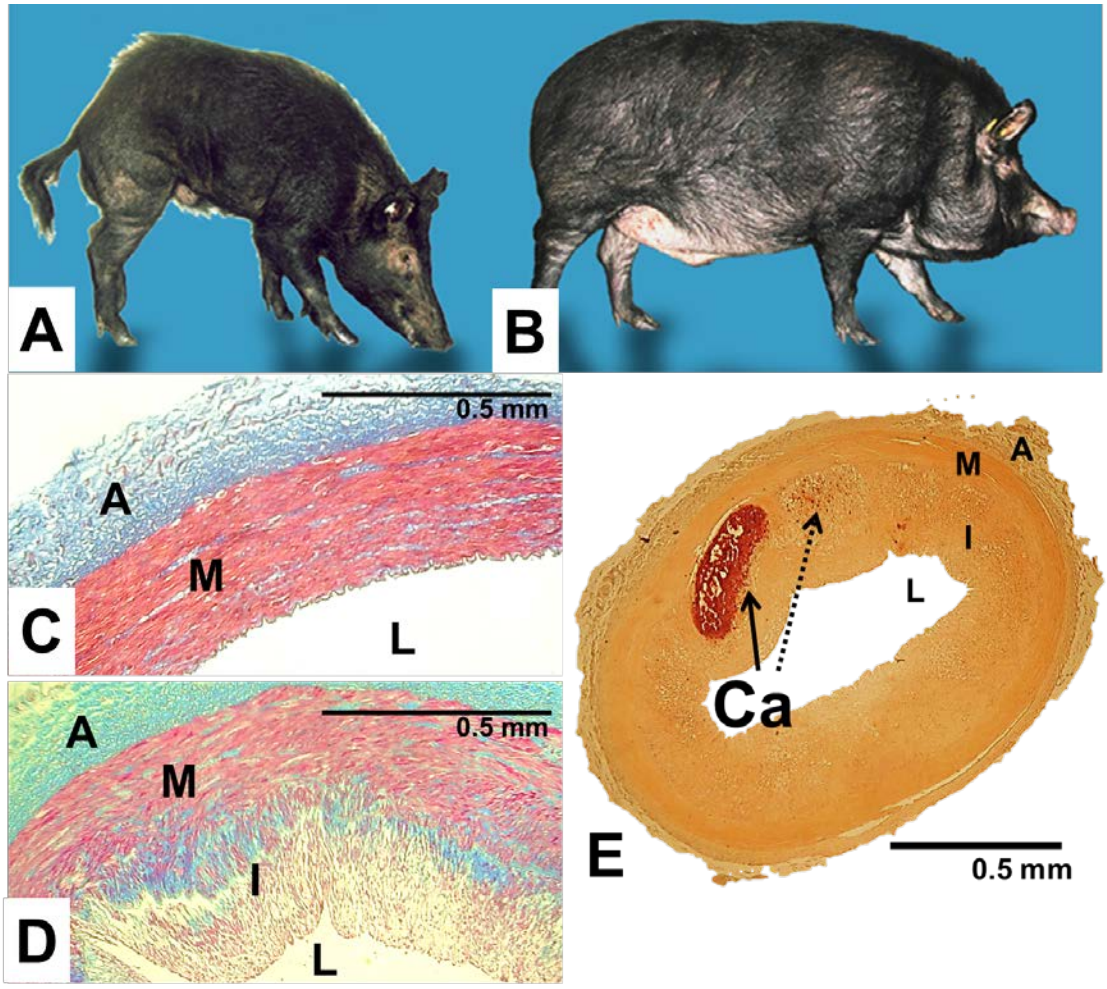

Figure 1.6

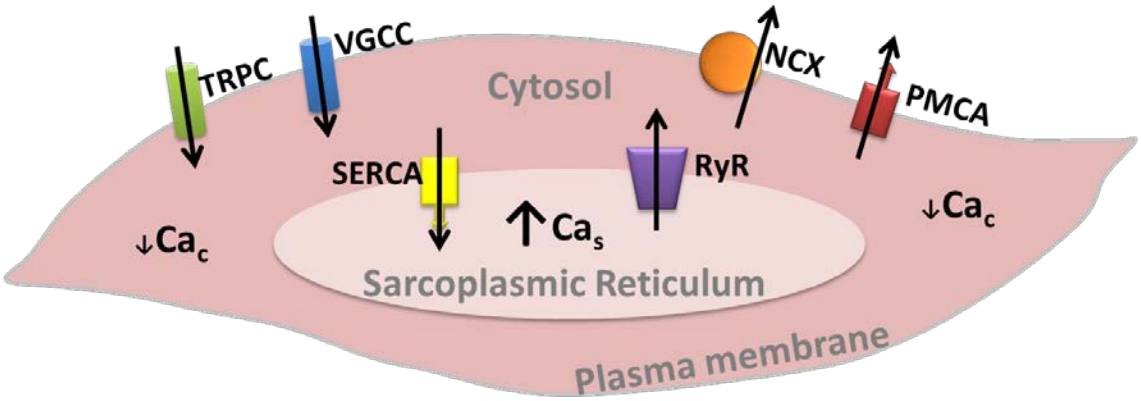

Influx mechanisms:

- VGCC: L-type Voltage-gated Ca channel
- TRPC: Transient receptor potential canonical

Extrusion mechanisms:

- NCX: Na-Ca exchanger
- PMCA: Plasma membrane Ca ATPase

SR store mechanisms:

- SERCA: Sarco/endoplasmic reticulum Ca ATPase
- RyR: Ryanodine receptor

CHAPTER 2: EPICARDIAL ADIPOSE EXCISION SLOWS THE PROGRESSION OF PORCINE CORONARY ATHEROSCLEROSIS.

Mikaela L. McKenney, MS[1]*, Kyle A .Schultz, MS[1]*, Jack H. Boyd, MD[2], James P. Byrd[1], Mouhamad Alloosh, MD[1], Shawn D. Teague, MD[3], Arturo A. Arce-Esquivel, MD, PhD[4], John N. Fain, PhD[5], M. Harold Laughlin, PhD[4], Harold S. Sacks, MD[6], Michael Sturek, PhD[1]

*These authors contributed equally to this work.

[1]Departments of Cellular & Integrative Physiology, [2]Cardiothoracic Surgery and [3]Radiology, Indiana University School of Medicine, Indianapolis, IN 46202; [4]Department of Biomedical Sciences, University of Missouri, Columbia, MO, 65211; [5]Department of Molecular Sciences, University of Tennessee Health Science Center, Memphis, TN, 38163; [6]Endocrinology and Diabetes Division, VA Greater Los Angeles Healthcare System, Los Angeles, CA, 90073

Abstract

Background: In humans there is a positive association between epicardial adipose tissue (EAT) volume and coronary atherosclerosis (CAD) burden. We tested the hypothesis that EAT contributes locally to CAD in a pig model.

Methods: Ossabaw miniature swine (n=9) were fed an atherogenic diet for 6 months to produce CAD. A 15 mm length by 3-5 mm width coronary EAT (cEAT) resection was performed over the middle segment of the left anterior descending artery (LAD) 15 mm distal to the left main bifurcation. Pigs recovered for 3 months on atherogenic diet. Intravascular ultrasound (IVUS) was performed in the LAD to quantify atheroma immediately after adipectomy and was repeated after recovery before sacrifice. Coronary wall biopsies were stained immunohistochemically for atherosclerosis markers and cytokines and cEAT was assayed for atherosclerosis-related genes by RT-PCR. Total EAT volume was measured by non-contrast CT before each IVUS.

Results: Circumferential plaque length increased ($p<0.05$) in the proximal and distal LAD segments from baseline until sacrifice whereas plaque length in the middle LAD segment underneath the adipectomy site did not increase. T-cadherin, scavenger receptor A and adiponectin were reduced in the intramural middle LAD. Relative to control pigs without CAD, 11β-hydroxysteroid dehydrogenase (11βHSD-1), CCL19, CCL21, prostaglandin D_2 synthase,

gp91phox [NADPH oxidase], VEGF, VEGFGR1, and angiotensinogen mRNAs were up-regulated in cEAT. EAT volume increased over 3 months.

Conclusion: In pigs used as their own controls, resection of cEAT decreased the progression of CAD, suggesting that cEAT may exacerbate coronary atherosclerosis.

Background

In most recent reviews of human cross-sectional studies (61-63), the amount of epicardial adipose tissue (EAT), measured either as thickness by echocardiography over the right ventricle or as total volume by computed tomography (CT) scans, correlated directly with coronary artery disease (CAD) burden. Additionally, in prospective case-cohort (64) and in case-control (65) studies, EAT volume predicted future CAD events and myocardial ischemia. However, one report did not show that EAT volume added incremental predictive value over established CAD risk factors (66).

After regression analysis, EAT volume expansion in CAD occurs independently of associated increases in visceral abdominal and total body fat mass as well as changes in other CAD risk factors (62;63). This epidemiological evidence together with pathophysiological data showing increased chronic inflammatory cell infiltrates (67) and up-regulation of pro-inflammatory, redox, macrophage marker, and angiogenic gene expression specifically in EAT sampled from humans undergoing coronary artery bypass for severe CAD (20) is the basis for the hypothesis that EAT might contribute locally and detrimentally to coronary atherogenesis. However, to our knowledge, there is no direct experimental evidence that EAT plays a role in coronary atherogenesis.

Our laboratory has characterized Ossabaw miniature swine as a model of CAD. The “thrifty genotype” of Ossabaw swine has enabled survival in the feast and famine ecology, i.e. extreme variations in food availability, of Ossabaw Island (40). In the sedentary environment of captivity, our group induced CAD in this

breed of pigs by feeding them a hypercaloric, atherogenic diet (40;44) (42;59). This animal's coronary arterial supply more closely resembles that of humans compared to rodent research models. Additionally, rodent EAT is unpredictable in amount and not easily discerned, whereas the pig's EAT is clearly demarcated macroscopically (40;59), can be imaged radiologically (40), and potentially might be amenable to surgical removal (68). We tested the hypothesis that surgical excision of EAT in direct contact with the coronary artery (cEAT) of pigs would attenuate underlying plaque progression in vivo.

Methods

Animal Model and Protocol

We produced CAD in 9 castrated male Ossabaw miniature swine by feeding them 1000 g, once a day, of a high fat/cholesterol/fructose, atherogenic diet for 6 months starting at 6 months of age. The diet provided 16.3% kcal from protein, 40.8% kcal from complex carbohydrates, 19% kcal from fructose, and 42.9% kcal from fat. Fat calories derived from a mixture of lard, hydrogenated soybean oil, and hydrogenated coconut oil. It was supplemented with 2.0% cholesterol and 0.7% sodium cholate by weight (KT324, Purina Test Diet, Richmond, IN). Age- and gender-matched lean control swine were fed 750 g of regular chow (5L80, Purina Test Diet, Richmond, IN) containing 18% kcal from protein, 71% kcal from complex carbohydrates, and 11% kcal from fat once a day. All animals had free access to drinking water. After 6 months on the diet, CT was performed to quantify EAT surrounding the heart. Surgical excision of cEAT covering the middle segment of the left anterior descending (LAD) artery, which we termed selective coronary adipectomy, was then conducted via a thoracotomy, as described below, followed immediately by intravascular ultrasound (IVUS) quantification of CAD. Following the procedure, the same baseline diet was continued during a 3-month recovery period at the end of which identical CT followed by IVUS were performed prior to sacrifice and tissue collection. Control pigs did not undergo IVUS or adipectomy because they have been shown previously to develop minimal or no CAD over the time course of this experiment (42). In both adipectomy and control pigs at sacrifice, cEAT for

mRNA analysis was resected from the adventitial surface of the LAD just proximal to the middle LAD adipectomy site, and as a comparator, paracardial fat was sampled from the mediastinal surface of the pericardium towards the apex of the heart. Samples were stored at -80˚C. Biopsies of proximal, middle and distal LAD were taken and preserved for immunohistochemistry. All protocols involving animals were approved by an Institutional Animal Care and Use Committee and complied fully with recommendations in the *Guide for the Care and Use of Laboratory Animals* (69) and the American Veterinary Medical Association Panel on Euthanasia (70).

Intravascular Ultrasound

Following an overnight fast, swine received a 2.2 mg/kg of xylazine (Webster Veterinary, Devens, MA) and 5.5 mg/kg of telazol (Fort Dodge Animal Health, Fort Dodge, IA) intramuscular injection to induce anesthesia. Swine were intubated and anesthesia was maintained with 2-4% isoflurane in 100% O_2 as a carrier gas. The isoflurane level was adjusted to maintain anesthesia with stable hemodynamics. Heart rate, aortic blood pressure, respiratory rate, and electrocardiographic data were continuously monitored throughout the procedure. A 7F introducer sheath was inserted into the right femoral artery and heparin (200 U/kg) was administered under sterile conditions. A 7F guiding catheter (Amplatz L, sizes 0.75-2.0; Cordis, Bridgewater, NJ) was advanced to engage the left main coronary ostium. A 3.2F, 30 MHz IVUS catheter (Boston Scientific, Natick, MA) was advanced over a 0.014 inch diameter percutaneous

transluminal coronary angioplasty guide wire (Boston Scientific, Natick, MA) and positioned in the LAD. Automated IVUS pullbacks were performed at 0.5 mm/sec in the LAD. Throughout the procedure angiography was performed to place the guiding and IVUS catheters in their desired positions. The IVUS catheter, guide catheter, and introducer sheath were removed and the right femoral artery ligated. The incision was closed and the animal was allowed to recover. Cefazolin (1000 mg; WG Critical Care, Lake Forest, IL) was given twice a day for six days following the procedure.

All IVUS pullback images were analyzed off-line (Windows Media Player, Microsoft) at 1 mm intervals. The LAD was divided into 3 segments: proximal (0-15 mm), middle (15-30 mm) and distal (30-45 mm) with 0 mm starting at the bifurcation of the left main into LAD and circumflex. Three IVUS pullback images were captured per vessel segment. Using the Image-Pro Plus software (Media Cybernetics, Rockville, MD), lumen area (LA) was found by tracing the vessel lumen. From LA, lumen circumference (LC) was calculated for each vessel segment by the following formula: $LC=2\pi\ [\sqrt{\ }(LA/\pi)]$. To derive wall coverage (WC) by plaque, the circumference of each cross-sectional image was divided into 16 equal segments. Percent wall coverage was calculated as (# segments containing atheroma ÷ 16) x 100. From the product of average WC x LC, a circumferential plaque length for each vessel segment was found. As an example, the following results are presented from a proximal coronary artery segment:

LA 21.40 mm^2; LC 16.40 mm; WC 29.58%; circumferential plaque length = 4.85 mm. Pullbacks were used for 7 out of 9 animals due to restrictions from vasospasms or lumen diameter. Using a 2-way analysis of variance (ANOVA), average circumferential plaque length per vessel segment was compared pre- and post-adipectomy.

Selective Adipectomy

Under general anesthesia, cardiovascular monitoring (both as described above), and using aseptic surgical techniques, all adipectomies were performed on the LAD with access via left thoracotomy by the cardiac surgeon. Figure 2.1A shows the anatomical structures and distribution of EAT over the epicardium of a representative pig heart ex vivo. A Thoratrak Retractor (Medtronic; Minneapolis, MN) was utilized for minimal rib spreading and as a base for the Octopus cardiac stabilizer (Medtronic; Minneapolis, MN) (Fig. 2.1B). The pericardium was opened and cradled to the drapes exposing the LAD. The Octopus was then positioned to stabilize the middle LAD segment. Using the bifurcation of the left main into LAD and circumflex as the reference point, cEAT was excised sharply starting 15 mm distal to this landmark for a distance of 15 mm along the length of the LAD and 3-5 mm on both the right and left lateral aspects of this part of the vessel (Fig. 2.1C). Non-absorbable Prolene sutures were placed to control epicardial venous bleeding from resected fat typically to the left side of the LAD. The ligatures demarcated this site for later tissue collection at sacrifice. When possible, the pericardium was loosely approximated with interrupted sutures. The

chest was then closed in layers in the standard fashion. Pleural air was evacuated by means of suction on an intrapleural red rubber catheter being withdrawn during a valsalva breath and closure of the chest wall musculature. One of the 9 animals succumbed intra-operatively from an acute myocardial infarction complicated by refractory ventricular fibrillation documented by ECG and by subsequent autopsy that showed acute LAD thrombosis. There were no noticed post-operative complications in the remaining swine.

Immunohistochemistry

Sections of the LAD were prepared using techniques previously described by us (71). Samples of LAD were dissected and immersed in neutral-buffered 10% formalin for a minimum of 24 h and then processed to paraffin embedment. The proximal, middle, and distal samples of LAD were obtained consistently from the same location in all pigs. Five-micrometer sections were cut with an automated microtome (Microm, Thermo Fischer Scientific, Bellefonte, PA), floated onto positively charged slides (Thermo Fischer Scientific), and deparaffinized. The slides were then steamed in citrate buffer at pH 6.0 (Dako target retrieval solution S1699; Dako, Carpenteria, CA) for 30 min to achieve antigen retrieval and subsequently cooled for 30 min. Next, the slides were stained manually with sequential Tris buffer or water wash steps performed after each protocol step. Sections were incubated with avidin biotin two step blocking solution (Vector SP-2001; Vector Laboratories, Burlingame, CA) to inhibit background staining and in 3% hydrogen peroxide to inhibit endogenous

peroxidase. Nonserum protein block (Dako X909; Dako) was applied to inhibit nonspecific protein binding. Immunostaining was performed using scavenger receptor A (SRA-ES; 1:100 dilution, Transgenic Inc. #KT-022), tryptase (1:600 dilution, Dako #M7052), CD-3 (1:600 dilution, Dako #A0452), monocyte chemoattractant protein-1 (MCP-1; 1:100 dilution, PeproTech #500-P76), resistin (1:800 dilution, Phoenix Pharmaceuticals #H-02840), T-cadherin (1:1000 dilution, Abgent #CDH13, AP14346), adiponectin (1:200, Chemicon #MAB 3604) or tumor necrosis factor-alpha (TNF-alpha; 1:100 dilution, R&D #AF690). All the primary antibodies were diluted using antibody diluent (S0809; Dako) and were incubated with the tissue sections overnight at 4-C. After the appropriate washing was completed, sections were incubated with biotinylated antimouse or rabbit link secondary antibody and then peroxidase-labeled streptavidin (LSAB+ kit, peroxidase, K0690; Dako). Diaminobenzidine (K3468; Dako) was applied for 5 min and allowed visualization of primary antibody staining. Sections were counterstained with Mayer hematoxylin for 1 min, dehydrated, and coverslipped. For negative controls, histological sections were prepared as described, but incubation in primary antibody was replaced with Tris buffer.

Immunostaining analysis was performed in the entire vessel wall (i.e. intima to external elastic lamina boundaries) in order to quantify the presence of SRA, tryptase, CD3, MCP-1, resistin, T-cadherin, adiponectin or TNF-alpha. Sections were examined using an Olympus BX61 photomicroscope (Olympus, Melville, NY), and pictures were captured at 20x magnification. Image-Pro Plus (version 6.2.0.424; Media Cybernetics, Inc., Silver Spring, MD) was used to

identify and quantify the positive area of staining. Percent staining of the vessel wall was calculated from the data for positive staining and total area. An experienced investigator that was blinded to treatment group's identities performed the selection of target areas, photography, and image analysis.

mRNA Analysis

mRNA Isolation. Approximately 0.2 to 0.5 g of frozen cEAT and paracardial fat from adipectomy and control animals was homogenized with 5 ml of a monophasic solution of phenol and guanidine isothiocyanate (TRIzol reagent, Invitrogen, Carlsbad, CA).

RT-PCR. The mRNA assay involved real-time quantitative PCR. Transcriptor First Strand cDNA synthesis Kit from Roche Diagnostics was used on equal quantities of RNA to prepare the complementary DNA (cDNA). The Roche Lightcycler 480 Real-time RT-PCR system and Roche's Universal Probe Library of short hydrolysis Locked Nucleic Acid (LNA) dual hybridization probes combined with the primers recommended by their web-based assay design center [http://www.universalprobelibrary.com] were used for mRNA quantification. Integrated DNA Technologies (Coralville, IA) synthesized the primers. Twenty five genes related to atherosclerosis were selected (Table 2). Fifteen mRNAs were targeted for their roles in inflammation, 4 for their roles in oxidative stress as well as reactive oxygen species regulation and 6 in control of angiogenesis and endothelial cell function. In each assay, 55 ng per tube of total RNA (determined by absorption at 260 nm in a nano spectrophotometer) was

used. The data were obtained as crossing point values (Cp) obtained by the second derivative maximum procedure as described by Roche Applied Science technical notes LC10/2000 and 13/2001 [http://www.roche-applied-science.com/sis/rtpcr/htc/index.jsp]. Relative quantification of the data was calculated using the absolute Cp values based on analyzing the same amount of total RNA in each assay as recommended by Bustin (72).

Computed Tomography

CT scans to quantify changes in EAT were analyzed by one observer. EAT was defined as fat between the inner surface of the visceral pericardium and epicardial surface of the myocardium (15;73). Paracardial fat was defined as fat lying within the mediastinum superficial to the parietal pericardium (15;73). Representative images are shown in Figures 2.2A-C. The pigs were scanned using a Philips Brilliance 64 detector scanner (Cleveland, OH) while sedated using 4% Isoflurane (Webster Veterinary, Devens, MA) supplied by mask. Imaging was performed with retrospective electrocardiogram (ECG) gating and without the administration of intravenous contrast from above the aortic arch to below the heart. Additional scan parameters included a 64 x 0.625 collimation, pitch of 0.2, rotation time of 0.4 seconds, 120 kVp, and 800-1000 mAs. Images were reconstructed with a slice thickness of 0.67mm and increment of 0.67mm using a CB filter. A batch was first created to ensure equal amounts of data were analyzed and included for each image set. The baseline and pre-sacrifice images were then aligned side-by-side to ensure similar magnification and

orientation. Transverse images were analyzed by starting at the superior aspect of the atrial appendage. Sternal, vertebral body and cardinal landmarks were utilized to insure similar alignment. The slice thickness of each image produced was 3 mm without overlap, yielding about 40 images per heart in each batch. Regions of interest (ROI) were drawn by hand using quantitative computer tomography angiography (Q-CTA) software on a Philips Extended Brilliance Workspace (Version 3.5) to include the entire heart. Vessels leaving and entering the heart were included until they were noticeably detached from the heart. The Hounsfield unit (HU) value is similar for blood, muscle, and soft tissue, thus making the vessels appear as part of the heart until a visible distance is evident between the heart and the vessel. In all cases vessels were split in the ROI through their center as the pericardium encapsulates the most proximal regions of the vessels leaving and entering the heart. The software highlighted all tissue that matched the HU intensity of a reference ROI drawn in known subcutaneous fat (at the level of the carina). The fat area measurements of the images were then multiplied by their slice thickness to determine fat volume. Volumes of EAT were compared before adipectomy and at the end of the recovery period. Inter-operator coefficient of variation was 6.2%, while intra-operator variation was 1.0%.

Statistics

Statistical analysis was performed via Microsoft Excel 2010, utilizing ANOVA, regression analysis and post hoc 1- and 2-tailed paired student t-tests

to examine significance. All values are given as mean ± SEM. A p value <0.05 was considered statistically significant.

Results

Metabolic Characteristics

At adipectomy, pigs on the atherogenic diet had developed CAD and its risk factors including hypertension, obesity, increased LDL/HDL ratio, insulin resistance, glucose intolerance and increased triglyceride levels compared to age-matched lean controls (Table 2.1). Other than the increase in body weight, these characteristics remained constant during the 3 month recovery following adipectomy (data not shown).

IVUS

Representative IVUS images in Figure 2.3 show a normal coronary lumen (A) as well as partial (B) and complete circumferential (C) neointimal plaque formation. The results of IVUS pullbacks revealing atherosclerosis in each 15 mm length proximal, middle and distal portions of the LAD from its origin are shown in Figure 2.3D. Over 3 months, baseline mean circumferential plaque length in the proximal LAD increased from 4.45±0.54 to 8.24±1.03 mm ($p<0.05$, Two-way ANOVA and Bonferroni post-hoc) and in the distal LAD from 1.98 ± 0.35 to 5.74± 0.75 mm ($p<0.05$, Two-way ANOVA and Bonferroni post-hoc). By contrast, circumferential plaque length in the middle LAD increased from 5.60±0.90 to 7.64±1.03 mm, which was not statistically different ($p>0.05$, Two-way ANOVA and Bonferroni post-hoc). There was no difference between baseline mean proximal and middle LAD plaque lengths ($p=0.26$), whereas

middle LAD was higher than distal LAD ($p<0.05$) and proximal was also greater than distal ($p<0.05$).

Immunohistochemistry

On light microscopy of the LAD middle segment sections, a thinner layer of cEAT covered the adventitia than the adjacent two segments, suggesting no regrowth of remnant fat 3 months after adipectomy. Figure 2.4A shows representative photomicrographs of the presence, distribution and intensity of immunostaining of T-cadherin, SRA and adiponectin in the three segments of the LAD. T-Cadherin was strongly positive in the endothelial layer, but also present in the sub-endothelial neointima in proximal and distal LAD, but to a lesser extent in the middle vessel wall. SRA was present in the endothelial layer and neointima. Adiponectin was present in the endothelial layer and very dispersed over the media. As shown in Figure 2.4B (panel A), when these markers in all samples were quantitated, there was a significant reduction in mean percentage area of T-cadherin staining in the intima-media from 4.77±0.92% in the proximal and 4.71±0.66% in the distal LAD segments to 2.67±0.66% in the middle LAD (proximal to middle LAD $p<0.05$ and distal to middle LAD $p<0.05$ using 2-tailed t tests). SRA staining (Fig. 2.4B, panel B) was 0.73± 0.25% in the proximal LAD and 0.26±0.08% in the middle LAD which was significantly different ($p<0.05$) by a 1-tail t test with a trend towards significance ($p= 0.07$ in a 2-tailed t test), and 0.74±0.45% in the distal LAD which although higher than the middle LAD was not significantly different. Adiponectin staining (Fig. 2.4B, panel C) was significantly

lower in the middle LAD 3.28±1.04% versus the proximal 8.94±2.32% ($p<0.05$ in a 1-tailed t test versus a trend for significance $p=0.08$ in a 2-tailed t test). In the distal LAD, adiponectin measured 5.12±1.57%, which was not different to either the proximal or middle LAD. There were no differences in coronary wall percent staining for tryptase, CD3, TNFα, MCP-1 and resistin between the proximal, middle and distal LAD.

CT Quantification of Epicardial Fat

In Figure 5, CT scans done on 6 of the 8 surviving swine showed an increase in total EAT volume from 9.7 ± 1.1 cm^3 at adipectomy to 13.5 ± 0.7 cm^3 at time of sacrifice, representing a 39% increase ($p = 0.006$) over 3 months. Due to inadequate numbers of data points, CT data could not be correlated with the IVUS data to determine if a relationship existed between changes in EAT volume and total plaque burden.

Gene Expression

Table 2.2 shows the expression in cEAT and paracardial fat of genes linked to atherogenesis, namely those involved in inflammation, reactive oxygen species and redox reactions, angiogenesis and endothelial cell function. The data in each fat depot are expressed as the ratio of experimental to control pig fat depots. In EAT, there were significant and substantial fold increases in mRNA expression of pro-inflammatory 11β-hydroxysteroid dehydrogenase (11βHSD-1), CCL19, CCL21 and PGD2S; anti-inflammatory adiponectin; pro-oxidant

gp91phox [NADPH oxidase], angiogenic VEGF and VEGFGR1 and vascoconstrictive angiotensinogen. There were no changes in pro-inflammatory toll-like receptor 4 [TLR4], CCR7, TNFα, IL-1β, IL-6, IL-8, leptin, Unc5b, netrin-1 and NGF; redox genes eNOS, superoxide dismutase [SOD], cyclooxygenase 2 and cytochrome oxidase; and vasoconstrictor endothelin-1 and vasodilator adenosine receptor 1.By contrast, in paracardial fat relative to cEAT, 11βHSD-1 and CCL21 were normal; CCL19, PGD2S, adiponectin pro-oxidant gp91phox [NADPH oxidase] VEGF, VEGFGR1 and angiotensinogen were up-regulated to much lesser degrees; and the remaining genes were similar except for TLR4 and endothelin-1 which were modestly (~2 fold) increased.

Discussion

We present experimental evidence that, in Ossabaw miniature swine, selective surgical excision of adipose tissue in direct contiguity with one of the epicardial coronary arteries attenuated the progression of atherosclerosis, thus supporting the hypothesis that cEAT could contribute to underlying coronary atherogenesis (68). The findings are applicable to the early stages of CAD because of the relatively young age of the animals, the short duration of atherogenic diet feeding, and the lack of observed flow-limiting coronary stenosis typical of advanced clinical disease. We acknowledge the substantially high LDL cholesterol levels (>500 m/dL) in the obese group. We have conducted other studies in which the LDL was ~250 mg/dL (e.g. (42;44)) for a longer duration, which yielded substantial coronary atherosclerosis. We predict a similar result of adipectomy. This very high LDL cholesterol level for a short duration is similar to LDLR-/- humans, who have substantial atherosclerosis. Horton and colleagues refer to this phenomenon as the effect of cumulative LDL cholesterol in g/dL-years (74)**.**

We showed that in the middle LAD at the adipectomy site, progression of CAD was not significant compared to the significant increases in circumferential plaque in the adjacent, unperturbed proximal and distal segments. Thus, in the middle LAD segment, the increase in mean plaque length was 1.4-fold compared to 1.9- and 2.9-fold in the proximal and distal LAD, respectively. There were higher mean values and greater variability in baseline plaque length in the middle compared to the proximal and distal segments at the time of adipectomy,

suggesting that the attenuated progression of atheroma could have been the consequence of higher initial plaque thickness at the inception of the protocol. However, a two-tailed, paired t-test did not indicate that this baseline difference was statistically significant ($p=0.26$). The reason for the variability in the middle LAD plaque dimensions is not clear, since prior studies have indicated that mean plaque burden is greatest proximally and decreases distally in the LAD (42). One possibility is that adipectomy could have perturbed underlying plaque structure or vasomotor responses and interfered with IVUS measurements performed under heparin immediately after adipectomy. However, we have recently shown that cEAT has uniformly adverse effects on coronary artery function (75;75), in contrast to protective effect of PVAT in the aorta and other arteries. This explains why we observed no adverse mechanical changes after adipectomy.

We resected fat from one coronary artery for several reasons. Resection of as much fat as possible off the entire myocardium was not technically possible in vivo. cEAT on the LAD was the most accessible site within the operative field of exposure compared to either the circumflex or right coronary arteries, which would lessen both intraoperative trauma, morbidity and mortality, and the risk of post-operative complications. This strategy targeting one rather than two vessels was subsequently vindicated by the low intraoperative mortality (1 of 9 pigs) and no noticed post-operative complications. Finally, the longitudinal time course of the experiment enabled the pigs to act as their own controls.

Immunoreactivity for T-cadherin was predominantly localized to the endothelium as previously established (76), but also to the neo-intima. It is

considered to be a marker of active atherosclerosis (76) and a major receptor for adiponectin in the vasculature (77). T-cadherin and SRA, the scavenger receptor for LDL-cholesterol on plasma membranes of plaque macrophages and foam cells (78;79), were reduced in the middle LAD intima-media implying less atherogenesis. Paradoxically, anti-inflammatory immunoreactive adiponectin in the same LAD segment was reduced significantly by 68%, despite a ~7-fold upregulation of adiponectin mRNA expression in overlying cEAT; thus, one might surmise that adiponectin released by epicardial adipocytes might not have been able to penetrate the coronary wall if such a mechanism exists. While a majority of the literature describes a decrease in adiponectin expression in CAD patients, we speculate that the 6.7-fold increase in obese pig cEAT mRNA was a compensatory response and that there must be some block in mRNA translation. We have previously reported that serum adiponectin is decreased in obese versus lean Ossabaw swine (41). On the other hand, there were no changes in vessel wall CD3 (a T lymphocyte cell marker), tryptase (a basophil marker), TNFα, MCP-1, and resistin.

The mechanisms whereby selective adipectomy might have attenuated the progression of CAD remain to be established, but hypothetically include (i) the removal of factors generated by cEAT that could contribute to atherogenesis by direct diffusion through the porous adventitia into the coronary intima-media (73), such as reactive oxygen species (ROS) and pro-inflammatory cytokines and/or (ii) the disruption of vasa vasorum in the adventitia and in the closely adjacent cEAT (80), which might interfere with vasocrine signaling of atherogenic

adipokines (73) and restrict mononuclear cell access into the intima-media. The evidence for these suppositions includes the fact that relative to control cEAT, there was significant up-regulation in atherosclerotic cEAT of pro-inflammatory 11βHSD-1, CCL19, CCL21 and PGD2S; gp91phox [NADPH oxidase],a major source of vascular ROS; VEGF and VEGFGR1, which partake in vasa vasorum neogenesis and angiotensinogen, which promotes endothelial dysfunction and vasoconstriction. Similar to our current findings in pigs, we reported 3-fold up-regulation of 11βHSD-1 gene expression in human EAT adjacent to severe CAD over controls without CAD (20). Pharmacological inhibition of 11βHSD-1 prevented aortic plaque progression in a murine model of atherosclerosis, suggesting that 11βHSD-1 may play a role in atherogenesis (81). Lymphoid chemokines CCL19 and CCL21 are crucial for the recruitment of circulating naive T cells into lymph nodes. Increased levels of CCL19 and CCL21 have been reported within the atherosclerotic lesions of ApoE-/- mice, in human atherosclerotic carotid plaques, and in plasma of CAD patients (81). In mice, PGD2S deficiency induces obesity and facilitates aortic atherosclerosis (82), suggesting it is normally protective and anti-atherogenic in this species. The role of PGD2S in porcine atherosclerosis has not been reported, but -regulation of PGD2S in EAT in our study was associated with amelioration of atherosclerosis, suggesting the possibility that this pro-inflammatory prostanoid might otherwise be harmful either alone or in conjunction with other adipokines. No changes were observed in cEAT in the expression of TLR4 and acute phase cytokines TNFα, IL-1β, IL-6, IL-8 as well as the anti-oxidant genes eNOS and SOD. Finally, the

enhanced expression of a selected array of pro-atherosclerotic genes in cEAT over paracardial fat attests to the relative specificity of the genomic response of cEAT associated with CAD that has been similarly documented in humans with CAD (20).

Epicardial fat volume determined by sequential CT scans significantly increased over 3 months of hypercaloric feeding under the same conditions previously shown to result in major expansion of visceral retroperitoneal and intraperitoneal as well as subcutaneous abdominal fat depots in the same animal model (39). Although our experimental design using pigs as their own controls in a longitudinal study has its strengths, there are also limitations in the lack of sham-adipectomies in age- and gender-matched pigs fed hypercaloric atherogenic diet. Future studies should employ sham-operated animals; randomization of experimental and control pigs; blinding of both the ultrasonographer and two independent IVUS data analysts to the pig group designation; reversing heparin anti-coagulation during IVUS with protamine sulphate so that IVUS can be done before surgery; CT scanning using radio-contrast dye to delineate the coronaries and to quantitate cEAT area around coronary plaques per se rather than EAT covering the entire myocardium; and immunohistochemical and mRNA analysis of cEAT and the coronary wall for expression of genes and proteins known to be important mediators of or participants in atherogenesis. To make these studies more translatable to clinical treatment, more clinical outcomes studies in the swine model would be helpful,

for example, monitoring hard clinical endpoints such as MI, fatal events, etc. over a longer duration.

Our translational research project was done using experimental conditions prohibited in man by obvious ethical constraints and, with the provisos noted above, supports the human epidemiological evidence for a direct relationship between EAT and CAD. At this juncture and until more rigorous evidence is available one way or the other, it is premature to advocate an adipectomy as surgical treatment to attenuate the progression of CAD. Rather, it would be more appropriate from a clinical point of view if non-invasive methods were devised to shrink epicardial fat volume to serve the same beneficial purpose. In this regard, weight loss by caloric restriction and/or exercise in obese human subjects is associated with shrinkage of EAT volume by 9-32% of baseline in different reports (68;83), but it is not known whether this is accompanied by decreases in chronic inflammation in EAT or reduction in CAD burden (42).

Conclusions

The results of our pilot study are consistent with the hypothesis that selective coronary artery adipectomy attenuates the progression of early atherosclerosis, setting the stage for performing definitive future studies using sham operation controls. These studies will determine whether coronary adipectomy attenuates stable atherosclerotic plaques typically found in clinically advanced disease.

Acknowledgements

The authors would like to acknowledge Doug Bowles, PhD (University of Missouri) for his consultation on histology and review of the manuscript.

Funding Sources

NIH HL062552 (MS, MLM, KAS, JPB, MA), P01 HL052490 (MHL), Cardiometabolic Disease Research Foundation, Los Angeles, CA (HS, MS), and NIH/NCATS CTSI TL1 TR000162 (MLM).

Disclosures

None. The authors declare that they have no competing interests.

Figures & Tables

Figure 2.1. Removal of coronary epicardial adipose tissue from the left anterior descending artery. A. Ossabaw heart (left anterior view) ex vivo. **a**. epicardial adipose tissue; **b**. left anterior descending artery; **c**. circumflex artery; **d**. left ventricle; **e**. pulmonary artery; **f**. aorta. **B**. Adipectomy procedure with Octopus stabilizing the myocardium and left anterior descending (LAD) segment. **C.** Surgical landmarks for excision of epicardial adipose tissue; RC, right coronary artery; LAD, left anterior descending artery; CFX; circumflex artery.

Figure 2.2. Epicardial fat computed tomography imaging. Transverse slices were taken at the level of the carina, approximately midway between the base and apex of the heart. **A**. Landmark CT: **a**. subcutaneous adipose tissue; **b**. sternum; **c.** heart; **d**. lungs; **e**. bronchi. **B**. Representative ROIs: **a**. subcutaneous reference ROI; **b**. ROI drawn to encapsulate pericardium (fat inside ROI considered epicardial fat); **C**. CT image after fat analysis (maroon=fat); **a**. ROI arrows drawn to show epicardial fat locations; **b**. paracardial fat. CT = computed tomography, ROI = region of interest.

Figure 2.3. Intravascular ultrasound images and analysis. A-C: IVUS images, distance between white dots =1.0 mm. **A**. Normal vessel with no intimal thickening; **a**. guidewire artifact **b**. IVUS catheter **c**. clear lumen **d**. lumen of parallel vessel. **B**. Analysis example; **a**. atheroma covering 3 segments of a 16

segment designation ~ 19%. **C**. **a**. Concentric neointimal ring of atheroma. **D**. Circumferential plaque length in each 15 mm of proximal, middle and distal left anterior descending coronary artery (LAD) at the time of adipectomy (survival, lower line) and at sacrifice (3 months later, upper line). Values are mean ± SEM for 7 pigs. Asterisk indicates $p<0.05$ between upper and lower proximal and distal LAD portions.

Figure 2.4. Left anterior descending artery immunostaining for inflammatory markers. A: Representative photomicrographs of brown immunostaining for T-Cadherin [**A**, upper panels], SRA [**B**, middle panels] and Adiponectin [**C**, lower panels] in the designated LAD segments. Arrows point to brown positive stains in the endothelial and sub-endothelial neo-intima for each marker. Scale bar=500 microns. **B:** Percent immunohistochemical staining of the proximal, middle and distal 15 mm segments of left anterior descending coronary wall intima-media for **a**; T-Cadherin, **b**; SRA and **c**; adiponectin. The same letters (a-a, b-b) indicate that the mean ± sem in the segments are significantly different (n = 8 separate samples from each segment, $p<0.05$).

Figure 2.5. Epicardial adipose tissue volumes of swine on high-fat diet before adipectomy and 3 months after the procedure. Letter a indicates significant difference, $p<0.05$.

Figure 2.1

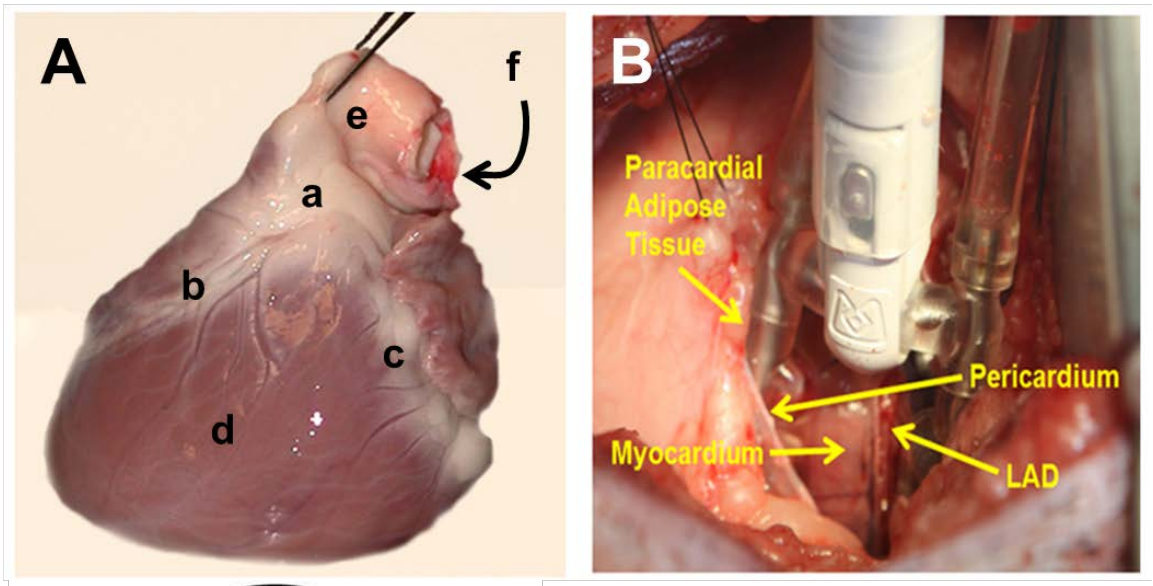
A
f
e
a
b
c
d
B
Paracardial
Adipose
Tissue
Pericardium
Myocardium
LAD

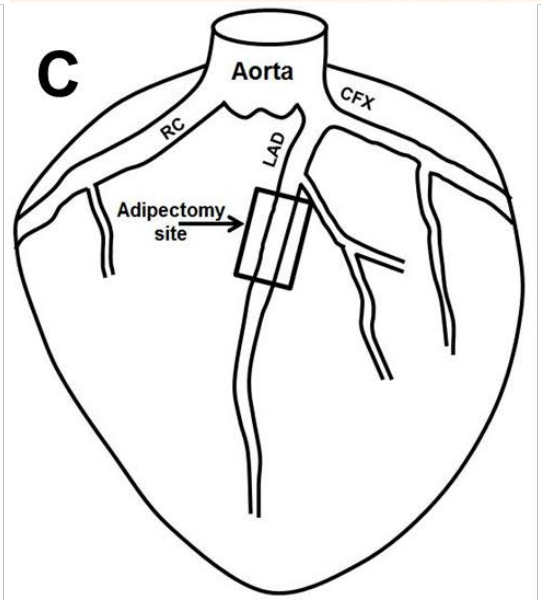
C
Aorta
CFX
RC
LAD
Adipectomy
site

Figure 2.2

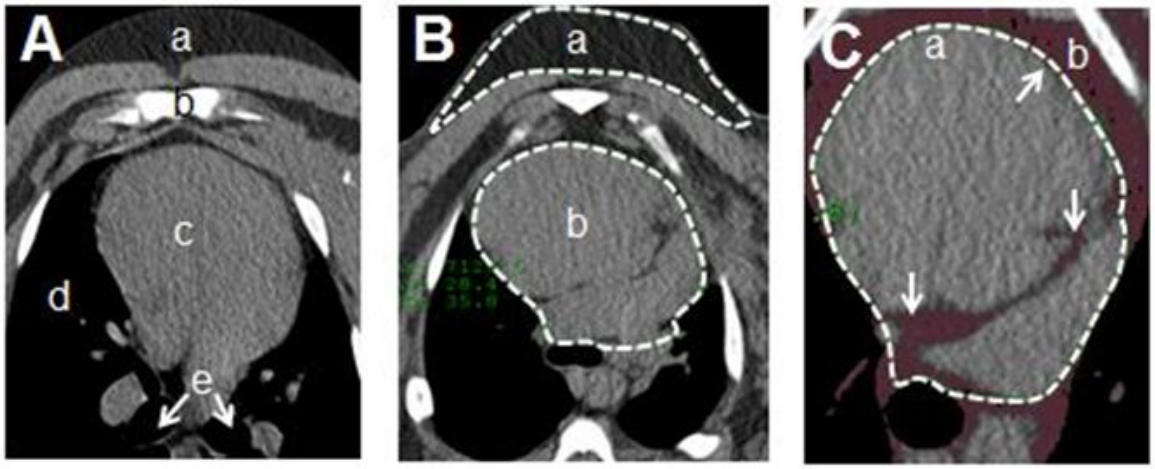

Figure 2.3

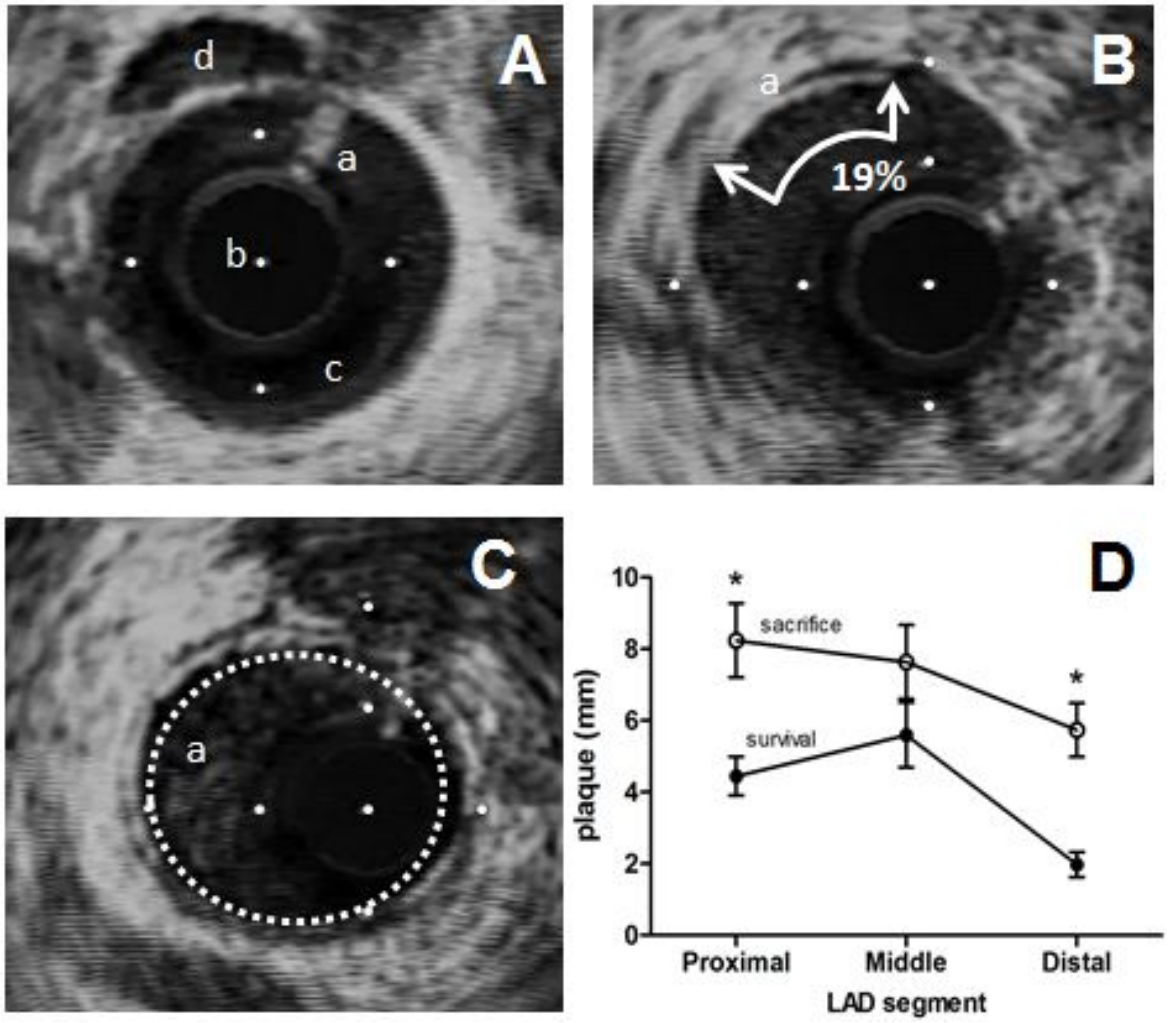
A
d
a
b
c
B
a
19%
C
a
D
plaque (mm)
10
8
6
4
2
0
sacrifice
survival
*
*
Proximal
Middle
Distal
LAD segment

Figure 2.4

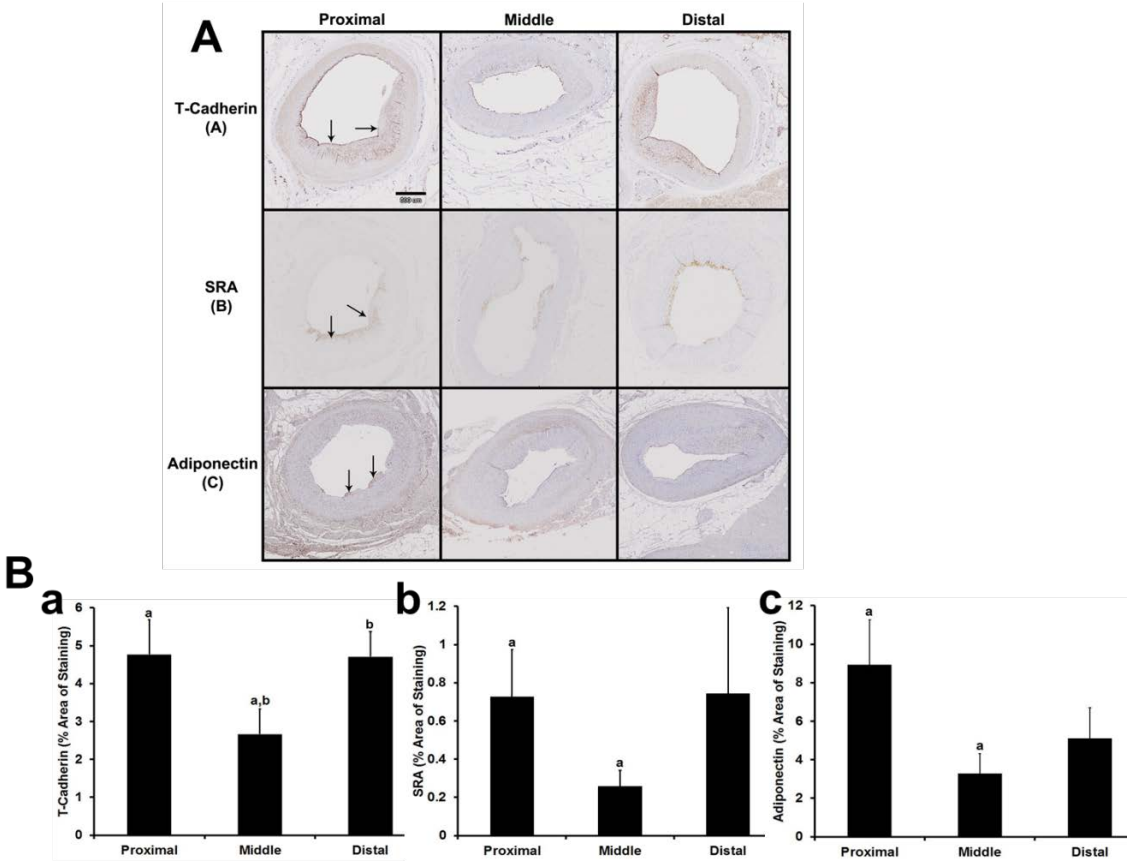
A
Proximal
Middle
Distal
T-Cadherin (A)
SRA (B)
Adiponectin (C)
B
a
T-Cadherin (% Area of Staining)
a
a,b
b
Proximal
Middle
Distal
b
SRA (% Area of Staining)
a
a
Proximal
Middle
Distal
c
Adiponectin (% Area of Staining)
a
a
Proximal
Middle
Distal

Figure 2.5

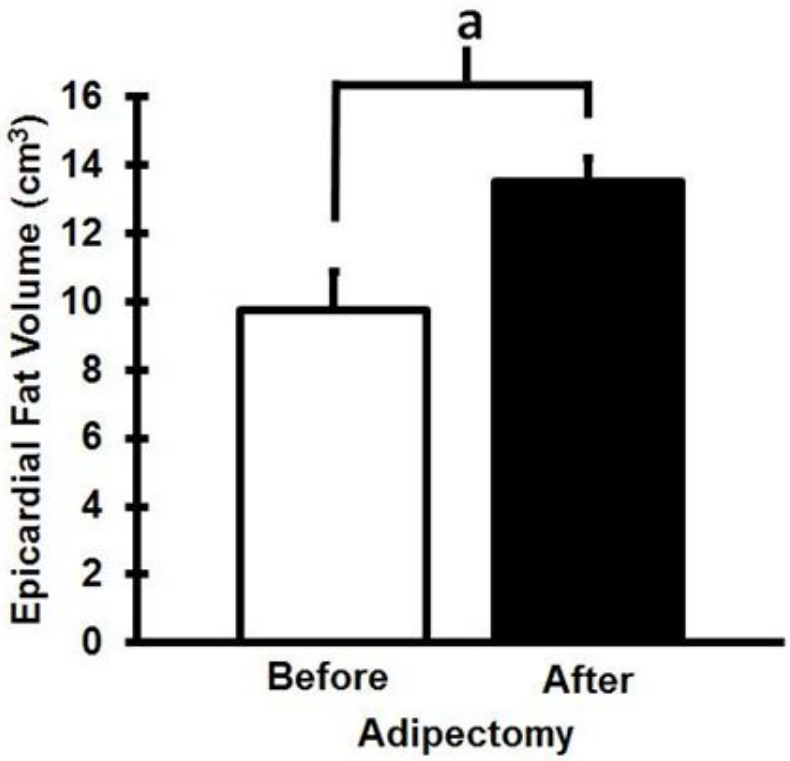
a
16
14
12
10
8
6
4
2
0
Epicardial Fat Volume (cm3)
Before
After
Adipectomy

Table 2.1. Metabolic characteristics of Ossabaw swine.

Parameter	Obese (n=9)	Lean (n=9)	P value
Weight at Adipectomy (kg)	77 ± 3	N/A	N/A
Weight at Sacrifice (kg)	91 ± 1	54 ± 2	< 0.001
Total Cholesterol (mg/dL)	576 ± 40	57 ± 6	< 0.001
Fasting Triglycerides (mg/dL)	108 ± 21	32 ± 3	< 0.001
LDL (mg/dL)	502 ± 36	33 ± 1	< 0.001
HDL (mg/dL)	53 ± 7	24 ± 2	< 0.005
LDL/HDL Ratio	11 ± 2	1 ± 0.1	< 0.001
Fasting Glucose (mg/dL)	80 ± 5	73 ± 6	0.334
Plasma Glucose Peak (mg/dL)	820 ± 35	527± 24	< 0.001
Plasma Glucose AUC	17138 ± 1004	9274 ± 377	< 0.001
Fasting Insulin (µU/ml)	21 ± 6	5 ± 1	0.020
Plasma Insulin Peak (µU/ml)	172 ± 19	33 ± 4	< 0.001
Plasma Insulin AUC	4413 ± 432	667 ± 121	< 0.001
Systolic Blood Pressure (mmHg)	138 ± 2	110 ± 3	<0.001
Diastolic Blood Pressure (mmHg)	79 ± 2	67 ± 2	<0.030

Adipectomized obese swine were age matched to lean swine. Values for adipectomized swine were obtained just prior surgery (n=9), except for body weight at sacrifice (n=8). AUC = area under curve, HDL = high density lipoprotein, LDL = low density lipoprotein

Table 2.2. Ratio of gene expression in fat from obese and lean Ossabaw pigs.

	Ratio of obese/lean	
mRNA	Epicardial Fat	Paracardial Fat
Inflammatory adipokines or proteins associated with inflammation		
11β HSD-1	16.0*	1.2
CCL19	14.0*	4.4*
Adiponectin	6.7*	5.0*
Prostaglandin D_2 synthase	5.3*	3.0*
CCL21	3.1*	1.0
TLR4	1.8	2.0*
IL-6	1.7	1.8
NGF	1.6	1.6
IL-8	1.6	1.4
Unc5b	1.4	1.1
Netrin-1	1.3	0.6
CCR7	1.2	0.8
TNF	1.1	1.7
IL-1β	0.8	0.6
Leptin	0.7	1.5
Oxidative stress/reactive oxygen species regulation		
gp91phox [NADPH oxidase]	72.0*	5.4*
SOD	2.0	1.5

cytochrome C oxidase	1.5	1.5
cyclooxygenase 2	2.2	1.1
	Angiogenesis and endothelial cell function	
VEGFa	16.0*	4.3*
Angiotensinogen	5.3*	1.6
VEGFGR1	4.3*	4.3*
Endothelin-1	2.5	1.7
eNOS	1.1	1.4
adenosine receptor 1	0.7	0.9

mRNA ratios of obese (n=8) to lean (n=8) swine.

CHAPTER 3: VALIDATION OF 18F-NAF PET IMAGING AS A DIAGNOSTIC TOOL FOR EARLY CORONARY ARTERY CALCIFICATION

Mikaela L. McKenney, Ph.D.*, Paul R. Territo, Ph.D. †, Ali Salavati, M.D., MPH‡, Sina Houshmand‡, Scott Persohn †, Yun Liang, Ph.D. †, Mouhamad Alloosh, M.D.*, Sharon M. Moe, M.D.§, Connie M. Weaver, Ph.D. ‖, Abass Alavi, M.D., Ph.D. (Hon)‡, Michael Sturek, Ph.D.*

Department of Cellular & Integrative Physiology, Indiana University School of Medicine, Indianapolis, IN*, Department of Radiology & Imaging Sciences, Indiana University School of Medicine, Indianapolis, IN†, Department of Radiology, University of Pennsylvania, Philadelphia, PA‡, Department of Medicine, Indiana University School of Medicine, Indianapolis, IN§, Department of Nutrition Science, Purdue University, West Lafayette, IN‖

Abstract

Objectives: We sought to validate ^{18}F-NaF positron emission tomography (PET) imaging as a diagnostic tool for early coronary microcalcification in a preclinical swine model of metabolic syndrome (MetS) and coronary artery disease (CAD). We compared multiple imaging modalities: PET, computed tomography (CT), IVUS, and histopathology for their sensitivity to measure early coronary artery calcification.

Background: ^{18}F-NaF uptake has been investigated as an *in vivo* biomarker of early vascular calcification and high-risk atherosclerotic plaque in humans. Vascular calcification increases risk of fatal cardiac events in CAD patients, thus making early diagnosis and clinical intervention extremely important. To our knowledge, no studies to date have investigated early calcification before clinically significant CAD.

Methods: MetS Ossabaw swine (n=11) with early-stage CAD underwent ECG-gated ^{18}F-NaF PET/CT scans followed by IVUS and histology. Both global cardiac and coronary tracking techniques were used to measure ^{18}F-NaF uptake. Total calcium deposition was measured in the left ventricle by an HCl extraction assay. Finally, specimens of the proximal right coronary artery were obtained to histologically examine CAC.

Results: MetS swine (n=11) with CAD had almost 2-fold increased ^{18}F-NaF uptake in the conduit coronary arteries ($p<0.05$) compared to lean (n=3), as well as 2.5-fold increased global molecular calcium score ($p<0.05$). IVUS identified a local calcified lesion in 1 MetS pig. All pigs, lean and MetS, had Agatston calcium scores of 0. Histological staining of proximal right coronary specimens revealed microcalcifications present in 45% of MetS pigs.

Conclusions: We have provided evidence that ^{18}F-NaF uptake is a marker of early coronary artery calcification. This uptake occurs at a stage of CAD and microcalcification prior to clinically significant, ossified lesions that can be detected by IVUS and CT imaging.

Background

In the United States, coronary heart disease alone caused 1 in every 6 deaths in 2010, which translates to approximately 380,000 total deaths per year. Annually, an estimated 620,000 Americans suffer a new coronary attack, while 295,000 have recurrent attacks, and an estimated additional 150,000 Americans suffer from silent first myocardial infarctions (4).

It is widely accepted that coronary artery calcification (CAC) contributes to local inflammation and, therefore, coronary artery disease (CAD) progression (84-87). CAD must be recognized as a dynamic, progressive disease involving various stages of plaque severity (43;88) that if left untreated could result in plaque rupture and a potentially fatal cardiac event. The direct cause of plaque rupture is still poorly understood, however, evidence suggests early CAC within the atherosclerotic plaque contributes to this increase in patient cardiovascular risk due to plaque instability (29;89-97).

Currently, the method for the identification of at-risk patients is computed tomography (CT) imaging and Agatston scoring for coronary calcium (31). While its high spatial resolution provides information on plaque morphology and the presence of macrocalcifications, CT lacks the ability to provide metabolic information from activity occurring at the molecular level of microcalcifications, which are known to be a higher risk to the patient. This shortcoming in CT imaging forces clinicians to rely on information from consecutive scans over a period of time to yield CAC progression data (32). By using an imaging modality that provides metabolic activity information in one imaging session such as

positron emission tomography (PET), the number of scans and, therefore, amount of radiation exposure, could be minimized in patients. Also, it is unclear at what threshold microcalcifications exceed the necessary density to become macrocalcifications that can be quantified by CT. If microcalcifications indicate high-risk, vulnerable plaque, we need an alternative method for identifying these patients sooner than currently possible with CT.

Areas of active microcalcification contain hydroxyapatite, a main component of bone (98). This fact allows use of the well-recognized bone tracer, ^{18}F-NaF, as a biomarker of active plaque calcification (33;34). Combining the strengths of both techniques, PET/CT hybrid imaging can be performed to obtain images with both high spatial resolution and high sensitivity for mineral metabolism and microcalcification activity.

^{18}F-NaF has previously been identified as a biomarker of active tissue calcification that can predict atherosclerotic disease progression in various vascular tissues (36;99-103), but recently it has been recognized as the first non-invasive method to identify high-risk patients for coronary plaque rupture (38). Joshi and colleagues (26) correlated patients with myocardial infarction to the highest coronary ^{18}F-NaF uptake in culprit vessels. This striking advancement in the field is consistent with the hypothesis that ^{18}F-NaF is an early marker of CAC and predictor of plaque instability. More definitive validity would have been provided by invasive coronary measures, i.e. histopathology, or demonstration that ^{18}F-NaF uptake occurs before CAC.

We have therefore conducted a study in our preclinical swine model that has coronary atherosclerosis in all stages of development from clinically insignificant fatty streaks through necrotic, flow-limiting lesions with macrocalcification detectable by intravascular ultrasound (IVUS) (42;43). We performed invasive measures of CAC (IVUS, histopathology) to correlate with ^{18}F-NaF uptake in the coronary arteries. We tested the hypothesis that ^{18}F-NaF PET imaging can detect CAC earlier than the current gold standard non-invasive CT scanning and invasive IVUS. We concluded that ^{18}F-NaF uptake into the conduit coronary arteries indicates an early stage of active calcium deposition and metabolism at sites of CAC that are too small to be detected by both CT and IVUS imaging, but correlates with plaque burden.

Methods

Animal Care

This protocol was approved by the Indiana University School of Medicine and the Purdue University Animal Care and Use Committees, and was conducted in accordance with NIH and USDA guidelines on animal care and use. Female Ossabaw miniature swine (n=11) were assigned to an excess-calorie, atherogenic custom diet for 6 months (16.3% kcal from protein, 40.8% kcal from complex carbohydrates, 19% kcal from fructose, and 42.9% kcal from fat). Animals were fed 1,500 grams once daily. The feed was supplemented with cholesterol (2.0%), hydrogenated coconut oil (4.70%), hydrogenated soybean oil (8.40%), cholate (0.70%), and high fructose corn syrup (5.0%) by weight resulting in the induction of metabolic syndrome (MetS) and CAD (40;42-45) (Table 3.1). Age- and gender-matched lean pigs (n=13) were fed 750 grams of a standard chow (5L80, Purina Test Diet, Richmond, IN; 18% kcal from protein, 71% kcal from complex carbohydrates, and 11% kcal from fat). All animals were kept in individual housing with free access to drinking water and a 12 hour light-dark cycle.

^{18}F-NaF PET/CT imaging & analysis

After 6 months on the diets, pigs underwent simultaneous PET/CT scans. The protocol is shown schematically in Figure 3.1. After overnight fast, pigs received 30-35 mCi ^{18}F-NaF injections through a percutaneous catheter in the jugular vein. Following a 90 min uptake period swine received 2.2 mg/kg of

xylazine (Webster Veterinary, Devens, MA) and 4.4-6.6 mg/kg of telazol (Fort Dodge Animal Health, Fort Dodge, IA) via intravenous injection to induce anesthesia. Pigs were intubated and anesthesia was maintained throughout the procedure by 2-4% isoflurane gas in 100% oxygen as the carrier. Heart rate, electrocardiogram (ECG), aortic blood pressure, blood oxygen saturation and respiratory rate were consistently monitored. To control the heart rate, lidocaine was infused (60μg/kg/min) intravenously. Pigs were transferred to a Siemens Biograph64 PET/CT system to begin the dual phase ECG-gated Dynamic Contrast Enhanced (DCE) CT and ECG-gated ^{18}F-NaF PET scanning. A representative time course of the scanning protocol as well as PET, CT, and hybrid images are displayed in Figure 3.1, where the total ^{18}F-NaF uptake time was 120 min.

Coronary tracking (Fig. 3.2) was performed by tracing individual arteries along the vessel mid-line, followed by planar re-curve analysis on DCE CT images (31) and CAC scores were obtained using the Agatston scoring system. DCE CT and PET images were coregistered across gates using Analyze 11.0 (AnalyzeDirect, Inc.), employing normalized entropy methods of Studholme (104), and semi-automated coronary segmentation of the left anterior descending (LAD) artery and right coronary artery (RCA) were performed on end diastolic contrast enhanced CT images and then applied to coregistered PET images for quantification. Due to a significant discrepancy in body weight between the two groups ($p<0.05$, $n=14$), data were expressed as percent injected dose (%ID/g) according to:

$$\%ID/g\ (n,i) = \frac{R(n,i)}{D(n)} * 100$$

Where, R, D, n, and i are the coronary region in Bq/ml, decay corrected injected dose in Bq, subject number, and region index (LAD or RCA) respectively.

Concurrently, ^{18}F-NaF cardiac uptake was measured by a Global Molecular Calcium Score (GMCS) technique as previously described (36). Two experienced readers analyzed PET scans in a blinded manner using advanced PET/CT review software (Extended Brilliance Workstation, Philips Healthcare, Bothell, WA) by manually drawing regions of interest on each PET/CT image around the heart on transverse slices from base to the apex and corresponding average NaF uptake and volume of each slice was calculated and recorded (Fig. 3.4A). Global Molecular Calcification Score (GMCS) was calculated by multiplying each slice volume by the average NaF generated from same ROI and summing the resulting numbers among the entire set of ROI analyzed. After scanning, animals were transported to their individual pens for decay of radioactive material before the next day's interventional cardiology procedure.

Intravascular Ultrasound

Following the same anesthesia methods described above, pigs (n=15) were transported to the cardiac catheterization lab for IVUS imaging of the LAD and RCA. Methods were almost identical to those previously described in detail (21;40;42;44), except that the Volcano CORE instrument and 40 MHz IVUS catheter were used.

IVUS pullback images were obtained offline (Volcano DICOM Viewer v4.98) at 1 mm intervals for the proximal 15 mm of each coronary artery. Using ImageJ software (NIH), percent plaque burden measures were obtained. The initial lumen (IL) was traced around the elastic lamina. The actual lumen (AL) was traced just inside the intimal layer of the vessel wall. Using the equation (IL-AL)/IL x 100, plaque burden were quantified for every 1 mm of the proximal 15 mm in the two coronaries.

Concurrently, a secondary measure of CAD was performed to quantify percent wall coverage over the entire length of the artery as previously published (40;42;44). Our laboratory has used wall coverage analysis to quantify CAD in pigs with early stage atherosclerosis, prior to the stage of clinical significance.

HCl Ca extraction

To address whether or not GMCS quantification of ^{18}F-NaF uptake in the heart was measuring calcium in the ventricles, HCl extraction assays were performed on left ventricular specimens flash-frozen in liquid nitrogen immediately upon excision of the heart. Total calcium was measured from a 1 cm^3 left ventricle specimen from each pig. This biochemical assessment was performed as previously described by Chen et al. (105).

Coronary & myocardial histopathology

RCA samples from the proximal 1.5 cm were fixed in formalin before being embedded in paraffin blocks. 2-3 slices per artery were obtained for staining with hematoxylin and eosin (H&E) and von Kossa (43).

Left ventricular specimens were also fixed and embedded prior to staining. Von Kossa mineral stain and Masson's trichrome collagen stain were used to assess the myocardium and microvasculature.

Statistics

Data are described as mean ± 1 SEM, where $p \leq 0.05$ was considered statistically significant. One-tailed Student's t-test, one-way ANOVA with Student-Newman-Keuls post-hoc test, and Pearson's correlation were used in PRISM software (GraphPad, San Diego, CA).

Results

Metabolic data

Pigs on the atherogenic diet developed MetS, as indicated by the risk factors of increased bodyweight, total cholesterol, triglycerides, and diastolic blood pressure (Table 3.1). Measures were significantly increased compared to age- and gender-matched lean pigs.

^{18}F-NaF PET/CT imaging

All pigs, lean and MetS, revealed no significant evidence of CAC by CT with Agatston calcium scores of 0. Simultaneous PET imaging revealed almost a 2.5-fold increase of ^{18}F-NaF uptake in the hearts of MetS pigs compared to lean (351 ± 17 vs 145 ± 26, $p<0.05$) by the GMCS technique (Fig. 3.3A&B). These data significantly correlated with percent plaque burden in both the LAD ($p<0.05$, $r=0.78$) and RCA ($p<0.05$, $r=0.86$) from all pigs (Fig. 3.3C&D).

DCE CT and coronary tracking allowed for direct measures of ^{18}F-NaF uptake in the LAD and RCA arteries. Using %ID/g as a discrete regional measure of uptake, significantly more ^{18}F-NaF uptake was measured in the proximal region of both LAD and RCA of MetS pigs compared to lean (LAD: 0.95 ± 0.11 %ID/g vs 0.51 ± 0.05 %ID/g, $p<0.05$; RCA: 0.98 ± 0.11 %ID/g vs. 0.54 ± 0.03 %ID/g, $p<0.05$) (Fig. 4A & 4C). In the LAD of lean and MetS pigs, ^{18}F-NaF showed a weak correlation with plaque burden measures in the same region of the artery ($p=0.08$, $r= 0.48$) (Fig. 3.4C). However, in the RCA of all pigs, this correlation between microcalcification measured by ^{18}F-NaF uptake and state of

CAD measured by the IVUS plaque burden measure was strong ($p<0.05$, $r= 0.87$) (Fig. 3.4D).

IVUS plaque burden

In Figure 3.5, images from coronary pullbacks in the proximal 15 mm of the artery show the lack of atherosclerotic plaque burden in lean pigs (Fig. 3.5A, LAD: 1 ± 0%, RCA: 0.2 ± 0%) compared to an early stage of CAD in MetS pigs with plaque burden development (Fig. 3.5B, LAD: 25 ± 1%, $p<0.05$, RCA: 20 ± 0%, $p<0.05$), ~25-fold greater than Lean (Fig. 3.5C). Of the MetS pigs with CAD, only one pig showed evidence of CAC by IVUS (Fig. 3.5D). The ~15% wall coverage by calcification in Figure 3D contrasted with the complete absence of even early stage intimal thickening in the other ~85% of this arterial cross-section shows the heterogeneity of the CAC process.

Left ventricle HCl Ca extraction and histopathology

Biochemical assessment revealed no significant difference in total calcium in the left ventricle from lean (1.11 ± 0.05 μmol/g) and MetS pigs (1.17 ± 0.06 μmol.g) ($p=0.24$) (Fig. 3.6A&B).

Von Kossa mineral staining of LV specimens from lean and MetS pigs revealed no evidence of myocardial or microvascular calcification in either group (Fig. 3.6C). Masson's trichrome stains were used for structural comparison and assessment of myocardial collagen deposition (Fig. 3.6D).

Right coronary artery histopathology

H&E (Fig. 3.7A) and von Kossa (Fig. 3.7B) staining of proximal RCA specimens were positive for 45% of MetS pigs (n=11).

IVUS wall coverage analysis

The percent wall coverage IVUS measure of the entire artery was more variable compared to the percent plaque burden data. As shown in Figure 3.8A, a pig with early CAD, and therefore a low percent plaque burden, has concentric wall coverage and a high probability of heighted cellular activity during that evolving stage of CAD. Wall coverage was measured for every 1 mm of the entire LAD in lean and MetS pigs. As expected, MetS pigs had ~14-fold greater intimal thickening compared to the leans (51 ± 6% vs. 3 ± 1%, $p<0.05$) (Fig. 3.8B). When compared to ^{18}F-NaF %ID/g in the LAD of each pig, the wall coverage data significantly correlated with microcalcification activity measured by PET ($p<0.05$, $r=0.67$)) (Fig. 3.8C).

Discussion

Clinically the use of CT CAC has been standardized and currently serves as the non-invasive gold standard for evaluating plaque burden. Based on the current work and the relevant literature suggesting that microcalcifications are present in early plaques, the question then remains, if these microcalcifications are too small to be measured by CT CAC scoring, why focus on this measure for clinical diagnosis of cardiovascular risk? Detrano et al. found CT CAC scoring is not more effective than risk-factor information and is not an accurate predictor in these asymptomatic patients with early CAD (106). Also, McEvoy et al. make the key point in their state-of-the-art review that CAC progression is an essential clinical measure, rather than a patient's CAC score alone (32). This requires multiple CT scans per patient to observe changes in plaque structure and severity. However, a single PET/CT scan may reveal current molecular activity and mineral metabolism, which is well-established to indicate plaque progression.

CAD is a highly complex disease progressing through stages of inflammation, lipid accumulation, calcium deposition, thrombosis, and finally fibrosis. CAC is classically observed in the vicinity of lipid-rich regions within atherosclerotic plaques in close proximity to inflammatory cells (107). The earliest form of calcium deposits in the coronary vasculature has been observed in type IV lesions from histological studies (26). A type IV lesion characterization involves plaque that is lipid laden, but not yet containing thick layers of fibrous connective tissue and are not yet largely calcified (type V) (43;88). These non-

calcified or micro-calcified lipid-rich plaques are the most vulnerable for plaque rupture (10), however, these type IV lesions can return a CAC score of 0 from CT imaging (32). In the current work, we have extended the concept of CAC by showing in an outstanding preclinical swine model of CAD (40;42-45) that ^{18}F-NaF PET-CT can detect CAC in type I, II, and III lesions.

Cocker et al. (108) corroborate the viewpoint that monitoring CAD time course with multiple imaging modalities (^{18}F-FDG, ^{18}F-NaF, and CT) is important to better understand the progression of CAC. Several groups have identified ^{18}F-FDG as an indicator of CAD progression by inflammation and macrophage activity (109-112). However, recently it has not proven to be reliable for detection of high-risk plaque (38). The major limitation of this tracer is its high uptake in the myocardium due to high metabolic activity, thus leading to a low target to background ratio when measuring in the coronaries. By contrast, ^{18}F-NaF has limited myocardial and blood uptake yielding very high target to background ratios. Therefore, of the available commercial tracers ^{18}F-NaF may provide the best opportunity for detection of early CAD/CAC progression.

In this preclinical PET/CT study, we have demonstrated that increased ^{18}F-NaF uptake in the coronaries can detect early calcium metabolism in pigs with CAD that lack frank evidence of calcification by both IVUS and CT imaging. These findings render the interpretation that ^{18}F-NaF binds to microcalcifications that are on a molecular level which is too small to be detected using standard clinical imaging modalities. Evidence for this conclusion lies within our

histopathology data revealing the presence of microcalcifications within the proximal region of the RCA, which were only detected by ^{18}F-NaF PET imaging.

Because wall coverage is a quantitative analysis of early CAD, i.e. type I, II, and III lesions composed of fatty streaks and intimal thickening, our data correlate superbly with ^{18}F-NaF uptake because it is indicating early, active mineral metabolism. This evidence for early phase CAC in type I, II, and III lesions is unprecedented in human clinical medicine or preclinical animal studies. Nonetheless, the evidence is consistent with substantial data showing dysfunctional intracellular calcium signaling in coronary smooth muscle in diabetic dyslipidemia and metabolic syndrome reviewed recently (46). It is reasonable to propose that dysfunctional smooth muscle calcium signaling leads to extracellular microcalcification that is detected by ^{18}F-NaF uptake into the wall. Mechanistically, the overloaded CSM calcium stores and/or cytosol would enhance matrix vesicles formation providing the target for ^{18}F-NaF, similar to the calcium-dependent mechanism proposed by Kapustin et al. for the role of smooth-derived matrix vesicles in vascular microcalcification when calcium homeostasis is lost (113). This mechanism has been shown to be exacerbated in inflammation by macrophage-derived matrix vesicles (114). Electron micrographs showing numerous vesicles / caveolae at the sarcolemma of coronary smooth muscle are consistent with the notion of matrix vesicle formation (115). These vesicles have been observed in athero-prone areas of the human aorta (116) and in fibrous caps of vulnerable plaque (117).

It is also important to note that our colleagues Wastney et al., have previously used ^{41}Ca kinetic modeling to show increased rate of calcium deposition into the coronary tissue of MetS Ossabaw compared to lean (118). The increase in ^{18}F-NaF uptake in MetS Ossabaw coronaries found in this current study corroborate with their previous findings.

Study limitations

Documentation of progression of CAC from ^{18}F-NaF whole artery uptake and global molecular calcification by longitudinal measures in the same pig as CAD/CAC progressed to IVUS, histopathological, and CT resolvable CAC would have strengthened the study.

Conclusions

We have shown in a preclinical swine model of CAD (40;42-45) that ^{18}F-NaF PET-CT can detect CAC in early atherosclerotic lesions, thereby extending the concept of CAC to significantly earlier in the pathogenesis of CAD. The data also argue for more widespread use of ^{18}F-NaF measures of CAC in humans.

Acknowledgements

The authors would like to acknowledge and thank James P. Byrd, Josh Sturek, Brandy L. Sparks, M.S., Stacey L. Dineen, John Martin, M.S., Jay D. Patel, M.S., Neal X. Chen, Ph.D., Gary Hutchins, Ph.D. (Indiana University School of Medicine), William G. Van Alstine, Ph.D., Berdine Martin, Ph.D. and Alyssa Phillips, M.S. (Purdue University) for their contributions to this work.

Funding Sources

NIH HL062552 (MS, MA, MLM), NIH/NCATS CTSI TL1 TR000162 (MLM), Pharmavite LLC, the Dairy Research Institute, Dairy Australia, Fonterra Co-operative Group Limited, Kraft Foods Inc., Nestle (CMW)

Disclosures

None. (MS, MA, MLM) Pharmavite advisory board (CMW).

Figure & Tables

Figure 3.1. Ossabaw swine underwent simultaneous PET/CT cardiac imaging. A. Timeline for PET/CT protocol. After ^{18}F-NaF injection (blue arrow, -90 min), pigs were transferred to the scan room (red arrows, 0-30 min). PET imaging (red dots, 30-90 min) began 120 mins post tracer injection. Non contrast CT (green arrows, 0-20 min), contrast injection (IsoVue, blue arrow, 25 min), and DCE CT imaging (green dots, 25-60 min) followed. **B.** High spatial resolution in CT image allows for identification of anatomical structures. **C.** PET image reveals high ^{18}F-NaF uptake in the bones of the Ossabaw. **D.** Hybrid image of co-registered PET and CT images after intravenous contrast injection. PET= positron emission tomography; CT= computed tomography; DCE= dynamic contrast enhanced; R= right; A= anterior; L= left; P=posterior; Tr= trachea; PA= pulmonary artery; Ao= aorta; LV= left ventricle.

Figure 3.2. Dynamic contrast enhanced (DCE) Coronary Tracking. A. From DCE CT images, the artery was identified for every transverse slice through the heart. **B.** A 3-D reconstruction of the heart shows the path of the LAD (red line). **C.** Images were reformatted along the linear axis of the artery. PET images were co-registered to these images in order to measure tracer uptake in the coronaries. RV= right ventricle; LV= left ventricle; LAD= left anterior descending; other abbreviations are the same as Figure 3.1.

Figure 3.3. Global Molecular Calcification Score (GMCS). A. A region of interest was drawn around the heart on each transverse CT slice image. Using co-registered PET images, ^{18}F-NaF uptake was quantified and a GMCS was calculated for the entire heart using a previously described method (36). **B.** MetS pigs (n=11) had almost a 2.5-fold higher GMCS compared to lean pigs (n=2) ($p<0.05$). **C.** GMCS significantly correlates with LAD plaque burden (n=13, $p<0.05$). **D.** GMCS significantly correlates with RCA plaque burden (n=9, $p<0.05$). Abbreviations are the same as Figures 3.1-3.

Figure 3.4. Percent injected dose (%ID) per gram body weight (g) in the proximal coronary arteries. A. MetS pigs (n=11) had increased ^{18}F-NaF %ID/g in the LAD compared to lean (n=3) ($p<0.05$). **B.** Pearson's Product correlation revealed a trend towards a positive %ID/g and plaque burden relationship (n=13, $p<0.05$). **C.** MetS pigs had increased ^{18}F-NaF %ID/g in the RCA compared to lean ($p<0.05$). **D.** There was a significant correlation between RCA %ID/g and plaque burden (n=10,$p<0.05$). Abbreviations are the same as Figures 3.2-3.

Figure 3.5. Intravascular ultrasound (IVUS) imaging and quantification of coronary artery disease (CAD). **A.** Cross sectional view of lean Ossabaw coronary with vascular wall traced in red. **B.** MetS pigs with CAD; initial lumen (IL) or elastic lamina is traced in red; actual lumen (AL) traced in yellow; percent plaque burden = (IL-AL)/ILx100. **C.** MetS Ossabaw (n=11) had significantly greater CAD compared to lean (n=4) by plaque burden quantification in the

proximal 15 mm of the LAD ($p<0.05$) and RCA ($p<0.05$). **D.** One pig showed evidence of local, spotty calcification by IVUS (green arrow points to lesion, green dashed line outline acoustic shadowing effect). MetS= metabolic syndrome; CAD= coronary artery disease; RCA= right coronary artery; IVUS= intravascular ultrasound; other abbreviations are the same as Figure 3.2. Distance between dots is 1 mm.

Figure 3.6. Left ventricular total calcium. A. Specimen was collected from LV away from any conduit artery (yellow box). **B.** There was no difference in LV total calcium between lean (n=6) and MetS pigs (n=11). **C.** Histopathology of LV revealed no evidence of myocardial or microvasculature calcification in lean (n=6) and MetS pigs (n=11) with von Kossa mineral staining (mineral= black sediment). **D.** Masson's trichrome staining shows healthy, non-fibrotic myocardium. LV= left ventricle; abbreviations are the same as Figure 3.3.

Figure 3.7. Coronary histopathology revealed microcalcifications. A. A representative image of an H&E-stained proximal RCA wall from a MetS pig revealing evidence for atherosclerotic CAC (black arrows). **B.** A representative image of an von Kossa-stained proximal RCA wall from a MetS pig revealing evidence for atherosclerotic CAC (black arrows). CAC was observed in 45% of MetS pigs.

Figure 3.8. Early stage CAD was quantified as percent wall coverage using IVUS images. A. Example of a MetS pig with 100% wall coverage (concentric fatty streak, intimal thickening) and 25% plaque burden, which is not clinically significant. **B.** MetS pigs (n=10) had ~16-fold greater percent wall coverage compared to lean pigs (n=3) ($p<0.05$). **C.** Wall coverage quantification significantly correlated with %ID/g ($p<0.05$). Abbreviations are the same as Figures 3.3 & 5. Distance between dots is 1 mm.

Figure 3.1.

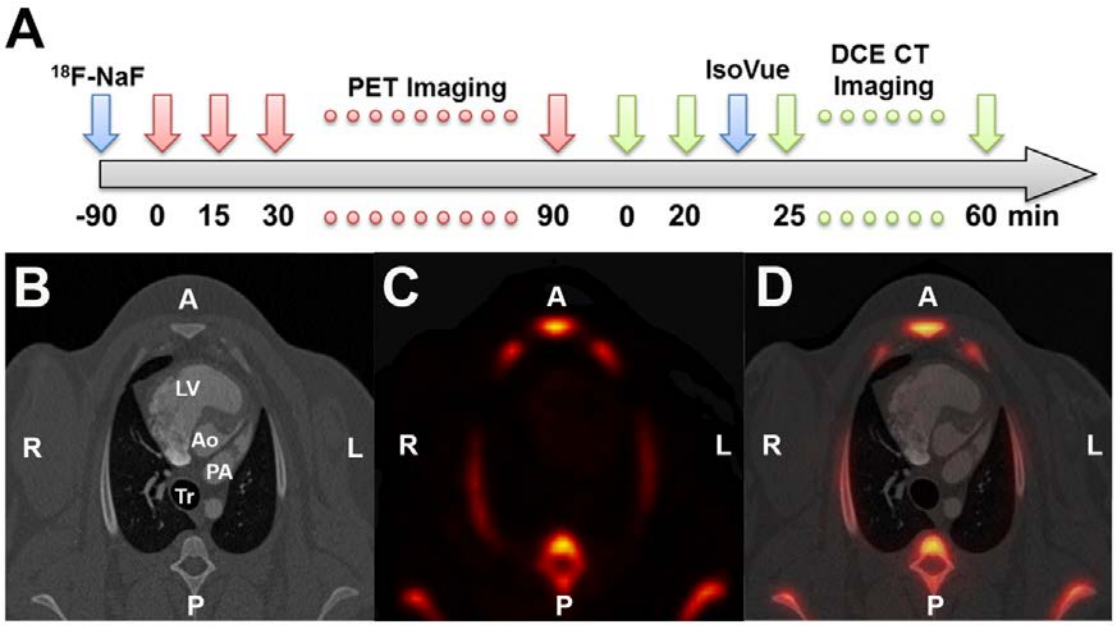
A
^{18}F-NaF
PET Imaging
IsoVue
DCE CT Imaging
-90 0 15 30 90 0 20 25 60 min
B
A
LV
R
L
Ao
PA
Tr
P
C
A
R
L
P
D
A
R
L
P

Figure 3.2.

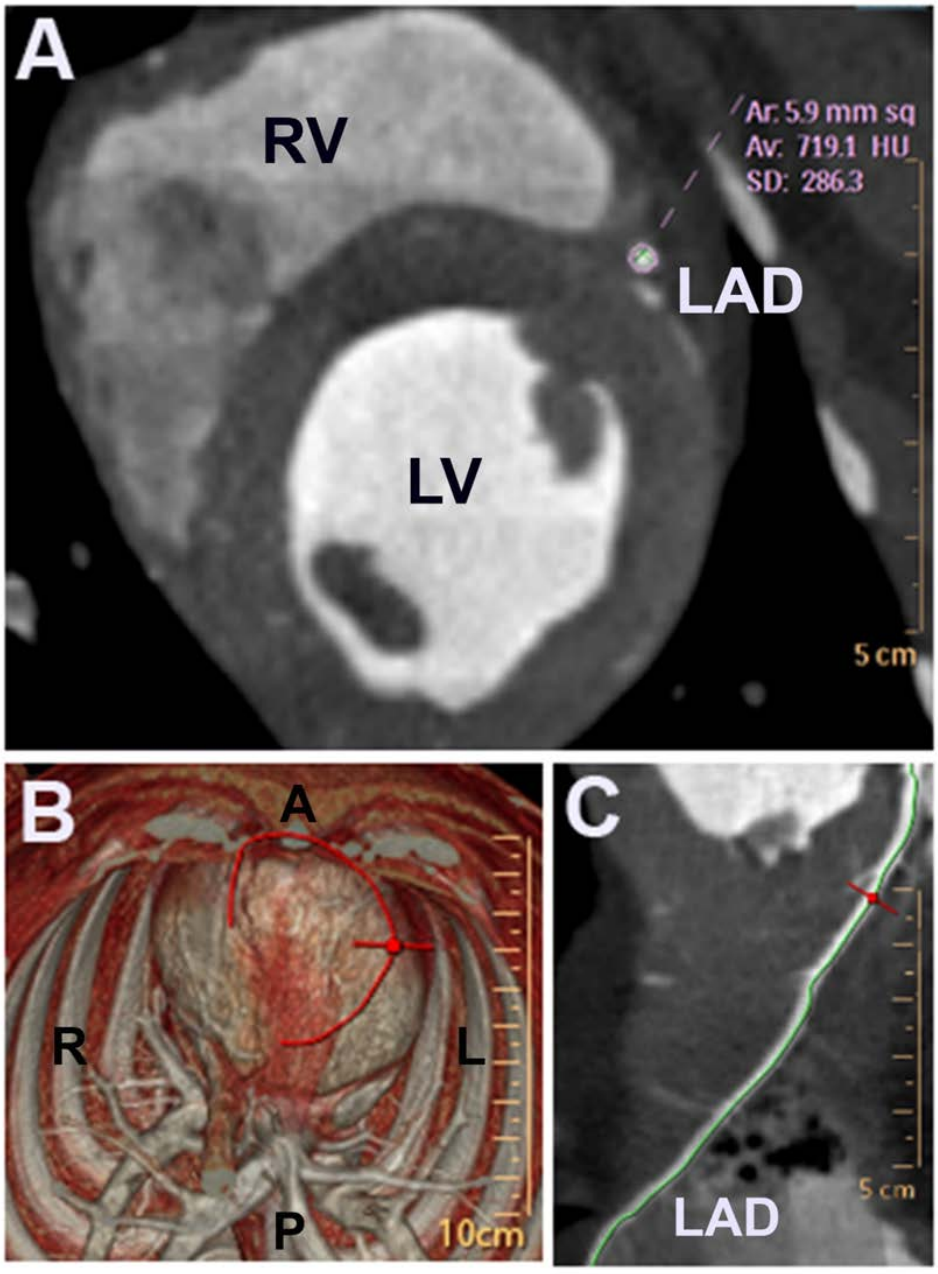

Figure 3.3.

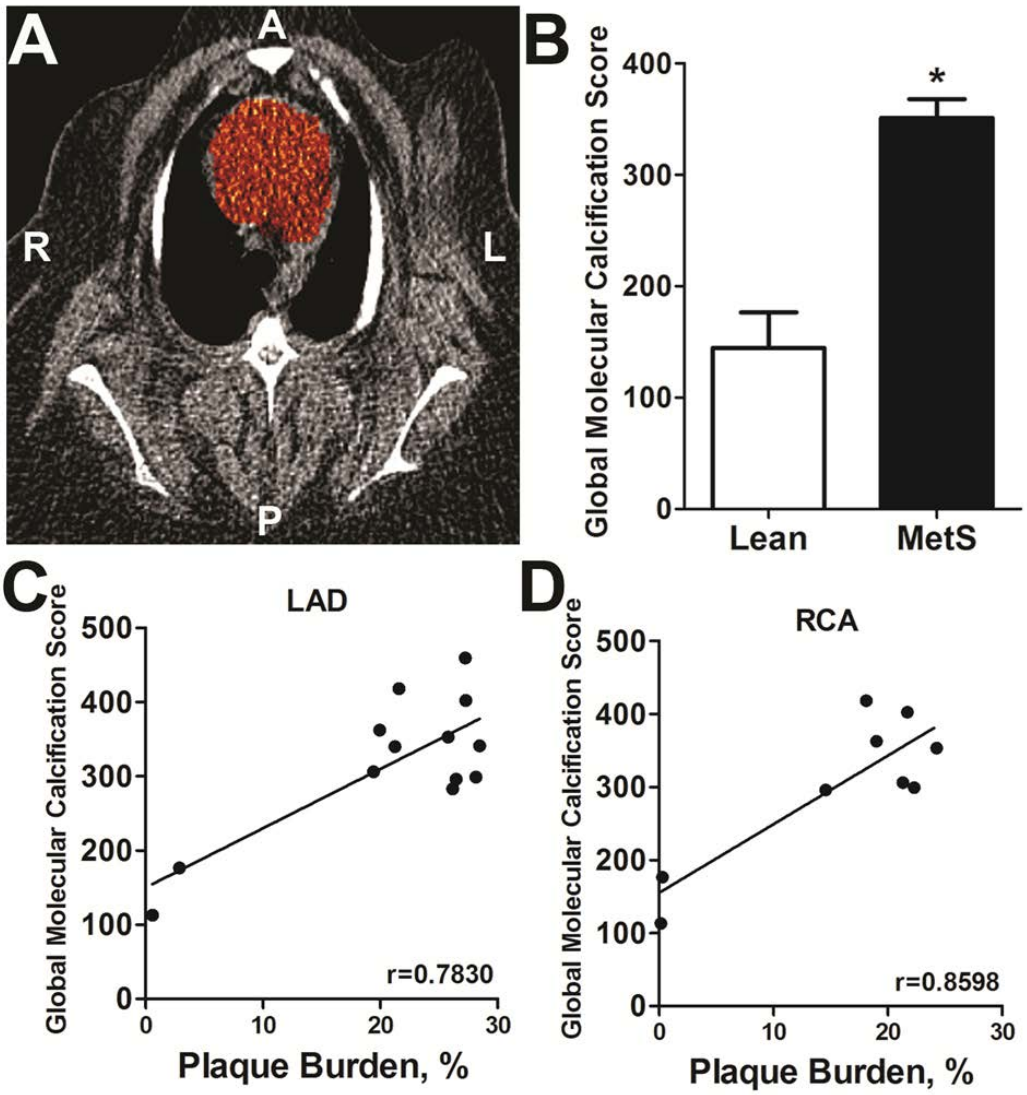
A
A
R
L
P
B
Global Molecular Calcification Score
400
300
200
100
0
*
Lean
MetS
C
LAD
Global Molecular Calcification Score
500
400
300
200
100
0
r=0.7830
0
10
20
30
Plaque Burden, %
D
RCA
Global Molecular Calcification Score
500
400
300
200
100
0
r=0.8598
0
10
20
30
Plaque Burden, %

Figure 3.4.

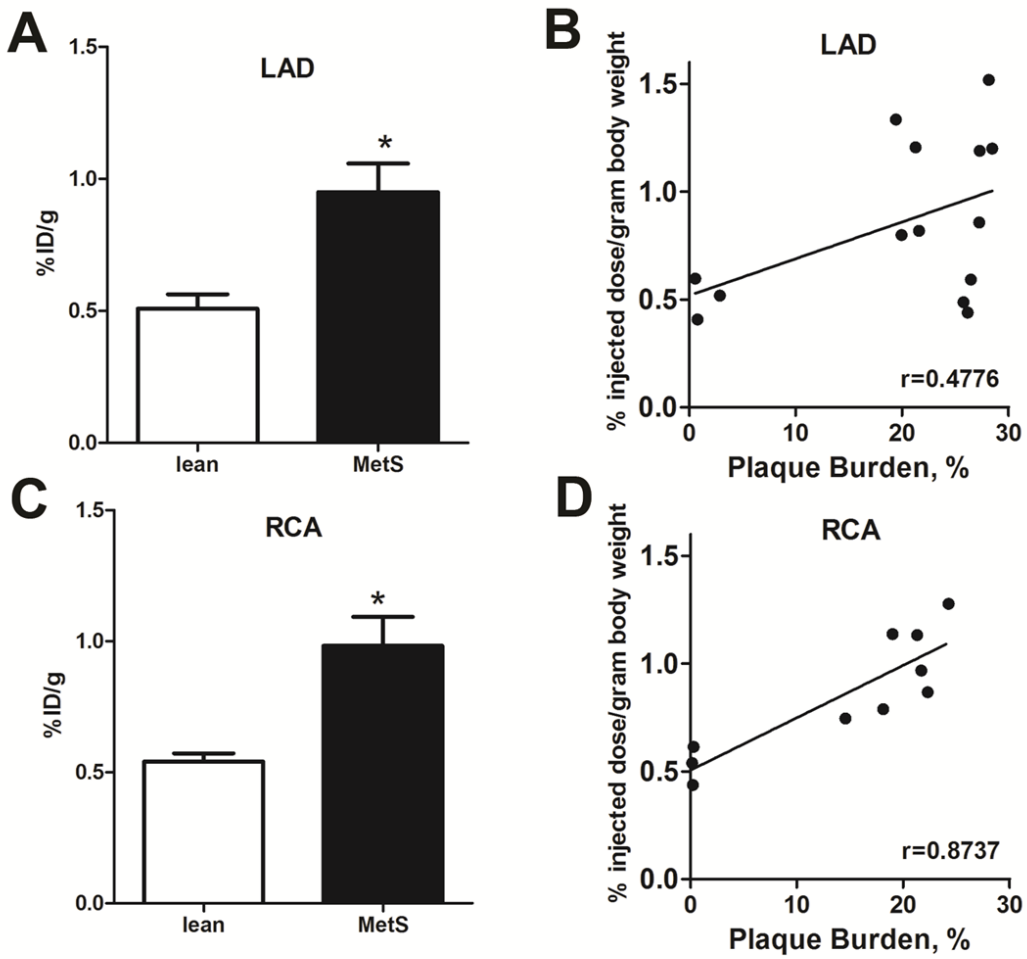
A
LAD
% ID/g
1.5
1.0
0.5
0.0
*
lean
MetS
B
LAD
% injected dose/gram body weight
r=0.4776
Plaque Burden, %
C
RCA
% ID/g
*
lean
MetS
D
RCA
% injected dose/gram body weight
r=0.8737
Plaque Burden, %

Figure 3.5.

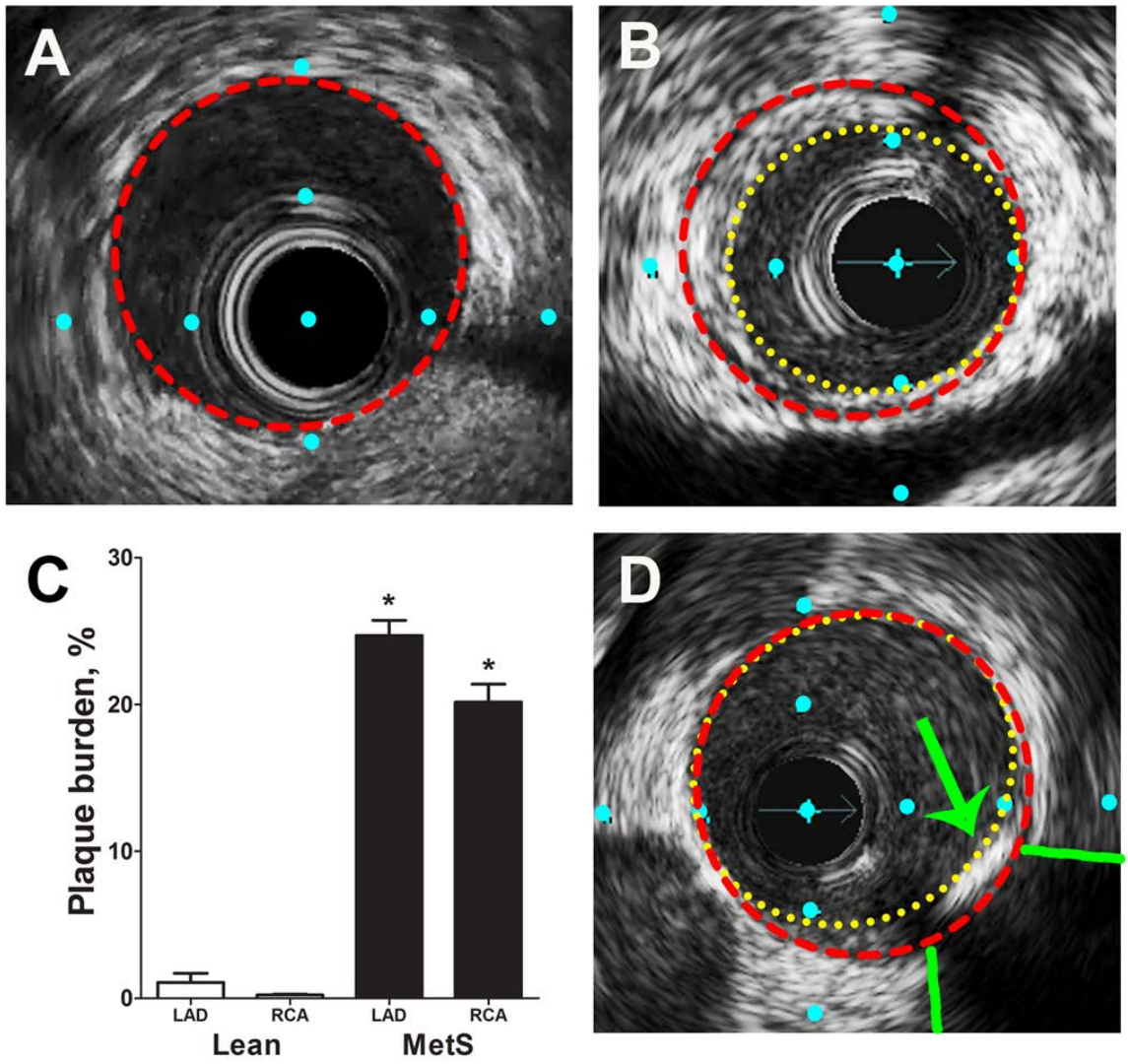

Figure 3.6.

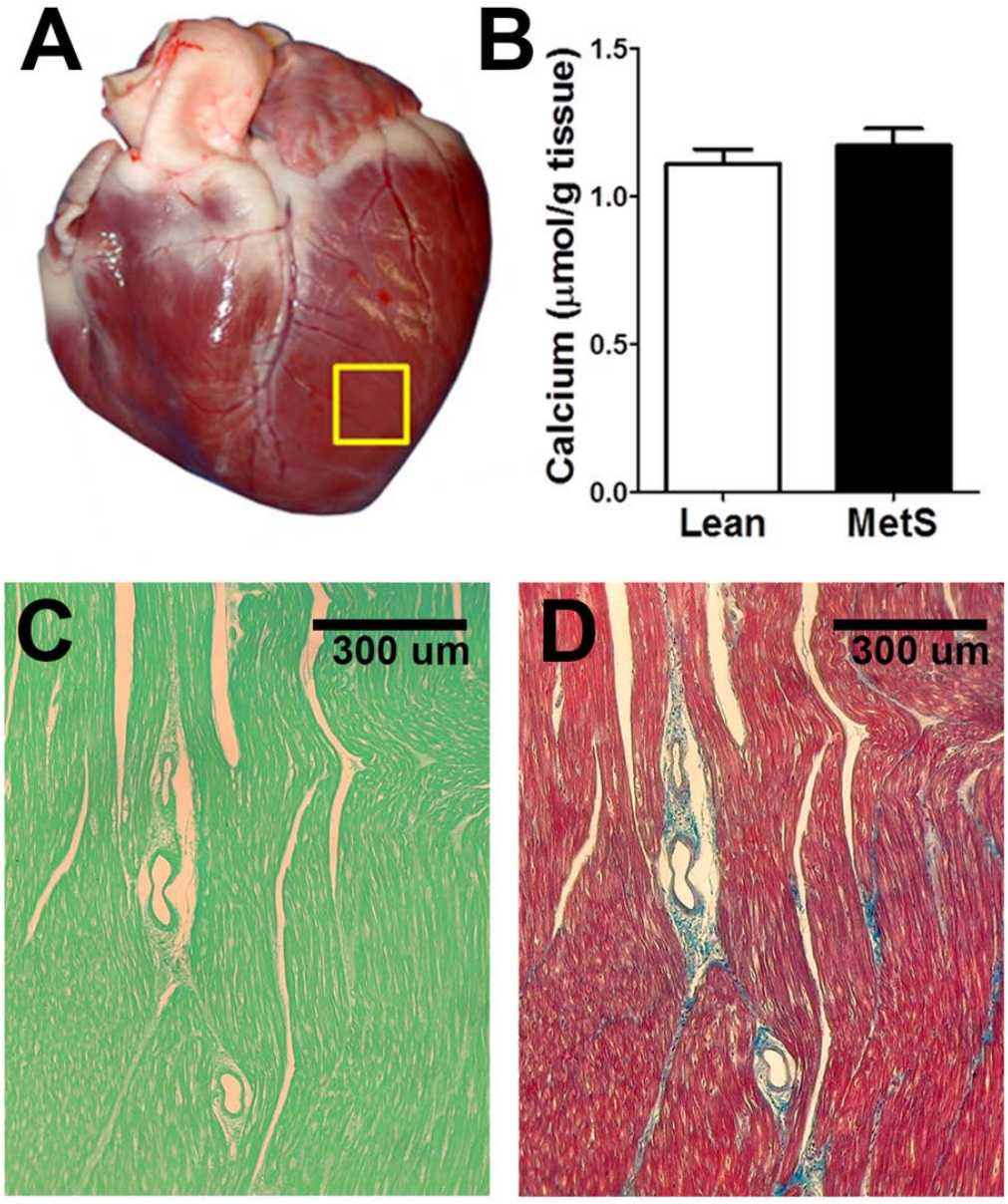

Figure 3.7.

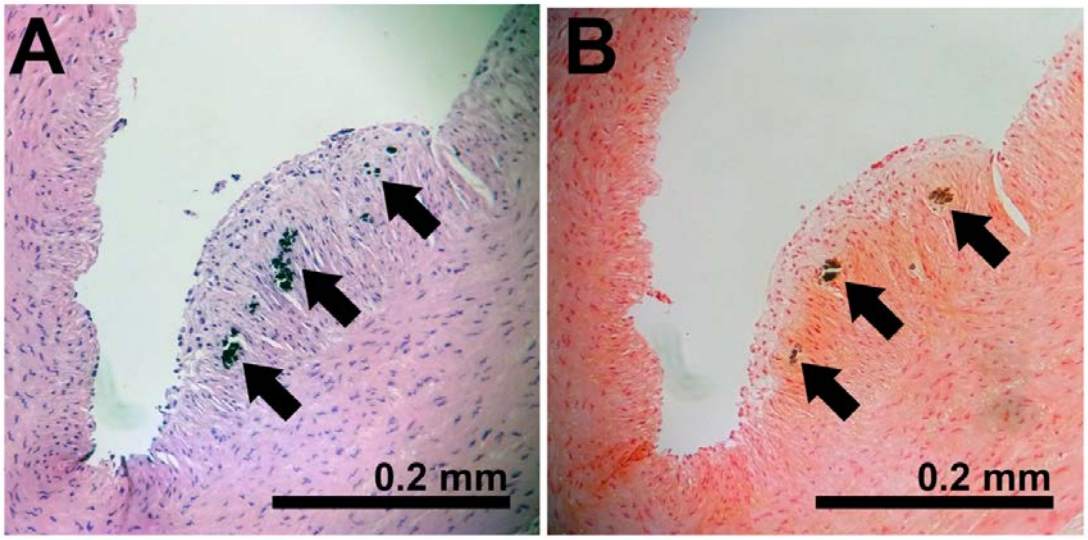

Figure 3.8.

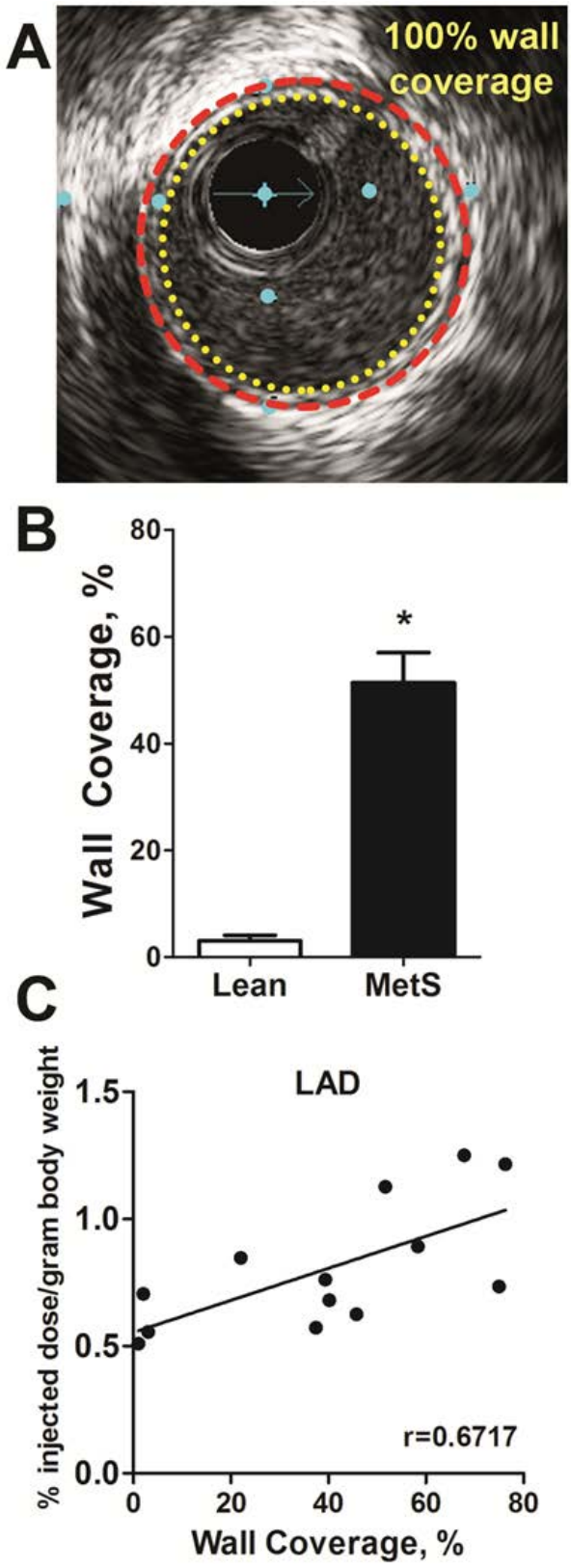
A
100% wall coverage
B
Wall Coverage, %
80
60
40
20
0
*
Lean
MetS
C
LAD
% injected dose/gram body weight
1.5
1.0
0.5
0.0
r=0.6717
0
20
40
60
80
Wall Coverage, %

Table 3.1. Metabolic Characteristics of Ossabaw miniature swine.

	Lean (n=13) Mean ± SEM	**MetS (n=11)** Mean ± SEM
Body Weight (kg)	70.7 ± 1.9	96.8 ± 4.3*
Fasting Blood Glucose (mg/dL)	62.2 ± 2.8	61.5 ± 3.3
Total Cholesterol (mg/dL)	57.6 ± 2.8	590.0 ± 45.5*
Triglycerides (mg/dL)	28.1 ± 4.3	110.4 ± 25.3*
Systolic Blood Pressure (mmHg)	128.3 ± 2.7	138.5 ± 5.6
Diastolic Blood Pressure (mmHg)	74.4 ± 3.9	97.1 ± 7.1*

One-tailed Student's t-test was performed to compare lean and MetS characteristics for each metabolic data set.

CHAPTER 4: RELATIVE CHANGES IN CSMC CA^{2+} REGULATION OVER THE TIMECOURSE OF CAD PROGRESSION IN THE SETTING OF METS

Mikaela L. McKenney, Ph.D., Meredith K. Owen, Ph.D., Kyle A. Schultz, M.S., Jillian N. Noblet, Mouhamad Alloosh, M.D., Johnathan D. Tune, Ph.D., Michael Sturek, Ph.D.

.

Department of Cellular & Integrative Physiology,

Indiana University School of Medicine, Indianapolis, IN 46202

Abstract

Alterations in coronary smooth muscle (CSM) Ca^{2+} regulation were studied in the Ossabaw swine model of metabolic syndrome (MetS) over the time course of coronary artery disease (CAD) progression. MetS was induced by excess calorie atherogenic diet for 6, 9, or 12+ months and compared to lean controls on normal standard diet. Isometric tension studies on isolated coronary arteries revealed that 9 months of MetS increased tension development to K depolarization vs. 6 months and lean controls, whereas at 12 months tension was significantly reduced. MetS increases CAD and CSM Ca^{2+} dysregulation. CSM were isolated enzymatically and imaged with the fluorescent Ca^{2+} indicator fura-2. There was no difference in basal Ca^{2+} levels between all groups. We released sarcoplasmic reticulum (SR) Ca^{2+} stores maximally with caffeine. The peak Ca^{2+} transient, which largely represents the caffeine-sensitive SR Ca^{2+} store capacity, was increased at 9 months and decreased at 12 months MetS vs. lean. There was no difference at 6 months. After the SR store depletion, a sustained Ca^{2+} signal above basal levels remained in the 9 month MetS group, reflecting store-operated Ca^{2+} entry as well as decreased Ca^{2+} extrusion ability. Intravascular ultrasound (IVUS) showed greater atherosclerosis correlates with length of atherogenic diet. Coronary artery calcification (CAC) was observed on IVUS in pigs fed for 12+ months with “late stage” CAD. In an organ culture model of CAC, nifedipine failed to inhibit induction of CAC, suggesting voltage-gated Ca^{2+} channels are not involved in CSM Ca^{2+} overload. Collectively, these data suggest that CSM undergo dedifferentiation from a contractile to a synthetic phenotype

defined by CSM proliferation and migration and increased intracellular Ca^{2+} signaling in “early stage” CAD. As CAD further progresses to “late stage”, CSM dedifferentiate to an osteogenic phenotype with decreased intracellular Ca^{2+} signaling and increased extracellular calcification.

Background

The latest report from the Centers for Disease Control and Prevention revealed that more than one-third of American adults are obese (1). While the American sedentary lifestyle undoubtedly plays a role in this epidemic, the *homo sapiens'* "thrifty genotype" is also contributing to the cause. This "thrifty genotype", first described in a classical report by Neel (2), is synonymous to a propensity to obesity. In his recent review, O'Rourke labeled modern day's overabundance of food and a lack of energy-intensive labor, both of which are fueling this American obesity epidemic, as an "obesogenic" environment (3).

This "obesogenic" environment has fueled a parallel catastrophic diagnosis for Americans – the metabolic syndrome (MetS), which is a combination of 3 or more of the following risk factors associated with metabolic abnormalities: central obesity, dyslipidemia, hypertension, impaired glucose tolerance, and insulin resistance (119). When an individual presents with multiple MetS risk factors, their chances for adverse or even fatal cardiovascular problems are far greater than if presenting one risk factor alone (6).

Together, obesity and MetS are fueling the number 1 killer of Americans, coronary artery disease (CAD). CAD progresses through a spectrum of stages (26;43) beginning with early clinically insignificant neointimal thickening due to lipid deposition in the arterial wall. Progression continues with further neointimal thickening due to further lipid deposition and inflammatory factors infiltrating the area (48;49). The coronary smooth muscle (CSM)-rich medial layer of the wall will also begin to thicken due to a shift in CSM phenotype from the differentiated,

contractile state (cCSM) found in healthy arterial walls to a dedifferentiated, synthetic phenotype (sCSM) known to proliferate and migrate in towards the coronary lumen. sCSM, most specifically recognized by the loss of smooth muscle myosin heavy chain (SM-MHC) (120), are also secretory cells that after further proliferation and migration into the neointimal lesion will enhance fibrosis and plaque complexity. A third more recently recognized phenotype of CSM is a dedifferentiated osteogenic cell (oCSM), which expresses bone-like genes (i.e., RUNX2) (30;51) and releases matrix vesicles (30;121) into the extracellular matrix leading to calcification within advanced CAD lesions.

Being a ubiquitous intracellular messenger, Ca^{2+} can signal CSM contraction, proliferation, migration, and gene transcription. It is imperative that CSM tightly regulate Ca^{2+} using various Ca^{2+} transporters (Fig. 4.1A). to compensate for changes in the local environment, specifically in a MetS milieu. Several reports have described changes in intracellular CSM Ca^{2+} signaling in health vs. disease and these characteristics of Ca^{2+} handling strongly influence the phenotypic state of the cell (50).

We cannot define just two divisions of CSM Ca^{2+} "health": before CAD onset vs. after CAD onset. The plasticity of CSM is much more complex than this, and more studies should observe the time course of intracellular CSM changes in correlation with the severity of CAD when interpreting the data. Here we utilize the Ossabaw miniature swine model of MetS and CAD (39-44) to study the changes in CSM Ca^{2+} signaling over a time course of CAD progression from healthy, lean pigs to obese, MetS pigs with advanced calcified CAD lesions.

Methods

Animal Care

Six month old Ossabaw miniature swine were fed 1 kg of an excess-calorie atherogenic diet (KT-324, Purina Test Diet, Richmond, IN; 16% kcal from protein, 41% kcal from complex carbohydrates, 19% kcal from fructose, and 43% kcal from fat) daily for 6 (n=6), 9 (n=7), or 12+(n=9) months. The feed was supplemented with cholesterol (2.0%), hydrogenated coconut oil (4.70%), hydrogenated soybean oil (8.40%), cholate (0.70%), and high fructose corn syrup (5.0%) by weight resulting in the induction of metabolic syndrome (MetS) and CAD (40;42-45). Lean control pigs (n=9) were fed 725 g of a standard diet (5L80, Purina Test Diet, Richmond, IN; 18% kcal from protein, 71% kcal from complex carbohydrates, and 11% kcal from fat). Animals were kept in individual housing with free access to drinking water and on a 12-hour light/dark cycle. This protocol was approved by the Indiana University School of Medicine Animal Care and Use Committee.

Intravascular Ultrasound (IVUS) for quantification of coronary artery disease

After an overnight fast, pigs received 2.2 mg/kg of xylazine (Webster Veterinary, Devens, MA) and 5.5 mg/kg of telazol (Fort Dodge Animal Health, Fort Dodge, IA) via intramuscular injection to induce anesthesia. Anesthesia was maintained throughout the procedure by 2-4% isoflurane gas in 100% oxygen as the carrier. Heart rate, the electrocardiogram (ECG), aortic blood pressure, blood

oxygen saturation, and respiratory rate were consistently monitored. Intravascular ultrasound (IVUS) imaging was performed on the left anterior descending (LAD) artery. Methods were similar to those previously described in detail (21;40;42;44).

Still frame IVUS pullback images were obtained offline at 1 mm intervals (Fig. 4.2A-C). Percent plaque burden measures were obtained using Image J software (NIH). The initial lumen (IL) was traced around the elastic lamina. The actual lumen (AL) was traced just inside the intimal layer of the vessel wall. Using the equation (IL-AL)/IL x 100, plaque burden was quantified for every 1 mm of the LAD. Quantification of % wall coverage over the entire length of the artery was performed as previously published (40;42;44). Our laboratory has used wall coverage analysis to quantify CAD in pigs with early stage atherosclerosis characterized by fatty streaks, and intermediate lesions (Type II, III) prior to later stages with more fibrous and complex lesions (Type IV-VI) (43;122).

Isometric tension studies for functional assessment of fresh and cultured coronary rings

Coronary rings (2-4 mm) were hung on pressure transducers in 37°C water-jacketed organ baths with a Ca^{2+}-containing Krebs solution (in mM: 131.5 NaCl, 5 KCl, 1.2 NaH_2PO_4, 1.2 $MgCl_2$, 25 $NaHCO_3$, 10 glucose, 4 $CaCl_2$). Optimal length was measured by contractions of isolated arteries to 60 mM KCl and passive tension was increased in gram increments until there was <10% change in active tension development to 60 mM KCl (typically equaled ~4 g) as

previously described (59;75;123). Once the arteries stabilized they were contracted with 10, 20, and 80 mM KCl and tension development was measured.

Fluorescent imaging for assessment of CSM intracellular Ca2^{+} signaling from freshly harvested and cultured coronary rings

Because vasoconstriction and CSM contraction are a result of increased Ca^{2+}, we wanted to directly compare tension development data to intracellular Ca2+ signaling. Ossabaw swine CSM were enzymatically isolated from freshly dissected coronary rings and loaded with 2.5 μM fura-2 AM (Molecular Probes, Life Technologies, Eugene, OR) as previously described (42;44;53;124). Fura-2 loaded cells were switched to a 2 mM Ca^{2+} physiologic salt solution (PSS), (in mM: 138 NaCl, 5 KCl, 2 CaCl2, 1 MgCl2, 10 HEPES, 10 glucose, titrated to a pH of 7.4 with NaOH) and kept on ice before being placed on a coverslip contained within a constant-flow superfusion chamber that was mounted on an inverted epifluorescence microscope (model TMS-F, Nikon). Whole-cell intracellular Ca^{2+} levels were measured at room temperature (22 to 25°C) using the InCa++ Imaging System (Intracellular Imaging, Cincinnati, OH). Loaded CSM were depolarized with 80 mM K^{+} (80K) (in mM: 2 CaCl2, 63 NaCl2, 1 MgCl2, 80 KCl, 10 HEPES, 10 glucose, titrated to a pH of 7.4 with NaOH) to initiate Ca^{2+} influx through voltage-gated Ca2+ channels (VGCC), stimulated with 5 mM caffeine (5CAF) to measure Ca^{2+} release from the sarcoplasmic reticulum (SR), and assessed for Ca^{2+} buffering ability/store-operated Ca^{2+} influx after the caffeine-induced elevation in cytosolic Ca^{2+} level (Fig. 4.1B).

In a second protocol, CSM from organ cultured domestic swine coronary rings (see methods below) were exposed to the same protocol, followed immediately by a 2 mM Ba^{2+} depolarizing solution (2Ba80K5Na) (in mM: 2 BaCl2, 63 LiCl, 1 MgCl2, 80 KCl, 10 mM HEPES, 10 mM glucose, titrated to a pH of 7.4 with NaOH) (Fig. 4.7A) . This solution contains low Na^{+}, which will inhibit NX and the 80 mM K will activate VGCC, which are highly permeable to Ba^{2+}. Barium was a good tool because it binds fura-2, but cannot be rapidly extruded by the inhibited NX and cannot be transported by Ca^{2+} pumps (125;126), allowing for a more pure measure of Ba (divalent cation) influx. Previously, exposure of the 2Ba80K5Na-activated cells to nifedipine, the VGCC inhibitor, confirmed activation of VGCC is inducing divalent cation (Ba / Ca) influx into the cell (125).

Sterile isolation of porcine coronary rings

Domestic farm pigs were anesthetized with telazol/ketamine/xylazine (1 mL/ 50 lb) and then euthanized by pentobarbital (1 mL/ 10 lb). Excision of the heart was performed with sterile gloves and tools. The heart was removed with the pericardial sac intact to help maintain sterility. In a sterile field, the pericardial sac was removed and the heart was rinsed with sterile-filtered PSS plus 1% penicillin streptomycin (PS) (Gemini Bio-products, Sacramento, CA). Gross dissection of coronary conduit arteries occurred immediately after removal of the heart and specimens were placed in ice-cold sterile-filtered PSS + 1% PS. The tissue was transported to the sterile hood for fine dissection. Arteries were trimmed of adventitia, cardiac and adipose tissues.

Coronary ring organ culture

To induce an advanced stage of *in vitro* CAD/CAC, domestic pig coronary rings were cultured in 12-well plates at 37°C with 4.6% CO_2 in a base media of normal glucose (100 mg/dL) DMEM (Sigma-Aldrich, St. Louis, MO) + 1% PS. After dissection, rings were randomly assigned to one of 4 groups: freshly harvested, control, calcification (CA), or calcification + nifedipine (NIF). Control rings were cultured in the base media alone. CA rings were cultured in the base media supplemented with 3.8 mM sodium phosphate and 7.5 U/mL alkaline phosphatase enzyme (Promega, Madison, WI) to induce CAC within the vascular wall. This CA media recipe has previously induced medial calcification in rat aortic ring cultures (127). NIF rings were cultured in base media supplemented with the CA media plus the specific VGCC inhibitor, nifedipine (1 μM; Santa Cruz Biotechnology, Santa Cruz, CA). Rings were cultured for 4 and 7 days. Fresh rings were also used for Day 0 measures (freshly harvested).

Coronary ring histopathology

Cultured rings were formalin-fixed for at least 24 hours. Samples were then transferred to plastic cassettes and placed in 70% ethanol. After paraffin embedding and slicing, slides were stained with Von Kossa mineral stain to assess calcification within the coronary wall and Masson's trichrome to assess collagen deposition as a measure of *in vitro* CAD progression. Analysis was performed using ImageJ software (NIH) similar to a previous method (128).

Statistics

Data are described as mean ± SEM with $p<0.05$ considered statistically significant. One-way analysis of variance (ANOVA) and two-way ANOVA with Student-Newman-Keuls (SNK) post hoc test were used in PRISM software (GraphPad, San Diego, CA).

Results

Metabolic characteristics of Ossabaw swine

Pigs on the atherogenic diet developed MetS as indicated by the risk factors in Table 1. Body weight, systolic blood pressure, diastolic blood pressure, total cholesterol, and triglyceride measures were increased in MetS compared to lean pigs.

Quantification of coronary artery disease (CAD) progression

Coronary artery plaque burden increased in MetS pigs with time on atherogenic diet (Fig. 4.2D), but did not significantly increase until pigs were fed for 12+ months (lean= 1 ± 0.2%, 6 months= 3 ± 1%, 9 months= 7 ± 2%, 12+ months= 21 ± 5%, $p<0.05$). Wall coverage, which shows mainly Type II and III lesions that are present in milder CAD, increased much earlier in the CAD progression time course (lean= 3 ± 1%, 6 months= 25 ± 7%, 6 months= 41 ± 7%, 12+ months= 41 ± 10%, $p<0.05$). These data support our statement that % wall coverage is a strong tool for quantification of early intimal CAD prior to the stage of more intimal plaque. From these quantification methods we have characterized pigs with CAD due to 6-9 months on atherogenic diet as “early stage” CAD and 12+ months on atherogenic diet as “late stage” CAD.

Fresh coronary ring tension development

Functional assessment of coronary rings from lean pigs revealed no effect of age on tension development to 20 mM KCl (average= 1.8 ± 0.3 g, $p= 0.1$) (Fig.

4.3A). Rings from MetS pigs revealed a biphasic change in tension development to 20 mM KCl as CAD progressed (6 months= 1.8 ± 0.6 g, 9 months= 5.0 ± 1.0 g, 12 months= 0.7 ± 0.1 g, $p<0.05$) (Fig. 4.3B). When compared to age-matched leans, rings from MetS pigs with “early stage” CAD after 9 months of atherogenic feeding developed significantly more tension to 20 mM KCl (5.0 ± 1.0 g vs 1.4 ± 0.3 g, $p<0.05$). Once coronary plaque burden significantly increases in MetS pigs fed atherogenic diet for 12+ months, tension development dramatically decreases below that of rings from lean age-matched pigs (0.7 ± 0.1 g vs. 2.8 ± 0.4 g, $p<0.05$) (Fig. 4.3C).

Fresh coronary smooth muscle (CSM) intracellular Ca^{2+} signaling

Intracellular imaging of CSM from varying stages of Ossabaw CAD progression revealed a similar biphasic pattern as seen in the functional tension development data. CSM from pigs with “early stage” CAD had greater Ca^{2+} influx through VGCC after activation by 80K compared to cells from age-matched lean pigs as quantified by area under the curve (18 ± 2 vs. 10 ± 0.1, $p<0.05$). CSM from pigs with “late stage” CAD lost this transient increase in VGCC activation (Fig. 4.4B). Release of the SR store with 5CAF revealed a significantly heightened Ca^{2+} transient in CSM from MetS pigs with “early stage” CAD compared to CSM from age-matched leans (0.41 ± 0.07 vs. 0.20 ± 0.01, $p<0.05$). Again, this increased Ca^{2+} signal in CSM from pigs with “early stage” CAD was lost in CSM from pigs with “late stage” CAD. (Fig. 4.4C). Finally, Ca^{2+} buffering impairment along with simultaneously store-operated Ca2+ influx was assessed

after SR store depletion. While this revealed a trend towards the same biphasic pattern of Ca^{2+} changes during the time course of CAD progression, no significant changes were observed (Fig. 4.4D).

Induction of coronary artery calcification (CAC) by organ culture

Coronary wall medial thickness and collagen deposition were not statistically different between organ culture groups (data not shown). Evidence for early coronary calcification was observed in rings from 7 days in CA and NIF medias (Fig. 4.5C&D), but not in fresh or control rings.

Cultured ring tension development

Control media

Compared to freshly isolated coronary rings, rings cultured for 4 and 7 days in the control media were functionally no different after exposure to 10, 20, or 80 mM KCl. However, tension development to 20 mM KCl was significantly increased at 7 days in culture compared to just 4 days (5.0 ± 1.4 g vs. 1.4 ± 0.3 g, $p<0.05$). This trend was observed in rings cultured for 7 days compared to freshly isolated rings (Fig. 4.6A).

Calcification (CA) media

After 4 days in CA media, tension development was not different from fresh rings. However, after 7 days in CA media, a significant increase in tension development to 20 mM KCl compared to just 4 days was observed (5.3 ± 0.6 g vs. 2.3 ± 0.5 g, $p<0.05$). When comparing functional assessment of freshly

isolated coronary rings to rings cultured in CA media for 7 days, a significant increase in cultured ring tension development was observed from 20 mM KCl (5.3 ± 0.6 g vs. 2.8 ± 0.6 g, $p<0.05$) and 80 mM KCl (8.1 ± 0.8 g vs. 6.3 ± 0.7 g, $p<0.05$) stimulation (Fig. 4.6B).

Calcification + Nifedipine (NIF) media

After 4 days of culture in NIF media, tension development was severely blunted to both 20 mM KCl (0.4 ± 0.1 g vs. 2.8 ± 0.8 g, $p<0.05$) and 80 mM KCl (1.1 ± 0.3 g vs. 6.3 ± 0.7 g, $p<0.05$) compared to freshly isolated rings. After 7 days in culture, tension development to 80 mM KCl was still severely blunted compared to freshly isolated rings (1.7 ± 0.4 g vs. 6.3 ± 0.7 g, $p<0.05$) while tension development to 20 mM KCl recovered to be functionally no different. When comparing 4 and 7 days of organ culture in NIF media, there was no functional difference between tension development to 10, 20, or 80 mM KCl (Fig. 4.6C).

Tension development to 20 mM KCl after 7 days in organ culture

After 7 days of culture in NIF media, tension development to 20 mM KCl was blunted compared to rings cultured in both CA media (5.3 ± 0.6 g vs. 1.5 ± 0.3 g, $p<0.05$) and control media (5.0 ± 1.34 g vs. 1.5 ± 0.3 g, $p<0.05$) (Fig. 4.6D). There was no significant difference between overall tension developments of rings in control media compared to CA media.

Tension development to 80 mM KCl after 7 days in organ culture

After the first 4 days of culture in NIF media, tension development to 80 mM KCl was blunted compared to rings cultured in both CA media (8.3 ± 0.9 g

vs. 1.1 ± 0.3 g, $p<0.05$) and cotnrol media (5.7 ± 1.0 g vs. 1.1 ± 0.3 g, $p<0.05$). After 7 days of culture in NIF media, tension development to 80 mM KCl was still blunted compared to rings cultured in CA media (8.1 ± 0.8 g vs. 1.7 ± 0.4 g, $p<0.05$) and control media (6.6 ± 1.6 g vs. 1.7 ± 0.4 g, $p<0.05$) (Fig. 4.6E). There was no significant difference between overall tension developments of rings in control media compared to CA media.

Cultured ring CSM intracellular Ca^{2+} signaling

Independent of time in culture and media, no difference was observed in CSM baseline Ca^{2+} levels (Fig. 4.7B). Fresh CSM had significantly greater caffeine-sensitive Ca^{2+} release compared to all CSM from all cultures ($p<0.05$). While no statistical difference was revealed among CSM from cultured rings, a trend of decreased SR Ca^{2+} store is seen in CSM from 4 and 7 days in CA media compared to both control and NIF (Fig. 4.7C). Finally, rate of Ba^{2+} influx was assessed as a pure influx measure during 2Ba80K5Na exposure. No difference was seen between any of the CSM groups (Fig. 4.7D).

Discussion

Several association studies have been conducted correlating CSM Ca^{2+} regulation and transporter expression in CAD (for review (46)). However, it is important to acknowledge at which stage of CAD progression these changes occur. From the IVUS imaging, we classified two stages of CAD in these study pigs: “early stage” CAD (0-9 months on atherogenic diet) and “late stage” CAD (>9 months on atherogenic diet). The clear distinction between the two stages of disease is the shift from neointimal wall coverage to the significant increase in plaque burden observed in the pigs fed the atherogenic diet for 12+ months.

Previous studies in freshly isolated porcine CSM have demonstrated that impairment of Ca^{2+} extrusion mechanisms may be the initial deficiency in Ca^{2+} handling (52). These Ca^{2+} extrusion impairments include a decrease in the plasma membrane Ca2+ ATPase (PMCA) function and a loss of the physical coupling of intracellular Ca^{2+} store release and Ca^{2+} extrusion at the plasma membrane by both PMCA and Na+-Ca^{2+} exchanger (NX) (52). This decrease in CSM Ca^{2+} extrusion efficiency could explain the trend towards a sustained Ca^{2+} transient observed after caffeine exposure in CSM from MetS Ossabaw with “early stage” CAD (Fig. 4.4D). Consequently, if CSM are not able to buffer Ca^{2+} as levels increase in the cytosol, this would lead to increased CSM contraction due to sustained Ca^{2+} levels, which was observed in coronary rings subjected to isometric tension studies. Rings isolated from pigs with “early stage” CAD revealed increased tension development to 20 mM KCl, a characteristic that was lost in coronary rings from pigs with “late stage” CAD (Fig. 4.3C).

Ca^{2+} can be buffered from the cytosol in two manners: plasma membrane Ca^{2+} extrusion or intracellular store Ca^{2+} buffering. As a compensatory mechanism for impaired extrusion, CSM may increase Ca^{2+} buffering into intracellular cellular stores to reduce cytosolic levels. Increases in the sarco/endoplasmic reticulum Ca^{2+} ATPase (SERCA) expression (53) and function (53;129) has been observed in CSM from pigs with "early stage" CAD. Increased SERCA buffering could also explain the heightened caffeine-sensitive Ca^{2+} release via ryanodine receptors on the sarcoplasmic reticulum (SR) (Fig. 4.4C).

On the other hand, in "late stage" CAD, evidence has revealed a decrease in SERCA's compensation (42), which could explain the decrease in our caffeine-sensitive SR Ca^{2+} release observed in CSM from the pigs on atherogenic diet for 12+ months (Fig. 4.4C). Studies have linked a decrease in SERCA activity to cCSM dedifferentiation to sCSM (130;131), however, we interpret our findings that increased SERCA in "early stage" CAD, as evident by increased caffeine-sensitive Ca^{2+} store release (Fig. 4.4C), is characteristic of sCSM. Further along the CAD time course, as intimal sCSM reach a certain toxic Ca^{2+} threshold, the cell must adapt by inducing apoptosis or further dedifferentiating to the oCSM phenotype which is likely characterized by decreased SERCA (Fig. 4.4C).

The early increase in SERCA may also occur in order to combat the increase in voltage-gated Ca^{2+} channel (VGCC) activity and expression that has been observed in CSM from pigs with a similar state of early CAD (56). Here we have provided more evidence, by both coronary ring tension development (Fig.

4.3C) and CSM Ca^{2+} influx (Fig. 4.4B), for increased VGCC activity from pigs with “early stage” CAD. Upregulated VGCC has also been observed in a cell line of cultured arterial smooth muscle cells exposed to low-density lipoprotein (132). Although their findings were in human cardiac myocytes, Schröder et al. found increased availability and open probability of VGCC from left ventricular samples from heart failure versus non-heart failure patients (133). This shift in VGCC properties is reflected in our Ca^{2+} signaling data of CSM from pigs with “early stage” CAD.

Downregulation of VGCC has been shown in dyslipidemic swine (53;55). Bowles et al. accounted their observed decrease in VGCC to the hypercholesterolemia of their pigs (55), however, our pigs with the highest level of total cholesterol (9 months on diet) revealed the highest coronary ring tension development along with the largest amount of VGCC Ca^{2+} influx (Table 1). If VGCC are downregulated in sCSM, inhibition should not prevent CSM dedifferentiation, which was shown by Kaimoto et al. in cell culture and in rats (134). It is feasible to conclude that VGCC is upregulated in early CAD when CSM begin to proliferate and migrate, and then severely downregulated in later CAD when complicated lesions containing apoptotic and oCSM exist. However, a major question lingers: does downregulation of VGCC lead to CSM dedifferentiation or does CSM dedifferentiation lead to downregulation of VGCC?

While it is important to recognize changes in Ca^{2+} handling associated with CSM phenotype switching, future studies must focus on causal roles for these changes. Transient receptor potential 1 channel (TRPC1) expression has

been correlated with neointimal growth and sCSM in humans (57). TRPC expression and activity are also increased in MetS Ossabaw (44). A causal role for TRPC1-mediated Ca^{2+} influx in CSM proliferation was proposed because TRPC1 activity preceded IVUS-detectable CAD in the disease time course (135).

We used an organ culture model of vascular calcification (105) to investigate whether Ca^{2+} influx via VGCC plays a causal role in dedifferentiation to the oCSM phenotype. We confirmed oCSM dedifferentiation by identification of increased RUNX2 expression after CA organ culture using flow cytometry as previously described (136) (data not shown). It is reasonably well accepted that dedifferentiated CSM have a decrease in VGCCs and contractile characteristics (137;138), but studies suggest a causal role of VGCC in calcification (139;140). Evidence for inhibition of vascular calcification by VGCC antagonists has been shown in *in vitro* (127) and animal (139) models and in humans (140) with vascular calcification. However, the mechanism of VGCC antagonist attenuation of disease is not well understood and it still remains uncertain whether Ca^{2+} influx by CSM directly affects calcification (30).

Some functional differences were revealed by isometric tension studies; however, the lack of a phenotypic difference makes interpretation difficult. What we can determine from the functional data is viability of our tissue after 7 days in culture.

Overall, these data support a conclusion that VGCC activity is not likely involved in the induction of coronary artery calcification by oCSM. The most convincing observation was the induction of calcification in rings that were

exposed to the VGCC inhibitor, nifedipine (Fig. 4.5D(a)). We are confident the inhibitor was effective because of the blunting of tension development observed in NIF cultured coronary rings (Fig. 4.6C). Interestingly, dispersed CSM from NIF cultured rings did not reveal decreased Ca^{2+} influx via VGCC upon K+ exposure (Fig. 4.7D). We speculate that nifedipine was not thoroughly washed from the intact rings prior to isometric tension studies.

It seems reasonable that VGCC do not play a causal role in oCSM phenotype switching because expression is down in sCSM. In CAD, intimal plaque buildup due to proliferative sCSM occurs prior to extracellular calcification by oCSM. Because oCSM suffers from Ca^{2+} overload, it is likely that some other Ca^{2+} influx pathway is responsible. The TRPC family of sarcolemmal channels, specifically TRPC1, which has previously revealed a causal role in sCSM proliferation and its expression is increased in CSM from pigs with CAD (44;57;135), may likely play a role in oCSM dedifferentiation.

Acknowledgements

The authors would like to recognize Brandy L. Sparks, M.S. and James P. Byrd for their scientific contributions to this work.

Funding Sources

NIH HL062552 and Indiana University Health – Indiana University School of Medicine Strategic Research Initiative (MS), HL092245 (JDT), NIH/NCATS CTSI TL1 TR000162 (MLM).

Figures & Tables

Figure 4.1. Intracellular Ca^{2+} signaling in coronary smooth muscle cells. A. A model of CSM Ca^{2+} signaling. VGCC = voltage-gated Ca^{2+} channel; CP = Ca^{2+} pump; NX = Na^{+}-Ca^{2+} exchanger; S = SERCA (sarcoplasmic-endoplasmic reticulum Ca^{2+}) pump; TRP = Transient receptor potential channel; CAF = caffeine; Ca_C= cytosolic Ca^{2+}; Ca_{SR}= intracellular store Ca^{2+}; Green arrow= VGCC Ca^{2+} influx; Blue arrows: CAF-sensitive SR Ca^{2+} store release; Red X= Ca^{2+} buffering impairment during CAF exposure; Red arrow (dashed)= store-operated Ca^{2+} influx; red arrows= impaired Ca2+ buffering/extrusion. **B.** Representative tracing of CSM cytosolic Ca^{2+} flux during imaging experiment. Labels indicate solution changes through superfusion chamber with duration shown by the horizontal lines. VGCC = voltage-gated Ca^{2+} channel; Caf = caffeine; green area under the curve = Ca^{2+} influx due to VGCC activation after 80 mM K+ membrane depolarization; blue double-headed arrow = Ca^{2+} transient due to Caf-sensitive release of the intracellular SR Ca2+ store; red double-headed arrow = delayed recovery to basal C_C levels due to impaired Ca^{2+} buffering and store-operated influx.

Figure 4.2. Intravascular ultrasound imaging of coronary arteries with varying stages of coronary artery disease. A. Cross-sectional view of a coronary artery from a lean pig reveals no evidence of intimal thickening of CAD. **B.** Cross-sectional view of a coronary artery from a MetS pig with “early stage”

CAD. A thin layer of concentric intimal thickening can be seen between the elastic lamina (yellow dotted line) and the lumen (red dashed line). **C.** Cross-sectional view of a coronary artery from a MetS pig with “late stage” CAD. Plaque burden can be quantified between the lamina (yellow dotted line) and the lumen (red dashed line). Within this luminal narrowing lesion, bright white areas of calcification (traced in solid green lines) can be observed as evident by the acoustic shadowing effect in the adventitial region (green dotted lines). **D.** CAD progression was quantified by both wall coverage and plaque burden. CAD continues to progress in MetS pigs that are fed an atherogenic diet over a longer course of time with wall coverage significantly increasing in “early stage” CAD (0-9 months) and plaque burden not increasing until “late stage” CAD (orange box, >9 months). (lean= 4 pigs, MetS 6 months= 5 pigs, MetS 9 months= 5 pigs, MetS 12+ months= 7 pigs) Distance between blue dots is 1 mm.

Figure 4.3. Functional assessment of coronary rings with varying stages of coronary artery disease. A. Age of lean pigs had no effect on tension development to 20 mM KCl. **B.** Coronary rings from MetS pigs fed an atherogenic diet for 9 months revealed the greatest tension development compared to rings from MetS pigs on diet for both 6 and 12+ months. **C.** Coronary rings from MetS pigs were paired with rings from age-matched leans. After 9 months on atherogenic diet, rings from MetS pigs acquired greater tension to 20 mM KCl compared to age-matched lean pigs (5.03 ± 0.94 g vs 1.36 ± 0.29 g, $p<0.05$. After 12+ months on atherogenic diet, rings from MetS pigs

acquired less tension to 20 mM KCl compared to age-matched lean pigs (0.70 ± 0.08 g vs 2.82 ± 0.35 g, $p<0.05$). (lean= 9 pigs, MetS 6 months= 6 pigs, MetS 9 months= 3 pigs, MetS 12+ months= 3 pigs)

Figure 4.4. Intracellular Ca^{2+} imaging of freshly dispersed coronary smooth muscle cells. A. The same representative tracing from Figure 4.1B, is replicated here for aid in data interpretation. **B.** Coronary smooth muscle (CSM) from MetS Ossabaw fed an atherogenic diet for 9 months revealed increased Ca^{2+} influx via voltage-gated Ca^{2+} channels (VGCC) due to exposure to 80 mM KCl compared to 6 and 12+ months (dashed lines, one-way ANOVA and SNK, 17.6 ± 2.3 vs 7.7 ± 0.5 and 9.1 ± 1.0, $p<0.05$). This increase in VGCC Ca^{2+} influx was also greater compared to CSM from age-matched lean pigs (solid line, two-way ANOVA and SNK, 17.6 ± 2.3 vs 10.1 ± 0.7, $p<0.05$). **C.** CSM from MetS Ossabaw fed an atherogenic diet for 9 months revealed increased Ca^{2+} release via ryanodine receptors after exposure to 5 mM caffeine compared to 6 and 12+ months (dashed line, one-way ANOVA and SNK, 0.41 ± 0.07 vs 0.17 ± 0.02 and 0.16 ± 0.02, $p<0.05$). This increase in caffeine-sensitive Ca^{2+} release was also increased compared to CSM from age-matched lean pigs (solid line, two-way ANOVA and SNK, 0.41 ± 0.07 vs 0.20 ± 0.01, $p<0.05$). **D.** By two-way ANOVA testing, no significant difference was revealed in sustained Ca^{2+} signal in CSM from MetS vs age-matched leans. However, MetS data alone showed an increase in the sustained Ca^{2+} signal in CSM from MetS Ossabaw fed an atherogenic diet for 9 months compared to 6 and 12+ months (dashed lines, one-

way ANOVA and SNK, 0.08 ± 0.01 vs 0.05 ± 0.01, $p<0.05$, and 0.04 ± 0.01, $p<0.05$). (lean= 9 pigs, cells= 60; MetS 6 months= 6 pigs, cells= 56; MetS 9 months= 7 pigs, cells= 68; MetS 12+ months= 9 pigs, cells= 92)

Figure 4.5. An organ culture model of coronary artery calcification. A. Fresh coronary arteries were fixed and stained for mineral (calcification) and collagen deposition. As expected, fresh tissue showed healthy coronary smooth muscle (red) in the medial layer of the arterial wall with little collagen deposition (blue) by Masson's trichrome staining (a) and no evidence of calcification (black/brown) by von Kossa mineral staining (b). **B.** After 7 days in control (CON) media, coronary rings lost the nice organization and structure of the medial wall seen in fresh rings, especially near the lumen suggesting medial inward thickening (a), and did not show any evidence of calcification (b). **C.** Rings cultured for 7 days in calcification (CA) media did not have increased medial thickening or collagen deposition (a&b), however, early calcification was induced in the media near the lumen (c&d). **D.** While not evident in all rings cultured in calcification + nifedipine (NIF) media for 7 days, calcification was induced in the same area as seen in CA rings (a). A closer look at the area of calcification reveals collagen deposition (blue) (b). A= adventitia; M= media; L= lumen; black arrows point to some but not all areas of calcification. (Fresh= 4 pigs, 4 rings; CON= 4 pigs, 8 rings; CA= 4 pigs, 8 rings; NIF= 4 pigs, 8 rings)

Figure 4.6. Functional assessment of cultured coronary rings. A. Rings cultured for 4 and 7 days in the control (CON) media were functionally no different than fresh rings after exposure to 10, 20, or 80 mM KCl. Tension development to 20 mM KCl was significantly increased after 7 days in culture compared to just 4 days (5.0 ± 1.4 g vs. 1.4 ± 0.3 g, $p<0.05$). **B.** After 4 days in CA media, tension development was not different compared to fresh rings, but after 7 days a significant increase in tension development to 20 mM KCl compared to just 4 days was observed (5.3 ± 0.6 g vs. 2.3 ± 0.5 g, $p<0.05$). Rings cultured in CA media for 7 days had a significant increase in tension development from 20 mM KCl compared to fresh rings (5.3 ± 0.6 g vs. 2.8 ± 0.6 g, $p<0.05$) and 80 mM KCl (8.1 ± 0.8 g vs. 6.3 ± 0.7 g, $p<0.05$) stimulation. **C.** Tension development of rings from 4 days in NIF media was severely blunted to both 20 mM KCl (0.4 ± 0.1 g vs. 2.8 ± 0.8 g, $p<0.05$) and 80 mM KCl (1.1 ± 0.3 g vs. 6.3 ± 0.7 g, $p<0.05$) compared to freshly isolated rings. After 7 days in culture, tension development to 80 mM KCl was still severely blunted compared to freshly isolated rings (1.7 ± 0.4 g vs. 6.3 ± 0.7 g, $p<0.05$) while tension development to 20 mM KCl recovered to be functionally no different. There was no functional difference between 4 and 7 days of NIF media. (* indicates Day 0 vs Day 4, + indicates Day 0 vs Day 7, # indicates Day 4 vs Day 7; green=CON, blue=CA, red=NIF) **D.** Tension development to 20 mM KCl was blunted after 7 days in NIF media compared to rings cultured in both CA media (5.3 ± 0.6 g vs. 1.5 ± 0.3 g, $p<0.05$) and CON media (5.0 ± 1.34 g vs. 1.5 ± 0.3 g, $p<0.05$). There was no significant difference between overall tension developments of rings in CON

media compared to CA media. **E.** Tension development to 80 mM KCl was blunted after 4 days in NIF media compared to rings cultured in both CA media (8.3 ± 0.9 g vs. 1.1 ± 0.3 g, $p<0.05$) and CON media (5.7 ± 1.0 g vs. 1.1 ± 0.3 g, $p<0.05$). Tension development to 80 mM KCl was still blunted after 7 days in NIF media compared to rings cultured in CA media (8.1 ± 0.8 g vs. 1.7 ± 0.4 g, $p<0.05$) and CON media (6.6 ± 1.6 g vs. 1.7 ± 0.4 g, $p<0.05$). There was no significant difference between overall tension developments to 80 mM KCl of rings in CON media compared to CA media. (* indicates CON vs CA, + indicates CON vs NIF, # indicates CA vs NIF; green=CON, blue=CA, red=NIF) (Day 0-Fresh= 4 pigs, 16 rings; Day 4-CON= 4 pigs, 9 rings; Day 4-CA= 4 pigs, 10 rings; Day 4-NIF= 4 pigs, 9 rings; Day 7-CON= 4 pigs, 10 rings; Day 7-CA= 4 pigs, 10 rings; Day 7-NIF= 4 pigs, 8 rings)

Figure 4.7. Intracellular Ca^{2+} imaging of coronary smooth muscle cells from cultured rings. A. A representative tracing of the experimental protocol performed on cells dispersed from cultured coronary rings. **B.** No difference in baseline Ca^{2+} was observed in fresh and all CSM from cultured rings. **C.** Sarcoplasmic reticulum caffeine-sensitive Ca^{2+} release was significantly greater in fresh CSM compared to CSM from cultured rings. No difference was observed between all culture groups, but a trend of further decreased Ca^{2+} release was seen in CSM from CA rings. **D.** The rate of Ba^{2+} influx was not different between fresh or any CSM from cultured rings. (Day 0-Fresh= 4 pigs, 57 cells; Day 4-CON= 4 pigs, 49 cells; Day 4-CA= 4 pigs, 43 cells; Day 4-NIF= 4 pigs, 48 cells;

Day 7-CON= 4 pigs, 42 cells; Day 7-CA= 22 cells, 10 rings; Day 7-NIF= 4 pigs, 23 cells)

Figure 4.1.

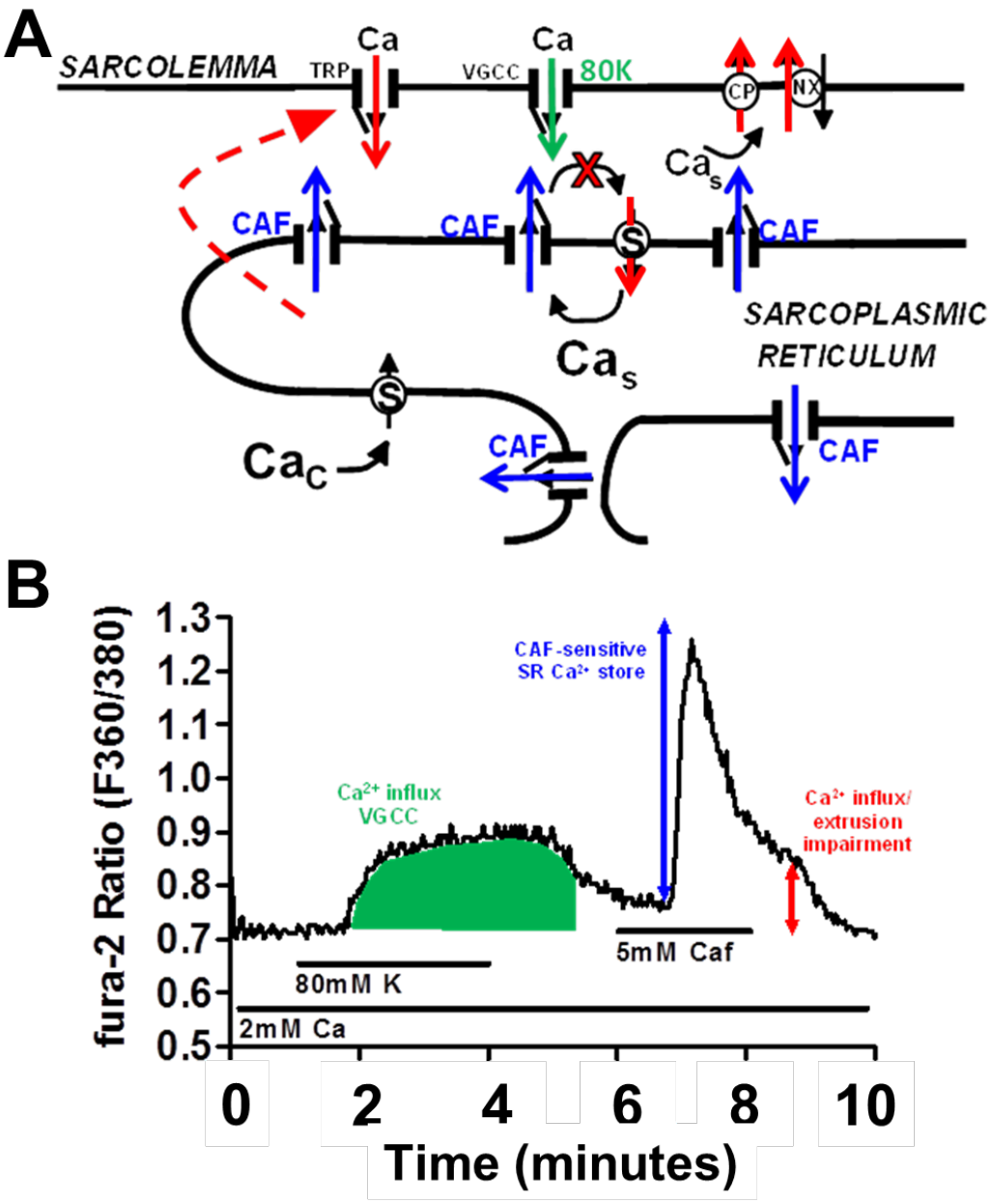
A
SARCOLEMMA
TRP
Ca
VGCC
Ca
80K
CP
NX
Ca$_s$
CAF
CAF
S
CAF
SARCOPLASMIC
RETICULUM
Ca$_s$
S
Ca$_C$
CAF
CAF
B
fura-2 Ratio (F360/380)
1.3
1.2
1.1
1.0
0.9
0.8
0.7
0.6
0.5
CAF-sensitive
SR Ca^{2+} store
Ca^{2+} influx
VGCC
Ca^{2+} influx/
extrusion
impairment
5mM Caf
80mM K
2mM Ca
0
2
4
6
8
10
Time (minutes)

Figure 4.2.

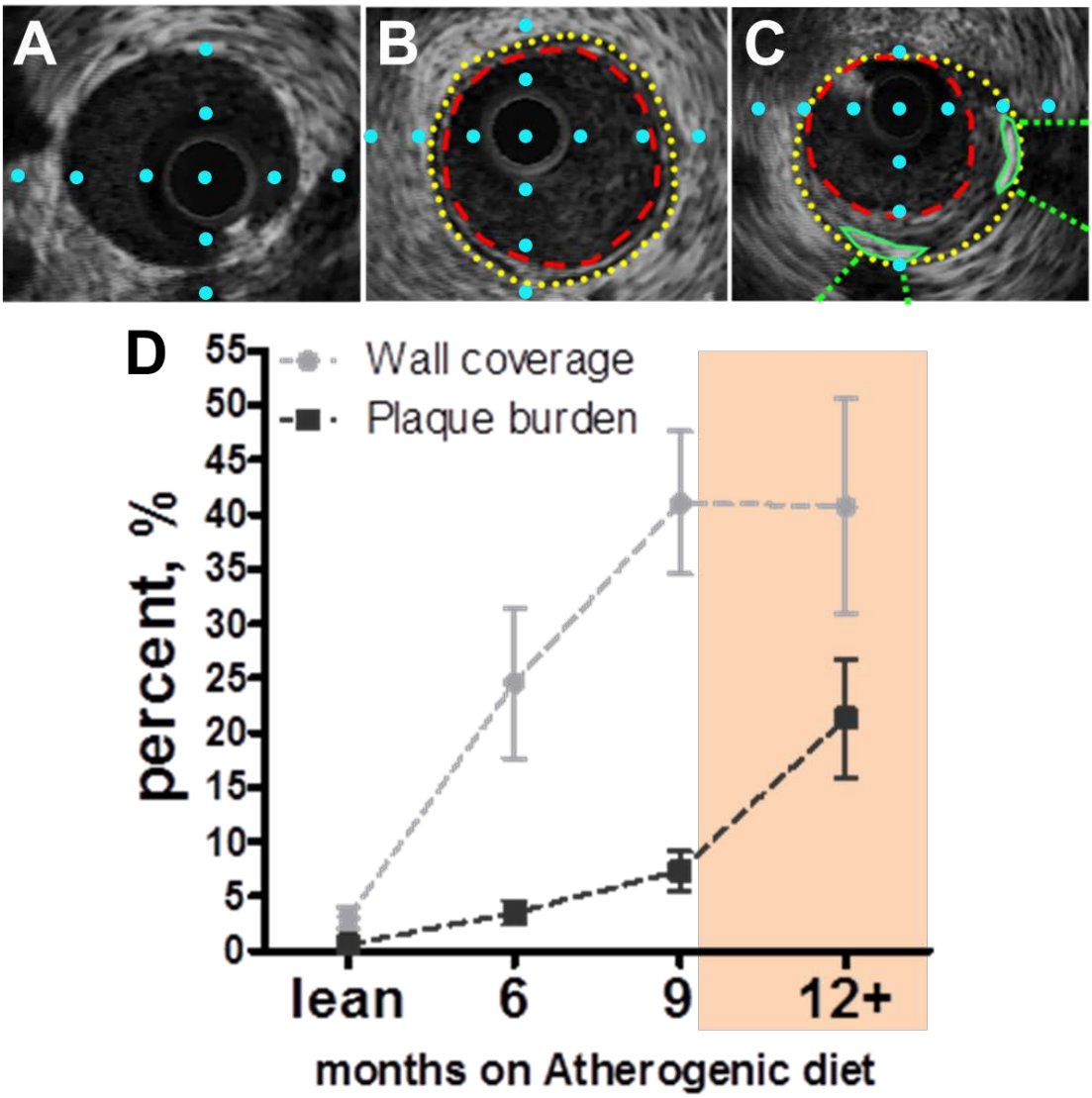
A
B
C
D
Wall coverage
Plaque burden
percent, %
55
50
45
40
35
30
25
20
15
10
5
0
lean
6
9
12+
months on Atherogenic diet

Figure 4.3.

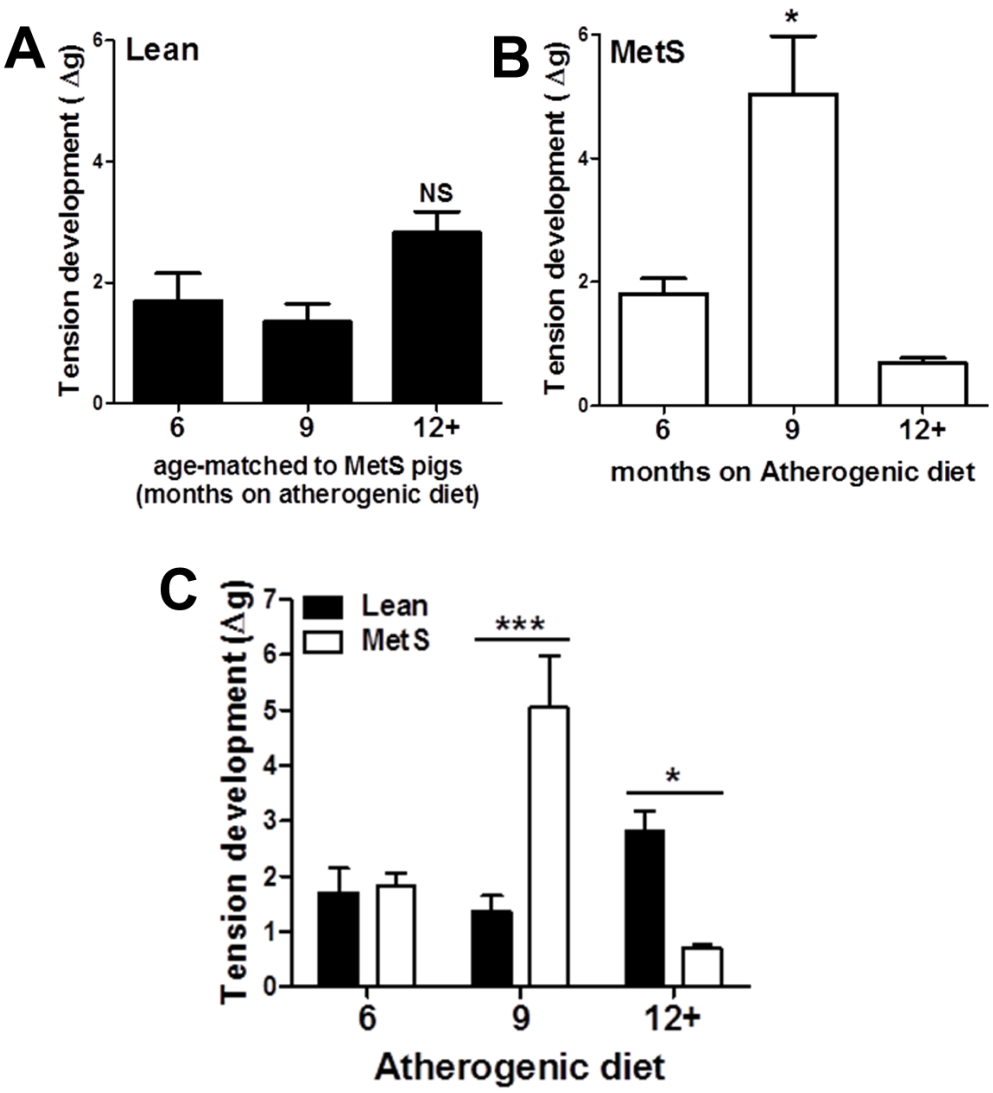
A
Lean
Tension development (Δg)
NS
6
9
12+
age-matched to MetS pigs
(months on atherogenic diet)
B
MetS
*
months on Atherogenic diet
C
Lean
MetS
***
*
Atherogenic diet

Figure 4.4.

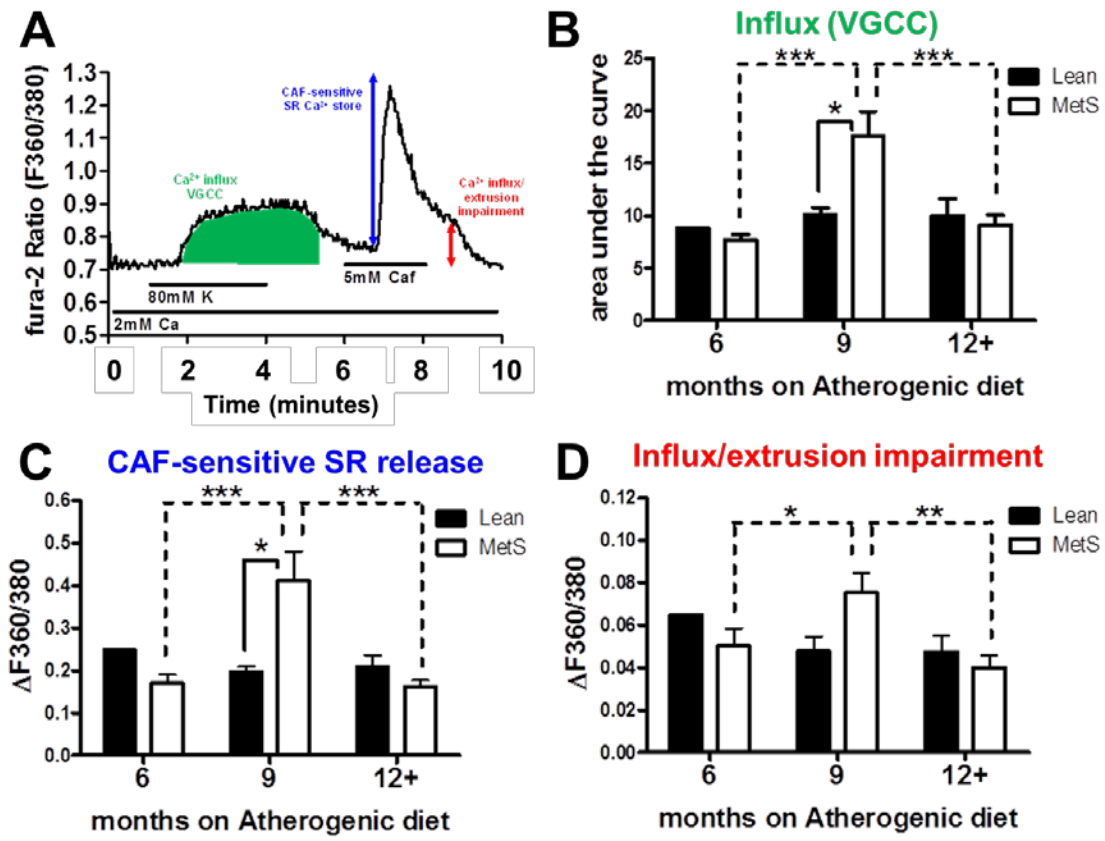
A
fura-2 Ratio (F360/380)
CAF-sensitive SR Ca2+ store
Ca2+ influx VGCC
Ca2+ influx/ extrusion impairment
5mM Caf
80mM K
2mM Ca
Time (minutes)
B
Influx (VGCC)
area under the curve
Lean
MetS
months on Atherogenic diet
C
CAF-sensitive SR release
ΔF360/380
months on Atherogenic diet
D
Influx/extrusion impairment
ΔF360/380
months on Atherogenic diet

Figure 4.5.

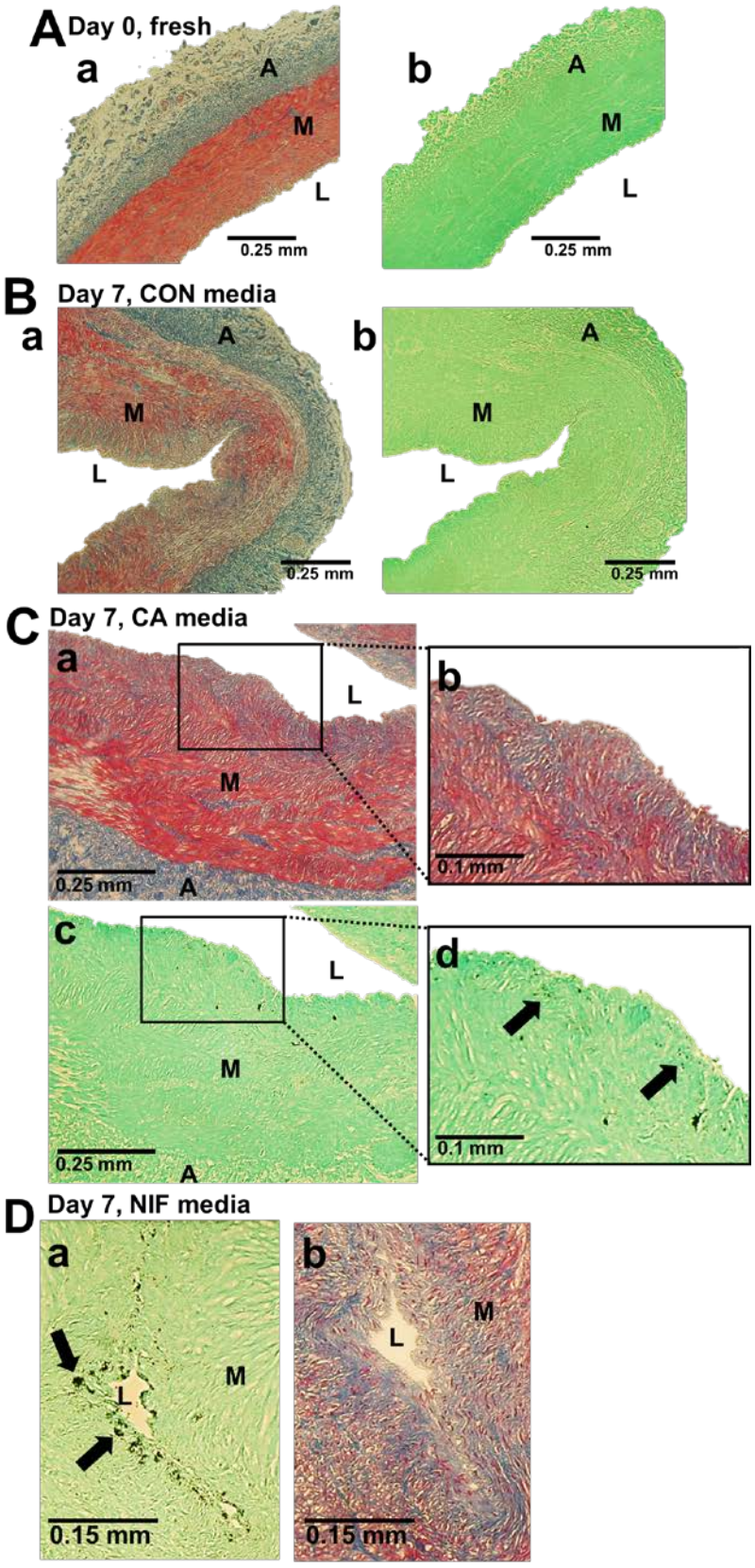
A
Day 0, fresh
a
A
M
L
0.25 mm
b
A
M
L
0.25 mm
B
Day 7, CON media
a
A
M
L
0.25 mm
b
A
M
L
0.25 mm
C
Day 7, CA media
a
L
M
0.25 mm
A
b
0.1 mm
c
L
M
0.25 mm
A
d
0.1 mm
D
Day 7, NIF media
a
M
L
0.15 mm
b
M
L
0.15 mm

Figure 4.6.

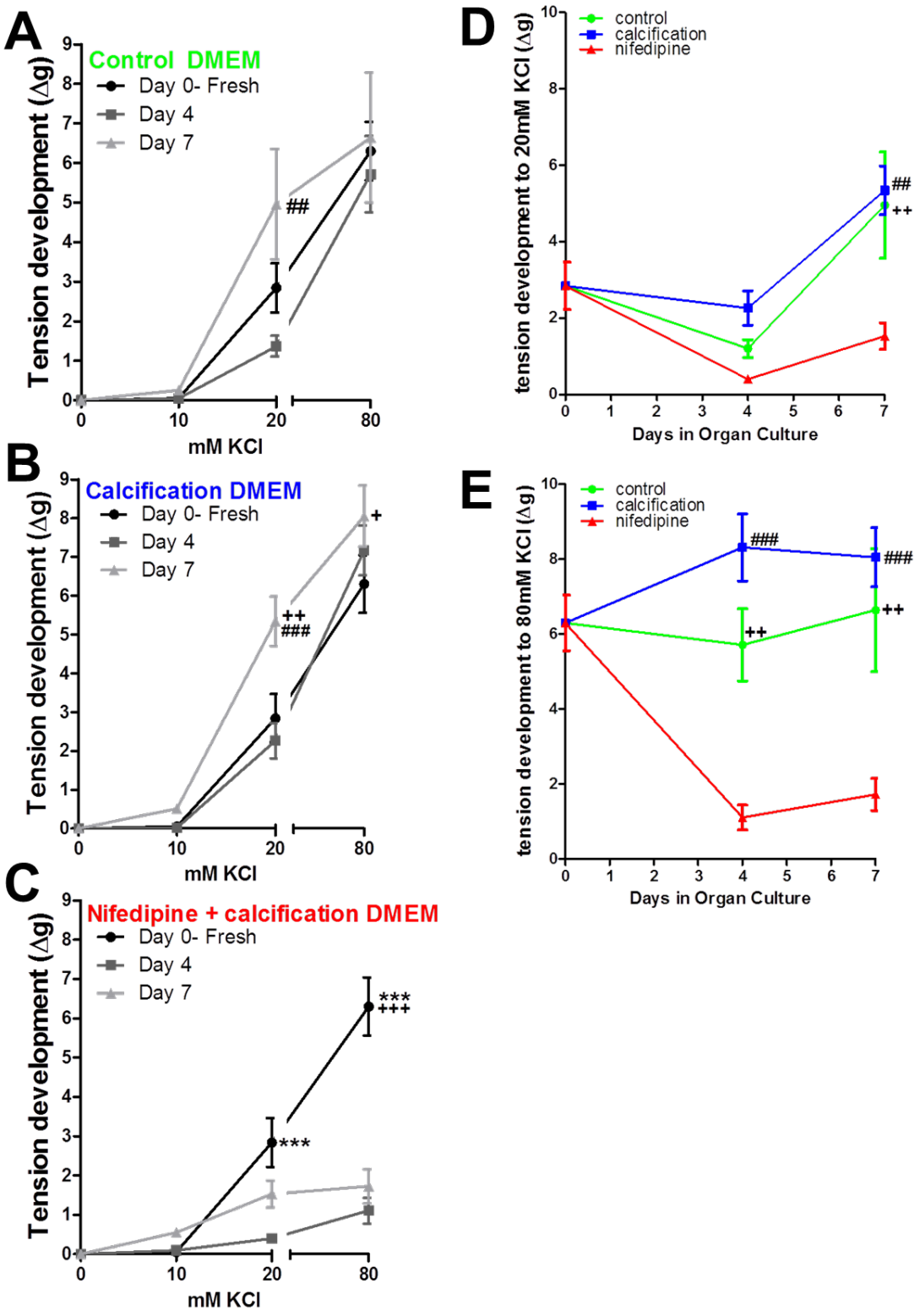
A
Control DMEM
Day 0- Fresh
Day 4
Day 7
Tension development (Δg)
mM KCl
##
B
Calcification DMEM
Day 0- Fresh
Day 4
Day 7
Tension development (Δg)
mM KCl
++
###
+
C
Nifedipine + calcification DMEM
Day 0- Fresh
Day 4
Day 7
Tension development (Δg)
mM KCl
***
***
+++
D
control
calcification
nifedipine
tension development to 20mM KCl (Δg)
Days in Organ Culture
##
++
E
control
calcification
nifedipine
tension development to 80mM KCl (Δg)
Days in Organ Culture
###
###
++
++

Figure 4.7.

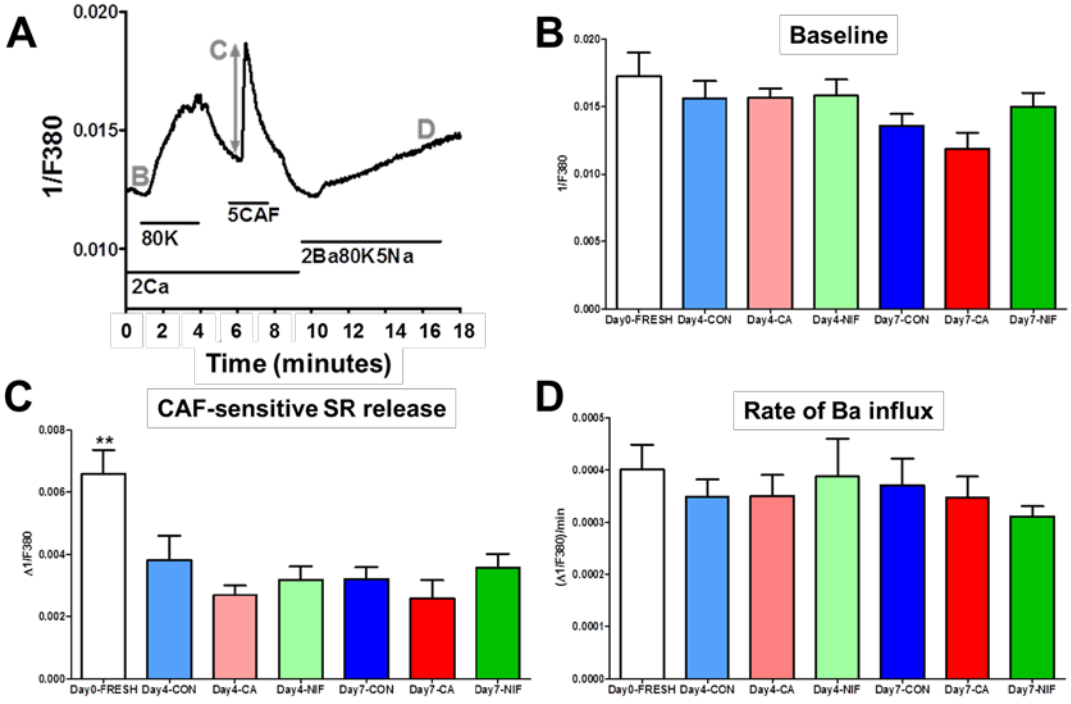
A
1/F380
0.020
0.015
0.010
B
C
D
5CAF
80K
2Ba80K5Na
2Ca
0 2 4 6 8 10 12 14 16 18
Time (minutes)
B
Baseline
1/F380
Day0-FRESH Day4-CON Day4-CA Day4-NIF Day7-CON Day7-CA Day7-NIF
C
CAF-sensitive SR release
Δ1/F380
**
D
Rate of Ba influx
(Δ1/F380)/min

Table 4.1. Metabolic characteristics of Ossabaw miniature swine groups**.**

	Lean	MetS 6 months	MetS 9 months	MetS 12 months	Significance
Body weight (kg)	62 ± 5	89 ± 2	87 ± 7	116 ± 2	12 > 9, 6 > lean
Fasting Blood Glucose (mg/dL)	84 ± 6	75 ± 2	82 ± 7	81 ± 2	NS
Systolic Blood Pressure (mmHg)	131 ± 7	150 ± 9	143 ± 4	170 ± 7	12, 9, 6 > lean
Diastolic Blood Pressure (mmHg)	63 ± 2	77 ± 5	85 ± 4	89 ± 5	12, 9 > 6, lean
Total Cholesterol (mg/dL)	57 ± 5	383 ± 39	546 ± 66	247 ± 17	12 > 9 > 6 > lean
Triglycerides (mg/dL)	25 ± 4	34 ± 4	98 ± 34	43 ± 6	9 > 12, 6, lean

All measures were tested by One-way ANOVA and SNK post-hoc.
NS = not significant.

CHAPTER 5: CONCLUSION

Summary of Findings

"Syndrome X" (5), "the deadly quartet" (141), and "a secret killer" (142) —all pseudonyms that have been used to describe metabolic syndrome (MetS), the condition with which 1/3 of Americans are diagnosed (143;144). It is well recognized that MetS is a risk factor for cardiovascular disease (CAD) and cardiovascular mortality. In 2006, Galassi et al. released their findings from an extensive literature search for studies that examined the association between MetS and CAD spanning almost 40 years (1966-2005) (145). From this analysis it was concluded that patients with MetS have a 61% increased risk for CAD (145), which is well-known as the leading killer of Americans (8).

To coincide with the high incidence in the United States, we have conducted our investigative aims using the Ossabaw swine model of MetS and CAD (39-44) to better replicate the human patient. Following is the summary of findings from this thesis research:

Investigative Aim 1. *Coronary epicardial adipose tissue (cEAT) contributes directly to CAD in Ossabaw swine and CAD progression was attenuated upon surgical removal of the local fat depot.*

The results of our pilot study are consistent with the hypothesis that selective coronary artery adipectomy attenuates the progression of early atherosclerosis. Along with attenuation of disease progression, multiple inflammatory markers were reduced at the site of adipectomy compared to

neighboring intact sites and cEAT from MetS pigs expressed an increased amount of inflammatory genes compared to control cEAT. These findings support the notion that local cEAT contributes to CAD by contributing to the inflammatory response within the coronary artery wall.

Investigative Aim 2. *^{18}F-NaF uptake in the coronaries of MetS Ossabaw with early stage atherosclerosis was higher than in lean Ossabaw and ^{18}F-NaF uptake can be detected at a stage prior to that measurable by computed tomography (CT).*

In this preclinical positron emission tomography (PET) study, we have demonstrated that increased ^{18}F-NaF uptake in the coronaries can detect early calcium metabolism in pigs with clinically insignificant CAD that lack evidence of calcification by both intravascular ultrasound (IVUS) and CT imaging. These findings render the interpretation that ^{18}F-NaF binds to microcalcifications that are on a molecular level, which is too small to be detected using other imaging modalities.

Investigative Aim 3. *Coronary smooth muscle (CSM) Ca^{2+} signaling and function are increased in "early" CAD, but significantly decreased in "later" stages of CAD progression. More specifically, fluctuation of voltage-gated calcium channel (VGCC) activity had no role in osteogenic coronary smooth muscle (oCSM) dedifferentiation and CAD progression to coronary artery calcification (CAC).*

In this time course study, we have demonstrated that CSM Ca^{2+} regulation is complex and changes as CAD progresses. In “early stage” CAD, coronary rings have increased vasoconstriction and their CSM have heightened Ca^{2+} signals. This is interpreted as an adaptation phase to the onset of a MetS milieu. If CAD progresses without intervention, coronary ring vasoactivity is dramatic blunted and CSM Ca^{2+} signaling is decreased as well. These findings suggest the importance of identifying the stage of disease at which measures are obtained. Further, we have demonstrated that VGCC inhibition does not inhibit CAC in organ culture, suggesting an alternative Ca^{2+} influx pathway is responsible.

Future Directions

A large volume of evidence supports the hypothesis that epicardial adipose tissue (EAT) volume is associated with CAD (22;146-151) and cardiovascular events (64;152) in humans, however, this association is difficult to experimentally test due to its anatomical location and research ethics. Our study in the Ossabaw swine model of MetS and CAD was the first of its kind in experimentally investigating the influence of cEAT on CAD progression (21). To more definitively connect the physical presence of cEAT and its impact on CAD, our initial study should be repeated with more pigs and using a definitive marker for the exact adipectomy location. With increasing the number of pigs, a sham group can serve as controls rather than the intra-animal controls used previously (21). Using an intra-animal control resulted in comparison of CAD progression between the LAD and CFX artery of each pig. While this was cost-effective, disease varies amongst the coronaries (153;154) and, therefore, a better control would be a sham LAD of another pig. Also, while CAD is diffuse in MetS Ossabaw (155), the greatest amount of disease remains in the proximal region of the LAD (153-155). Therefore, the adipectomy should be performed in the proximal region to observe greater and more obvious changes in CAD progression between groups. Finally, during the adipectomy procedure, it would be ideal to place radiopaque and echogenic markers at the proximal and distal locations (Fig. 5.1A) to ensure exact localization of the procedure site upon euthanasia. Using both angiography (Fig. 5.1B) and IVUS (Fig. 5.1C) to detect the markers, the location and length of the adipectomy region can be determined.

Studies have also found that intrapericardial adipose tissue, lying directly on top of the coronary arteries and myocardium, is associated with CAD risk factors and more specifically, CAC (22;156;157). CAC is in part a result of local inflammation due to macrophage secretion of cytokines that promote CSM osteogenic dedifferentiation (86;158;159). Our ^{18}F-NaF PET/CT study in Ossabaw swine was the first study to our knowledge to attempt to image CAC at such an early stage of CAD. At this stage, the CAD was clinically insignificant, with little plaque burden and no evidence of calcium by CT. Future studies of ^{18}F-NaF should entail much more variation in disease to better understand the characteristics of ^{18}F-NaF uptake throughout the time course of CAD/CAC. A hypothetical time course can be seen in Figure 5.2.

Prior to the formation of microcalcifications is a stage of local inflammation, which has interested researchers as a target for an *in vivo* imaging diagnostic tool. ^{18}F-fluorodeoxyglucose (FDG), a PET tracer that indicates glucose metabolism, has been investigated as a potential marker for macrophage activity in atherosclerotic plaque (108;109;111) (Fig. 5.2A). The downfall of ^{18}F-FDG has been its low target to background ratio in the heart due to glucose metabolism of the myocardium, evidenced by experimental findings (38). Aikawa et al. showed with *in vivo* imaging the close proximity of inflammation and calcification (86). While inflammation contributes to microcalcification, microcalcification activates macrophages in a positive-feedback fashion (84;85). This cycle will continue to drive more calcification if no clinical intervention takes place. We also know these microcalcifications increase

the risk of plaque rupture (91-93). It would seem that this is a critical stage in CAD/CAC progression where clinicians would want to identify patients using ^{18}F-NaF (Fig. 5.2B). Early diagnosis could assist in augmentation of disease progression perhaps by anti-inflammatory treatment at a reversible stage of CAD/CAC. It has also been suggested that reducing inflammation at this stage will aid in plaque stability (87). Further progression of CSM osteogenic dedifferentiation will result in macrocalcifications characterized by reduced inflammation and large, but stable calcified atherosclerotic lesions. Unfortunately, it is thought that macrocalcifications at this stage are irreversible. This is the stage at which CT can detect calcium in the heart (Fig. 5.2C). Interestingly, Dweck et al. found that 41% of patients with Agatston scores >1000 revealed no ^{18}F-NaF uptake (160). Therefore, it will be important to investigate the threshold at which active microcalcification ends and stable, quiescent macrocalcification begins. Future studies in animal models should focus on the time course of ^{18}F-NaF uptake across the disease spectrum. Ideally, animals with varying stages of disease can be imaged along with other *ex vivo* measures such as histopathology and protein/gene expression in order to better characterize CAD/CAC and CSM involvement.

The changes in CSM Ca^{2+} handling during transition from contractile CSM (cCSM) to synthetic CSM (sCSM) seems to be well characterized (161;162); however, little is understood about oCSM. With efforts in better understanding the time course of Ca^{2+} handling changes, we performed fura-2 Ca^{2+} imaging studies of CSM from pigs with progressing stages of CAD. To expand on the

associations we found and that were described in chapter 4, we specifically targeted the VGCC as a putative source of Ca^{2+} influx leading to oCSM dedifferentiation and activity because we saw increased activity in CSM from our pigs with “early stage” CAD. From our findings we concluded that VGCC activity did not play a causal role in CAC.

Future studies of CSM Ca^{2+} signaling should be more focused on specific Ca^{2+} transporters and their causal roles in CAD progression. For example, a causal role for TRCP1 has been found in dedifferentiation and proliferation in human saphenous vein (57) and pig (163) CSM. Additionally, Neeb et al. found that TRPC1 Ca^{2+} influx preceded CAD in MetS Ossabaw, further supporting its causal role in proliferation (135). Future studies should investigate the role of TRPC1 in oCSM dedifferentiation. It seems probable that a Ca^{2+} influx pathway will be responsible considering the cells are overloaded with Ca^{2+} (164) prior to the protective onset of matrix vesicle loading (165) (Fig. 5.3). Because we know sCSM express TRPC1, it is logical to think oCSM may as well. Rather than a linear path of dedifferentiation (cCSM → sCSM → oCSM), it is more likely an adaptation of cCSM to sCSM and/or oCSM to avoid apoptosis.

In the setting of chronic kidney disease, patients have medial calcification rather than atherosclerotic intimal calcification. In this case, cCSM in the medial layer of the arterial wall may be dedifferentiating directly to oCSM due to Ca^{2+} overload. Previously, we were not capable of imaging molecular calcification, but with ^{18}F-NaF we provided evidence that molecular calcification is occurring much earlier in the disease time course than we had thought. Concurrently, we may

find that TRPC1 channels are contributing to dedifferentiation and the Ca^{2+} overload of the oCSM phenotype. Increased Ca^{2+} influx past a certain threshold triggers matrix vesicle formation (113;164) and it is well understood that these matrix vesicles are loaded with calcification ingredients and dumped from oCSM into the extracellular matrix where hydroxyapatite calcifications are found (166). Another future direction for investigating CSM Ca^{2+} handling would be to try and better understand the effect of oCSM Ca^{2+} overload on matrix vesicle formation and dumping (Fig. 5.3.). Interestingly, microvesicles (smaller than matrix vesicles) have been found in athero-prone areas of human aorta (116). More specifically, these microvesicles are from intimal CSM at the pre-disease stage. This could be occurring in the early stage of transition from cCSM to sCSM prior to any intimal thickening. Also it is important to note that these microvesicles do not contain calcifying reagents; in fact, they contain inhibitors of calcification (116). It could be possible that CSM Ca^{2+} dysfunction as CAD progresses is what leads to the transition from protected microvesicles to pro-calcifying matrix vesicles.

Closing Remarks

This accumulation of research has led to the following all-encompassing working model: In the setting of MetS and CAD, cEAT is increased and therefore local inflammation around the conduit coronary artery. Pro-inflammatory factors and the MetS milieu disturb the quiescent CSM initiating intracellular Ca^{2+} dysregulation and dedifferentiation (Fig. 5.2A). Ca^{2+} dysregulation leads to CSM Ca^{2+} overload and progression of CAD. Further Ca^{2+} dysfunction in oCSM initiates adaptive matrix vesicle loading and extracellular microcalcification. At this stage, high inflammation and newly released microcalcifications are involved in positive feedback activity which can be detected by ^{18}F-NaF, but not the clinically standard CT (Fig. 5.2B). Diagnosis at this stage would be beneficial in disease intervention as risk of plaque rupture is increased due to microcalcification deposition in thin fibrous caps. If left untreated and no detrimental cardiovascular event occurs, microcalcifications will turn into large, stable macrocalcifications characterized by decreased inflammation and potentially blood flow limitations (Fig. 5.2C).

It is critical that we further investigate the effects of adipose-derived inflammation on CSM Ca^{2+} regulation and dedifferentiation, the specific changes in CSM Ca^{2+} dysregulation as CAD/CAC progresses, and finally the time course of CAD/CAC progression on a molecular level to use more sensitive imaging tools for earlier diagnosis and therefore earlier patient treatment.

Figures

Figure 5.1. Placement of ligature clips at the adipectomy site of MetS Ossabaw. (A) A retracted pericardial sac reveals two ligature clips at the adipectomy site above the LAD of a MetS pig. The adipectomy site is flanked at both proximal (yellow arrow) and distal (green arrows) ends. (B) An intravascular ultrasound (IVUS) image shows the echogenic ligature clip (green arrow) at the 4-5 o'clock orientation of the vessel (red dashed line). The placement of the clips can be imaged at the time of the adipectomy surgery; however, in the case that the clips fall off of the heart, anatomical landmarks can be used to identify the adipectomy site at euthanasia (~3 months post-surgery). In this image, a branch point can be seen at the 11 o'clock orientation of the vessel. Distance between dots is 1 mm. (C) The radiopaque clips can also be visualized by angiography (yellow and green arrows). (D) By flushing the coronary tree with contrast, anatomical landmarks can also be visualized by angiography. Traced in white, the same small branch seen in the IVUS image in panel B can be identified with angiography. This particular branch is faint, but more easily identified on the looped angiography video. The same distal clip is identified by the green arrow.

Figure 5.2. Multiple clinical imaging modalities can be used to assess progression of coronary artery disease and calcification. (A) Prior to the onset of coronary artery calcification (CAC) is a stage of coronary artery disease (CAD) characterized by macrophage infiltration and lipid deposition of the arterial

wall, and increased local inflammation detectable by ^{18}F-fluorodeoxyglucose (FDG) positron emission tomography (PET). (B) As inflammation remains, arterial intimal thickness and complexity increase due to dedifferentiation of coronary smooth muscle (CSM) to the osteogenic phenotype. CSM osteogenic activity leads to extracellular deposition of microcalcifications detectable by ^{18}F-NaF PET. Evidence suggests that this combination of chronic inflammation and active calcification in “early stage” CAD increases the risk of plaque rupture. Because these lesions are not flow-limiting, they are frequently asymptomatic, which is dangerous considering their risk of rupture. It is critical to identify patients at this stage of CAD/CAC. (C) Without intervention, and if a patient survives a plaque rupture event, the plaque will heal and CAD/CAC will progress to “later stage” CAD characterized by hardened, collagen-rich plaque containing large macrocalcifications. These large lesions can be stenotic (flow-limiting), but are likely stable due to reduced inflammation and stable calcium turnover (similar to mature bone activity). At this stage, macrocalcifications can be detected by computed tomography (CT) and IVUS.

Figure 5.3. Coronary smooth muscle cell adaptation to increased Ca^{2+} influx and local adipokines signaling. Coronary smooth muscle cells (CSM) are well known for their adaptive plasticity to the local environment. In the setting of obesity and metabolic syndrome (MetS), increased coronary epicardial adipose tissue (cEAT) volume is associated with increased CAD/CAC. Adipokines release from the local cEAT have been shown to effect CSM ion

channel function (75). These adipokines may penetrate the arterial wall or reach the CSM via the vaso vasorum where their effects influence CSM Ca^{2+} signaling and dedifferentiation to synthetic (sCSM) and osteogenic (oCSM) phenotypes. Specifically, sCSM are known to express increased TRPC1, potentially to compensate for the decrease in voltage-gated channel activity in “later stage” CAD. Increased sCSM/oCSM secretory activity increases the complexity of the extracellular matrix by collagen (purple rods), elastin (black ripple lines), and matrix vesicle deposition (light blue circles). Hypothetically, in “early stage” CAD, when CSM sarcoplasmic reticulum (SR) Ca^{2+} is elevated, sCSM vesicular activity is increased resulting in synthesis of extracellular matrix proteins (collagen/elastin). This forms an ideal environment for extracellular calcification (dark blue crystals, hydroxyapatite). Prior to the osteogenic phenotype, vesicles released from CSM to protect from intracellular Ca^{2+} overload will contain calcification inhibitors. Concurrently, and/or in “later stage” CAD, oCSM (characterized by RUNX2 and Ca^{2+} overload) adapt to adveristy by matrix vesicle release. Matrix vesicles are released into the extracellular matrix where they lay down hydroxyapatite on elastic/collagen fibers, contributing to plaque instability. Osteogenic matrix vesicles can transport Ca^{2+} and PO_4^{3-}, and due to lost calcification inhibitors can pre-form hydroxyapatite before release.

Figure 5.1.

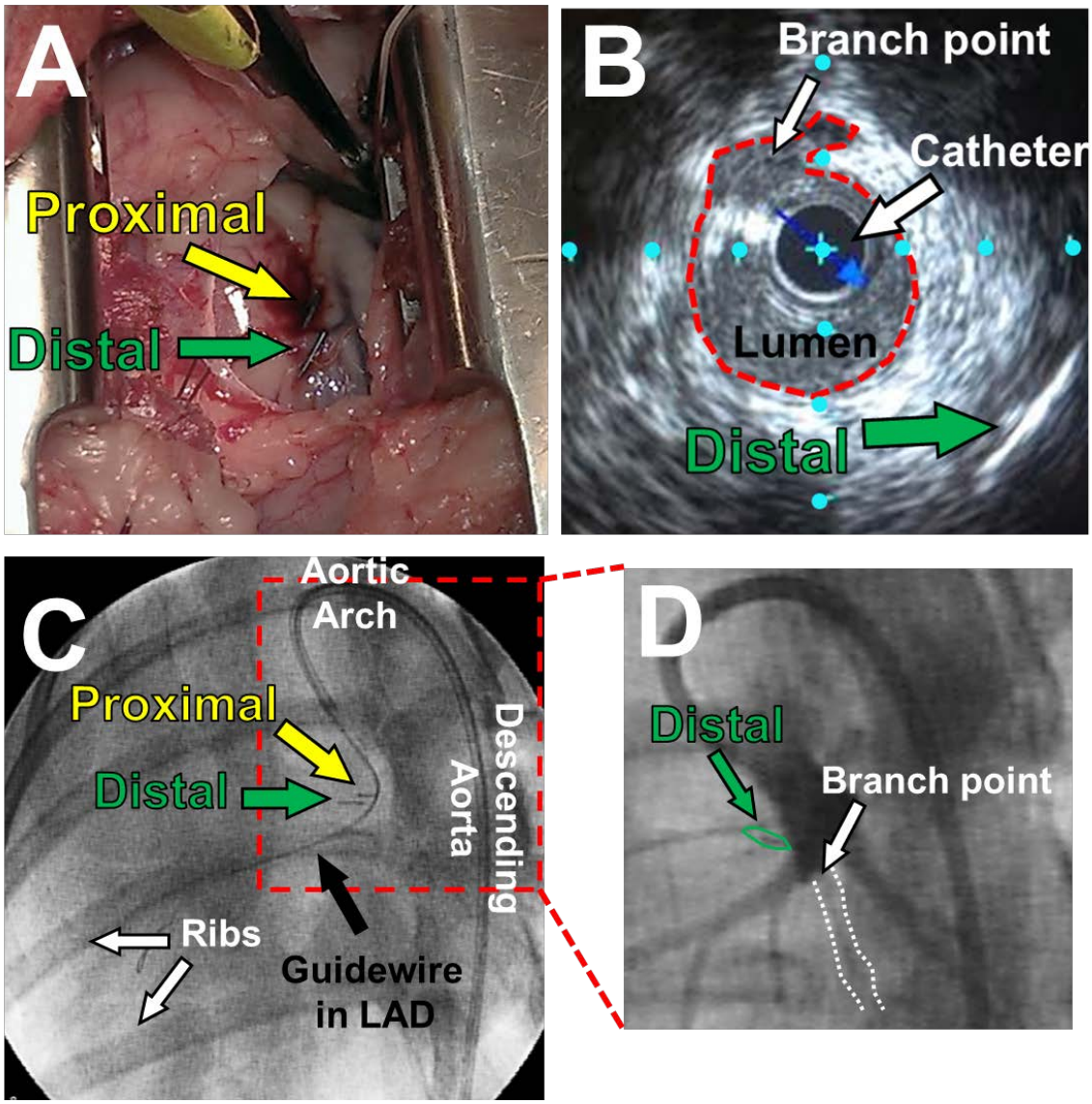
A
Proximal
Distal
B
Branch point
Catheter
Lumen
Distal
C
Aortic Arch
Proximal
Distal
Descending Aorta
Ribs
Guidewire in LAD
D
Distal
Branch point

Figure 5.2.

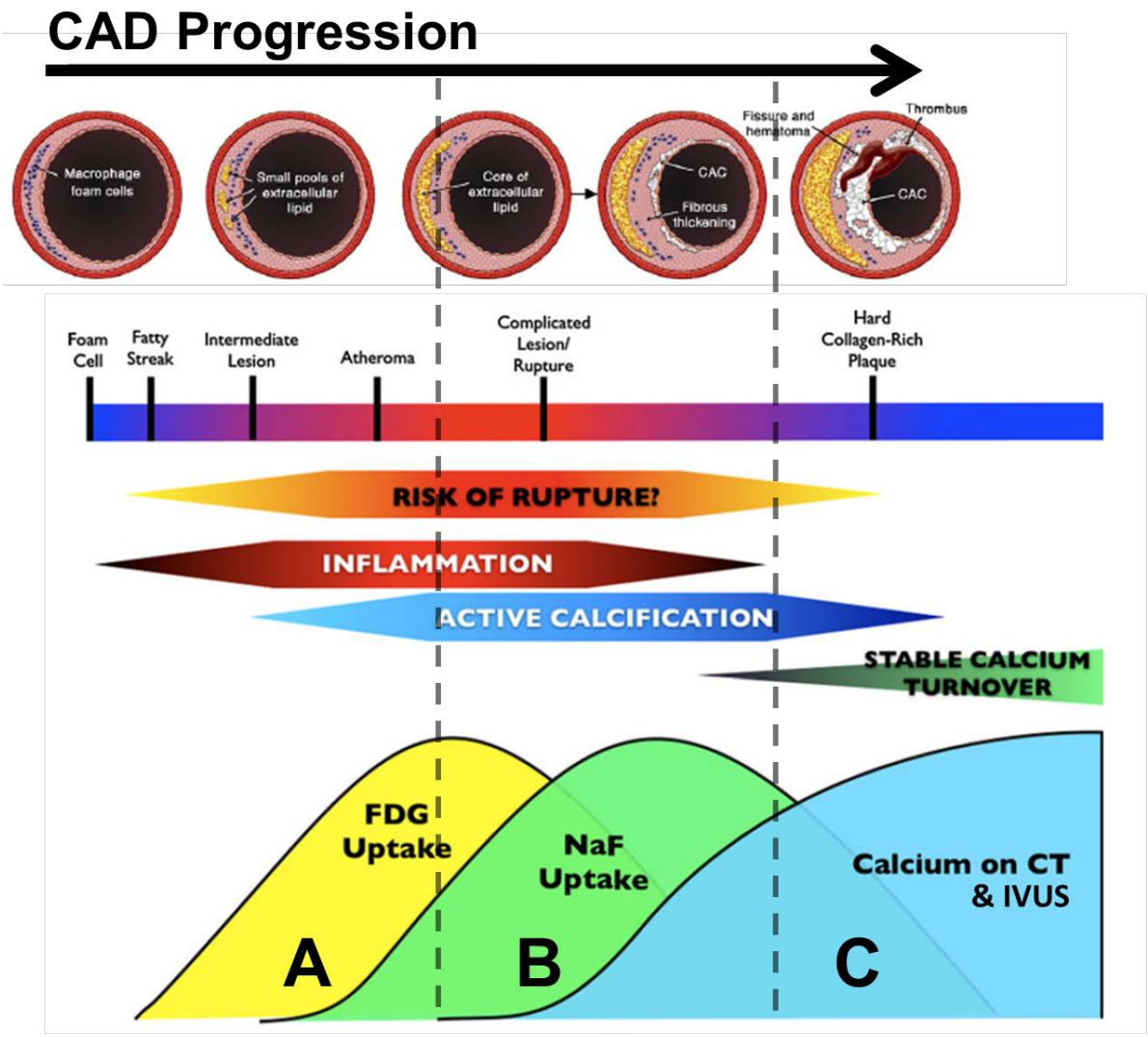
CAD Progression
Macrophage foam cells
Small pools of extracellular lipid
Core of extracellular lipid
CAC
Fibrous thickening
Fissure and hematoma
Thrombus
CAC
Foam Cell
Fatty Streak
Intermediate Lesion
Atheroma
Complicated Lesion/ Rupture
Hard Collagen-Rich Plaque
RISK OF RUPTURE?
INFLAMMATION
ACTIVE CALCIFICATION
STABLE CALCIUM TURNOVER
FDG Uptake
NaF Uptake
Calcium on CT & IVUS
A
B
C

Figure 5.3.

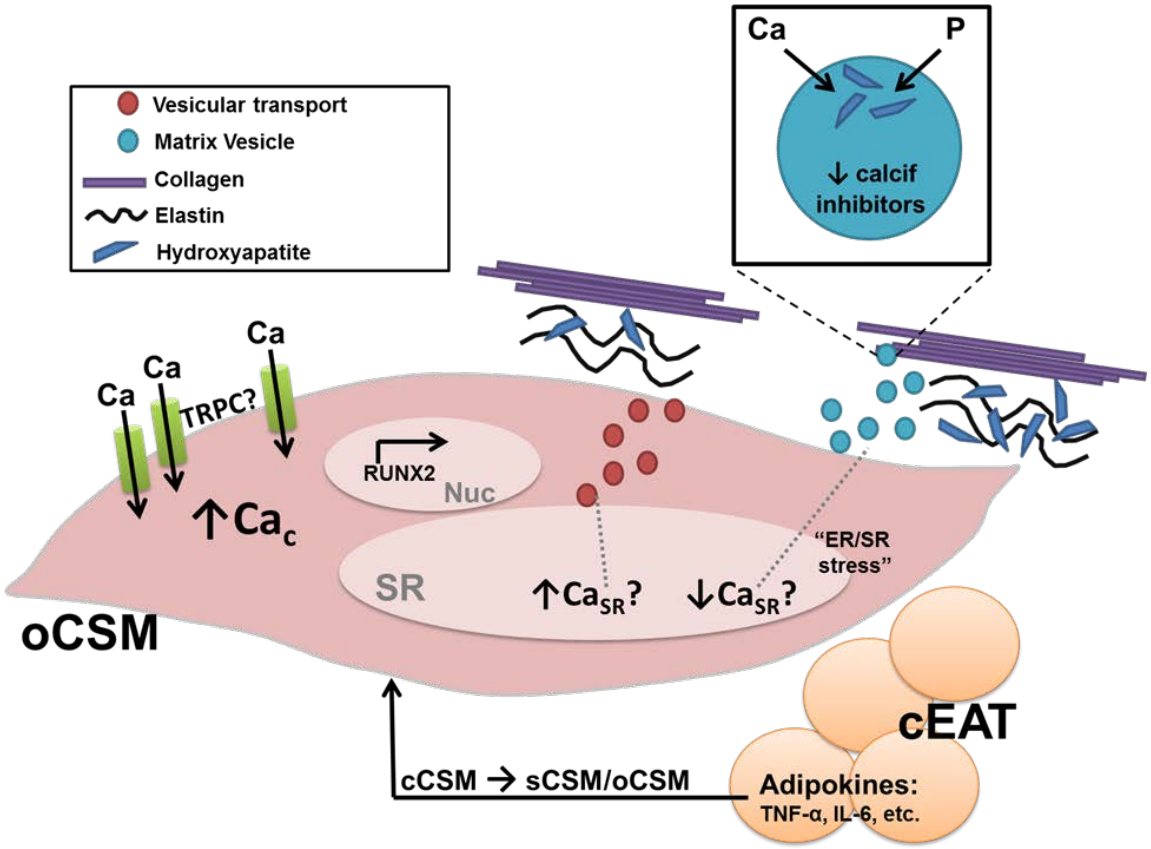
Vesicular transport
Matrix Vesicle
Collagen
Elastin
Hydroxyapatite
Ca
P
↓ calcif inhibitors
Ca
Ca
Ca
TRPC?
↑Ca$_c$
RUNX2
Nuc
SR
↑Ca$_{SR}$?
↓Ca$_{SR}$?
"ER/SR stress"
oCSM
cEAT
cCSM → sCSM/oCSM
Adipokines:
TNF-α, IL-6, etc.

LIST OF APPENDICES

APPENDIX A

PROCOTOL FOR 18F-NAF PET/CT IMAGING OF OSSABAW SWINE

Paul R. Territo, Ph.D.,10/02/12; Mikaela L. McKenney, 07/31/14

Study Protocol Title: Does high calcium intake exacerbate Atherosclerosis

Standard Conditions:

The Standard Conditions section includes baseline parameters for this model; Briefly describe differences below and in detail as necessary in the body of the protocol.	
Number of Animals	24
Number of Treatment Groups	2
Dosing Routes	IV – PET IV – CT
Dosing Frequency	IV – 1/PET IV – 1/CT
Strains	Ossabaw
Sex	Female
Species (1 per Template)	Swine
Duration of Live Phase	8 weeks
Study Type	chronic
Endpoints	PET/CT
Deliverables	Raw Images, Summary Data
Is this a Standard Study?	NO
If NO, briefly describe Non-Standard Conditions	This project will combine gated PET for determination of cardiac vascular calcifications with traditional measures acquired with gated CT angiography.

IIBIS Resource Areas:

Resource Needs:	☐ Clinical Pathology ☐ Histology ☐ Necropsy ☐ Animal/Vet Care ☐ Dose Formulations ☐ Sample Processing	☐ Surgery ☒ Imaging ☐ Imaging Histology ☐ Flow Cytometry ☐ Other:

1. Study Summary:

IIBIS Study Number	2013-00055
Sponsor Reference Number (Optional)	Ossabaw 26
Regulatory Status:	Non-GLP
☒Sponsor IACUC Protocol	3645
☐IIBIS IACUC Protocol	N/A
Test Facility:	IIBIS Core Department of Radiology & Imaging Sciences Indiana University 950 West Walnut, R2 Indianapolis, IN 46202
IIBIS PI	Paul R. Territo, Ph.D
Assay Name:	Large animal imaging
Assay Type:	Acute

Research Area:	Cardiovascular	
What are the deliverables:	☒Raw Images ☒Raw Data ☐Annotation Table ☒Analysis Data ☒Parametric Images ☒Graphs/Figures ☒Statistical Analysis	☐Specimens (Tissue /Samples) ☐Animals (Surgery) ☐Other: ☐Interim Report ☐Final Report
Study Purpose:	The purpose of the current study is to determine vascular calcification via NaF PET, and CTA methods.	
Success Measures:	Successful completion of the live phase.	
Expected Quantitative Controls:	Historical Study Data: No	
	Study References: N/A	
	Positive Control Value: N/A	
	Negative/Vehicle Control Value:	
	Variability within replicates: <50%	
	Minimum # of surviving animals/grp at end of study: 23	
Assay Specific Criteria:	N/A	
Assay Type:	☒Exploratory (Pilot) ☐Model Development ☐Pharmacological Validation ☐Statistical Validation ☐Model Transfer ☐Other:	

2. Key Personal:

2.1. Sponsor's Personnel

Sponsor Scientist:	Michael Sturek, Ph.D
Phone:	(317) 274-7772
Email:	msturek@iupui.edu
Sponsor Scientist:	Mouhamad Alloosh, MD
Phone:	(317) 503-4671 (cell)
Email:	malloosh@iupui.edu
Sponsor Scientist:	James Byrd
Phone:	(317) 278-3711 (317)-362-3005 (cell)
Email:	jvucheti@iupui.edu

2.2. IIBIS Personnel

IIBIS Scientist:	Paul R Territo, Ph.D
Phone:	(317) 278-3313
Email:	pterrito@iupui.edu
IIBIS Scientist:	Gary Hutchins, Ph.D
Phone:	(317) 274-3687
Email:	gdhutchi@iupui.edu
IIBIS Scientist:	Yun Liang, Ph.D
Phone:	(317) 274-1843
Email:	yliang1@iupui.edu
IIBIS Scientist:	Mandy Riley, RLAT
Phone:	(317) 278-7414
Email:	amariley@iupui.edu
IIBIS Scientist:	Wendy Territo, CNMT, RT(R)(N)
Phone:	(317) 274-2570
Email:	wterrito@iupui.edu
IIBIS Scientist:	Kevin Perry, CNMT
Phone:	(317) 274-2570
Email:	kperry2@iupui.edu

3. Dosing and Formulations - PET

Dose Description	All dose materials will be pre-formulated as aqueous solutions of ^{18}F-NaF
Dosing:	1/subject @ 30-35mCi ^{18}F-NaF
Vehicle:	Sterile Saline
Correct for Specific Activity:	N/A
Frequency of preparation:	Per day (3 doses total)
Dose Target Times:	(1 dose/day) 14:00-14:30 (2 dose/day) 14:00-14:30 16:00-16:30
Supplier:	Siemens PETNet, to be ordered by IIBIS personnel at least 1 week prior to study conduct.
Dose Uptake Interval	2.5h prior to initial PET scan
Dose Route	IV – Vascular access port via jugular vein
Alt. Dose Route	IV – Vascular access port via ear vein
Dose Times:	To be recorded according to atomic clock.
Clock Calibration: (IIBIS Personnel)	The atomic clock should be calibrated to the scanner time each day prior to study start.
Disposition/disposal of Materials Provided:	Per departmental SOP. All other materials and waste will be disposed of and documented by the sponsor.

4. Dosing and Formulations - CT

Dose Description	All dose materials will be pre-formulated as aqueous solutions of Isovue
Dosing:	Isovue 370 – 125ml (76%)
Power Injector Parts	Medrad Stellant (P/N 130745) 200ml syringe, 1 low pressure coil, 1 spike.
Dose Volume:	100 ml in total volume /subject
Dose Rate:	4 ml/sec for 25 sec total
Vehicle:	Sterile Saline
Supplier:	To be ordered by IIBIS personnel at least 1 week prior to study conduct.
Dose Uptake Interval	N/A
Dose Route	IV – Vascular access port via jugular vein
Alt. Dose Route	IV – Vascular access port via ear vein
Dose Times:	To be recorded according to scanner clock.

Disposition/disposal of Materials Provided:	Per departmental SOP. All other materials and waste will be disposed of and documented by the sponsor.

5. Animal Information

Species:	Swine
Strain:	Ossabaw
Vendor:	Purdue University - Breeding Program
Sex:	Female
Age/Weight:	50-120kg
Quantity to order	N/A (supplied by sponsor)
Quantity to enroll in the study:	24
Acclimation during Pre-Treatment Phase:	Per IACUC guidelines

5.1. Diet and Water

Diet Description/Supplier:	Provided by sponsor: KT324 with three different calcium's concentration
Water Type:	Indianpolis City Water

5.2. Housing

Housing:	Individually house in USDA approved space at LARC
Environmental Conditions:	Photoperiod: 12 hours light, 12 hours dark (may be interrupted for study-related activities). The animals were placed in normal light cycle i.e. from 6 pm to 6 am (dark cycle). Temperature: 72 ± 8°F Relative humidity: 20% - 80%

6. Pre-Treatment Phase

Clinical Signs:	Conducted by Sponsor Personnel
Body Weights:	Prior Imaging – Provided by Sponsor
Animal Distribution:	Animals will be segregated into individual pens with unique identification.
Pre-Treatment Requirements:	Animals should be in good health and acclimated for at least 2 days prior to study conduct.

7. Treatment Phase

Feeding/Fasting (type/date/time):	Animals should be fasted for a minimum of 12 hours prior anesthetic induction and/or tracer administration. In all cases, animals will have ad libitum access to water.

8. Terminal Phase

Animal Disposition:	• Dosed animals that are found dead contact the sponsor and alternate sponsors at the above listed numbers and email with findings. • Animals are to be transferred to sponsor for disposition of carcass according to RSO and NRC guidelines.
Euthanasia:	Per IACUC protocol guidelines

9. Necropsy Specimen Collection

Collection methods:	N/A

10. Phamacokinetics (PK)

Time Points:	N/A

11. Sample Analysis

Sample Preparation:	N/A

12. Study Procedures

Study Overview

In general, the study will composed of 18F-NaF list mode data acquisition with capture of ECG gating information. Gated Cardiac PET sequence, retrospectively gated into 8-16 phases of the cardiac cycle depending on image SNR. In addition, Static Abdominal PET images will be acquired at 3 bed positions which will encompass abdominal aorta from the apex or the heart through to femoral bifurcation. At completion of the PET, prospectively gated unenhanced CT for coronary calcium scoring and Contrast Enhanced Gated Cardiac CT Angiography will be acquired and retrospectively gated into 8-16 phases of the cardiac cycle, with matching bin alignment to PET sequence.

Animal Preparation

Up to 2 animals per day will be injected with 30-35mCi radiotracer described in ***"Dosing and Formulations - PET"***, and after 2.5 hr of tracer uptake, each animal will be induced at the LARC facility with Telazol (4.5-6.6 mg/kg) with Xylazine (2.2 mg/kg), intubated, and maintained on 1-5% Isoflurane (balance medical air) during transport from LARC to the placement on the imaging bed at IUH (Rm. 1117). Upon completion of the PET sequence, each animal will be infused with 100ml total of Isovue 370 contrast using the Stellant power injector wit materials and methods described in ***"Dosing and Formulations - CT".***

Study Sequence

Animals will be imaged using Siemens Biograph 64 PET/CT located at IUH according to the protocols and parameters outlined in "***Image Acquisition***". Images will be reconstructed according to the modality using the params found in the ***"Image Reconstruction"*** section of the protocol. In all cases, animals will generally follow the temporal sequence for study conduct as outlined in ***"Estimated Daily Study Schedules"***, where group replicates will be performed at regular intervals detailed in the ***"Estimated Weekly Study Schedules"***.

Image Naming Convention

Each animal's images should be named such that they can be uniquely identified by combination of Animal ID and IIBIS ID, as illustrated below:

Animal ID: Ossabaw Pig 2214
IIBIS ID: 2013-00055

PET/CT Field Name	Example Values
Last Name:	Ossabaw_Pig_2214
Patient ID:	2013_00055_ Ossabaw_Pig_2214

System:	Siemens BioGraph 64 PET/CT
Attenuation Sequence (1):	CT TOPOGRAM
Parameters (1):	Collimation 64x0.625 mm Slice thickness 0.60 mm Slice increment 1.00 mm Slice length 1024mm Voltage 140 kV Current 35 mA mAs 170 mAs Image matrix 512 x 512 Orientation Caraniocaudal
Acquisition Sequence (2): (Gated Cardiac PET)	PET_CARD_LM_SWINE
Parameters (2):	Isotope 18F Target Dose 10-15mCi Scan Mode Listmode Scan Range Match CT Localizer Scan Duration 30min Orientation Caraniocaudal Trigger ECG
Attenuation Sequence (3):	CT TOPOGRAM
Parameters (3):	Collimation 64x0.625 mm Slice thickness 5.00 mm Slice length 1370mm Voltage 120 kV Current 35 mA mAs 325 mAs Delay 4 s Scan Time 24.57 s Image matrix 512 x 512 Orientation Caraniocaudal
Acquisition Sequence (4): (Static Abdominal PET)	1_PETCT_WHOLEBODY_SWINE
Parameters (4):	Isotope 18F Target Dose 10-15mCi Scan Mode Normal Scan Range Match CT Localizer Bed Count 3 Scan Duration 5min/Bed Orientation Caraniocaudal Trigger None

Image Acquisition – CT/CTA

System:	Siemens BioGraph 64 PET/CT
Acquisition Sequence (5): (Coronary Calcium Scoring)	Coronary Calcium Scoring
Parameters (5):	Collimation 24x1.2 mm Slice thickness 1.20 mm Slice increment 1.20 mm Pitch 1 Rotation time 0.5 s FOV 500 mm Voltage 120 kV Current 600 mA mAs 300 mAs Image matrix 512 x 512 CTDIvol 26.2 mGy Gating phase 65%
Acquisition Sequence (6): (Gates-Contrast CTA)	CORONARYCTA_STUREKPIG
Parameters (6):	Collimation 64x0.6mm Slice thickness 0.6 mm Slice increment 0.4 mm Pitch 0.20 Rotation time 0.33 s FOV 180 mm Voltage 120 kV Current 606mA mAs 1000 mAs Image matrix 512 x 512 CTDIvol 47.0 mGy Contrast Isovue 370 Volume 100 Cc in total volume Injection Rate 4 cc/sec injection rate Gating phases 65%; and additional 16 in accordance with PET.

Image Reconstruction – PET

Acquisition Sequence (1):	CT TOPOGRAM
Parameters (1):	Method: FBP SP Filter Yes Adaptive Filter N0 Filter B Tagging None
Acquisition Sequence (2): (Gated Cardiac PET)	PET_CARD_LM_SWINE
Parameters (2):	Model Offline Method Backprojection Filter 70% Hanning FWHM 2mm Zoom 1.0 Tagging ECG Phases 16
Attenuation Sequence (3):	CT TOPOGRAM
Parameters (3):	Method: FBP SP Filter Yes Adaptive Filter N0 Filter B Tagging None
Acquisition Sequence (4): (Static Abdominal PET)	1_PETCT_WHOLEBODY_SWINE
Parameters (4):	Model Online Recon Backprojection Filter 70% Hanning FWHM 2mm Zoom 1.0 Tagging None

Image Reconstruction – CT/CTA

Acquisition Sequence (5):	CORONARY CALCIUM SCORING
Parameters (5):	Method: FBP SP Filter Yes Adaptive Filter No Filter B35F Heart View Medium Tagging 65%
Acquisition Sequence (6): (Gated-Contrast CT)	CORONARYCTA_STUREKPIG
Parameters (6):	Method: FBP SP Filter Yes Adaptive Filter Yes (Cardiac) Filter B25F smooth ++ Tagging ECG: 65% A Phases 16

Image Quantification

1. PET Imaging

PET images will be co-registered to CT images using a mutual information based normalized entropy, 3D-Voxel Registration, algorithm in Analyze 11.0 (AnalyzeDirect, BIR Mayo Clinic). CT images will be segmented into blood pool (cardiac chambers and major vessels) and myocardial tissue using either: 1) Object Extractor, an object based region growing algorithm, or 2) Manual segmentation. Segmented blood pool and myocardial tissue VOIs will then be applied to PET images and SUV (or %ID/g) in each volume of interest (VOI) will be calculated according to standard methods described previously [1]. In all cases, image segmentation and image quantification will be performed using Analyze 11.0 software (AnalyzeDirect, BIR Mayo Clinic).

2. CT/CTA Imaging

PET images, where appropriate, will be co-registered to CT using a mutual information based normalized entropy, 3D-Voxel Registration, algorithm in Analyze 11.0 (AnalyzeDirect, BIR Mayo Clinic) software according to [2]. Gated Non-Contrast CT will be analyzed utilizing the Philips EBW(Extended Brilliance Workspace, Philips Healthcare Nederland B.V. Best, The Netherlands). The Agatston scoring method (130 HU) Threshold, Density Mode: Maximum) will be performed on the images obtained. Curved Plane MPR and 3D Images of the CTA images will be extracted utilizing the Comprehensive Cardiac Software to evaluate the contrasted images.[3]. Upon request from the investigators, further analysis and statistics may be performed.

13. Estimated Study Schedule

Estimated Daily PET/CT Study Schedule #1 – 1 per day		
Session	**Time**	**Task**
Setup	16:30-17:00	Instrumentation Draping
Animal 1	14:30-16:30 16:30-16:45 16:45-17:00 17:00-17:05 17:05-17:35 17:35-17:50 17:50-18:20 18:20-19:00	Tracer Administration/Uptake Transfer from LARC to IUH Start Beta-Blockade Attenuation CT Gated Cardiac PET Static Abdominal PET Non-Contrast CT Gated Contrast CT
Cleanup	19:00-19:30	Instrumentation Decontamination
Estimated Daily PET/CT Study Schedule #2 – 2 per day		
Session	**Time**	**Task**
Setup	16:30-17:00	Instrumentation Draping
Animal 1	14:30-16:30 16:30-16:45 16:45-17:00 17:00-17:05 17:05-17:35 17:35-17:50 17:50-18:20 18:20-19:00	Tracer Administration/Uptake Transfer from LARC to IUH Start Beta-Blockade Attenuation CT Gated Cardiac PET Static Abdominal PET Non-Contrast CT Gated Contrast CT
Animal 2	16:30-18:30 18:30-18:45 18:45-19:00 19:00-19:05 19:05-19:35 19:35-19:50 19:50-20:20 20:20-21:00	Tracer Administration/Uptake Transfer from LARC to IUH Start Beta-Blockade Attenuation CT Gated Cardiac PET Static Abdominal PET Non-Contrast CT Gated Contrast CT
Cleanup	21:00-21:30	Instrumentation Decontamination

14. Statistics and Reporting

Evaluate image data for endpoints will be conducted in collaboration between respective scientists listed on the protocol, unless otherwise indicated.

15. Literature References

1. Dandekar, M., J.R. Tseng, and S.S. Gambhir, *Reproducibility of 18F-FDG microPET studies in mouse tumor xenografts.* J Nucl Med, 2007. **48**(4): p.

2. Studholme, C., D.J. Hawkes, and D.L.G. Hill, *A normalized entropy measure for multimodality image alignment.* Proc SPIE Medical Imaging 1998. **3338**: p. 132-143.
3. Otton, J.M., et al., *A method for coronary artery calcium scoring using contrast-enhanced computed tomography.* J Cardiovasc Comput Tomogr, 2012. **6**(1): p. 37-44.

16. Deliverables, Statistics and Reporting

Statistical analysis and interpretation of the results is the responsibility of the sponsor, unless stated otherwise.

IIBIS Statements of Study Conduct

17. Animal Care and Use Statement

All procedures in this protocol are in compliance with the U.S. Department of Agriculture's (USDA) Animal Welfare Act (9 CFR Parts 1, 2, and 3); the Guide for the Care and Use of Laboratory Animals, Institute of Laboratory Animal Resources, National Academy Press, Washington, D.C., 1996; and the National Institutes of Health, Office of Laboratory Animal Welfare. Whenever possible, procedures in this study are designed to avoid or minimize discomfort, distress, and pain to animals.

18. Alteration of Design

Prior to making changes to the approved protocol, the Lead Scientist or Alternate will consult the Sponsor as appropriate. The date that sponsor approval is received will be documented in all amendments.

19. Regulatory Compliance

This non-clinical laboratory study is not intended to be conducted in full accordance with the United States Food and Drug Administration (FDA) Good Laboratory Practice (GLP) regulations, 21 CFR Part 58, but will be conducted in accordance with IIBIS standard operating procedures.

20. Veterinary Care/Treatment

This study will comply with all applicable sections of the Guide for the Care and Use of Laboratory Animals (National Research Council 1996). Wherever possible, procedures used in this study are designed to avoid or minimize discomfort, distress, and pain to animals. All procedures are described in this study protocol or in written laboratory procedures. These procedures are based on the most current available technologies concerning proper laboratory animal use and management.

21. Palliative and Prophylactic Measures

Following study distribution, the study director and sponsor/designee (if possible) will be included in discussions of palliative and prophylactic procedures (nonlife-threatening conditions, including suspension of dosing and removal of animals from study) recommended by the attending veterinarian. Final authority for decision making will be with the Laboratory Animal Veterinarian.

22. Reports

22.1. Interim Report

An electronic copy of the interim report, if applicable, will be available to the sponsor.

22.2. Final Report

An electronic copy of the final report, if applicable, will be available to the sponsor.

23. Record Retention

The raw data, documentation, specimens, the protocol, and any study related materials requested in section 1 for this study will be stored in the IIBIS archives for at least 1 year after study finalization. The sponsor will be responsible for the maintenance of the test and control article reserve samples.

APPENDIX B

PROTOCOL FOR DISPERSION OF VASCULAR SMOOTH MUSCLE CELLS (SMC)

Michael Sturek Ph.D, MLM, 8/19/13, MLM SLD, 07/25/14

Current Date ___-___-___ Initials_____

1. Conduit coronary arteries of swine are typically used. The artery is classified as proximal, middle, and distal thirds. At euthanasia/tissue collection, grossly dissect vessels by first locating vessel and then making a transverse cut through myocardium near ostium. Remove entire length of conduit artery with minimal adjacent cardiac muscle, fat, etc. attached. Place the tissue into wide-mouth bottle containing »50-75 ml ice-cold 2CaNa. Place immediately into cooler filled with ice. (NOTE: in the case of overnight transport, store tissue in EH storage media on ice.)

[Animal: Pig# _____, Age _____, Time dead _____, Misc. _____]

[**Portion of artery**: Proximal ___, Middle ___, Distal

Artery: LAD___ RCA ___ CFX ___ Other?_____]

[**Date** ____-____-____, Time of storage _____]

2. Clean artery of adherent connective tissue, fat, cardiac muscle, etc. in cell culture hood in 100 x 20 mm culture dish in »30 ml Low Ca. (see COR OC_METv3.docx) Treat artery gently (do not stretch excessively, if possible).

****At this point, the artery can be stored in the refrigerator in storage media for 2-5 days, if necessary.**

[Storage media = EH + PS]

[In refrigerator: Date ____-____-____ Time _____]

3. Cut open artery longitudinally to reveal lumen. Pin down the artery with the lumen facing up in a 30 ml Sylgard jar with 2 mL Collagenase solution. (Approximately a 1 cm^2 area of vessel is enough to yield several million SMC.) Pin the artery segment on all corners and at the middle to increase surface area.

4. Place jar in 37° C shaking water bath (100 strokes/min; 5.5 on dial) for 60 min. The jar should be placed so that the long axis of the vessel segment is parallel with the direction of the shaking.

[Collagenase batch: Date made: ____-____-____, Made by: _____]

[**Dispersion 1**: Date ____-____-____,

Time started _____, Time ended _____]

5. Aspirate supernatant and pipette over artery several times to loosen isolated CSM. Place drop of supernatant in 35 mm petri dish on microscope and observe. (At this point expect mostly connective tissue, endothelial cells (EC), etc., but few CSM. EC are round and clump together in bunches.) Note appropriately and either: 1) discard_____, 2) save in 15 ml tube for immediate fura-2 or patch-clamp studies_____. If #2, transfer supernatant to 15 mL conical

tube and clearly label with pig number and cell fraction. Centrifuge at 900 rpm (**Not RCF**) for 4 min, remove supernatant (**Be careful not to aspirate the pellet!),** then resuspend pellet in 1 mL of freshly prepared 0.02%BSA in 2CaNa (20 mg BSA/10 mL 2CaNa). Add 2.5µL fura-2 AM and triturate several times. Place in 37° C water bath for ~30-45 mins.

Cell fraction: _____ (Ignore this section if discarded)

[Dye: Fura-2____, Other_____ Dye concentration _____]

[Loading: Date ____-____-____,

Time started _____, Time ended _____]

6. Add another 2 mL Collagenase solution to Sylgard jar and repeat steps 4 and 5 until isolation is complete.

Step 4:

[**Dispersion 2**: Time started _____, Time ended _____]

Step 5:

Cell fraction: _____

[Dye: Fura-2____, Other_____ Dye concentration _____]

[Loading: Date ____-____-____,

Time started _____, Time ended _____]

Step 4:

[**Dispersion 3**: Time started _____, Time ended _____]

Step 5:

Cell fraction: _____

[Dye: Fura-2____, Other_____ Dye concentration _____]

[Loading: Date ____-____-____,

Time started _____, Time ended _____]

7. Centrifuge cells at 900 rpm for 4 min, resuspend in EH solution and put in 37° C water bath for ~20 min.

[Time started _____, Time ended _____]

8. Centrifuge cells at 900 rpm for 4 min, resuspend in 0.02%BSA in 2CaNa and chill on ice. Wrap tubes in foil to protect from light exposure.

NOTES:

1. All steps following fura-2 loading, CSM are light-sensitive. When possible, minimize exposure to light.
2. "Overnight dispersion" - It is also possible to disperse by exposing cells to 2 mL collagenase in bottle at room temp. for »8-10 hours.

APPENDIX C

EXPERIMETNAL SOLUTIONS

8-20-13 ***Collagenase (in Low Ca)***

Component	Concentration	20 ml tot.	10 ml tot.	Stock
Collagenase, CLS II	300 U/mL	20 mg	10 mg	300 U/mg (04-12-12, Worthington)
BSA (Fraction V)	0.2% (wt/vol)	40 mg	20 mg	(09-94, Sigma-Aldrich)
Soybean Trypsin Inhibitor Type SI	0.1%	20 mg	10 mg	2.17 mg trypsin/mg (03-04-14, Worthington)
DNase I, Type IV	459 KUnitz/mL	4 mg	2 mg	2297 KUnitz/mg (06-04-14, Sigma-Aldrich)

[Batch: Date made: ____-____-____, Made by: _____]

1. Adjust pH of Low Ca to 7.55, then add collagenase and pH will be exactly 7.40. Filter.

2. Make in 10-20 ml quantities. Each isolation requires at least 4-6 ml collagenase. Remaining collagenase solution may be frozen at -20° C for up to 10 days.

8-3-14 ***2 CaNa***

Components	Conc. (mM)	1000 ml total
$CaCl_2$	2	20 ml of 0.1 M
NaCl	138	138 ml of 1.0 M
$MgCl_2$	1	10 ml of 0.1 M
KCl	5	5 ml of 1.0 M
HEPES	10	10 ml of 1.0 M
Glucose	10	1.8 g
pH (with NaOH)	7.4	3-4 ml of 1.0 M

NOTES:

1. Sterile solutions all contain PS and are sterilized by filtration through Millex-GS 0.2 µm filter or Millipore Stericup apparatus.
2. Penicillin Streptomycin (PS) 100 mg/ml (100 U/ml) is added in a 1:100 (vol:vol) ratio to yield a 1% PS solution.

7-9-87 ***Low Ca***

Components	Concentration (mM)	1000 ml total
$CaCl_2$	0.5	5.0 ml of 0.1 M
NaCl	135	135 ml of 1.0 M
$MgCl_2$	1	10 ml of 0.1 M
KCl	5	50 ml of 0.1 M
KH_2PO_4	0.44	4.4 ml of 0.1 M
Na_2HPO_4	0.34	3.4 ml of 0.1 M
$NaHCO_3$	2.6	26 ml of 0.1 M
Amino Acids	1X	20 ml of 50X
Vitamins	1X	10 ml of 100X
Phenol Red	0.001%	2 ml of 0.5%
HEPES	20	20 ml of 1.0 M
Glucose	10	1.8 g
pH	7.4	with NaOH
PS	1%	10 ml

NOTES:

1. Low Ca is exactly like EH, except that the Ca concentration is only 0.5 mM, and no horse serum is used.

2. Low Ca with horse serum may be used to facilitate acquisition of a seal when doing patch-clamp studies.

7-9-87 ***EH (aka Storage media)***

Components	Concentration (mM)	1000 ml total
$CaCl_2$	2.0	20 ml of 0.1 M
NaCl	135	135 ml of 1.0 M
$MgCl_2$	1	10 ml of 0.1 M
KCl	5	50 ml of 0.1 M
KH_2PO_4	0.44	4.4 ml of 0.1 M
Na_2HPO_4	0.34	3.4 ml of 0.1 M
$NaHCO_3$	2.6	26 ml of 0.1 M
Amino Acids	1X	20 ml of 50X
Vitamins	1X	10 ml of 100X
Phenol Red	0.001%	2 ml of 0.5%
HEPES	20	20 ml of 1.0 M
Glucose	10	1.8 g
pH	7.4	with NaOH
PS	1%	10 ml
Horse Serum	2%	20 ml

NOTES:

1. EH media is a type of Eagle's Minimal Essential Medium (EMEM), but also has HEPES as a pH buffer, so that bubbling the solution with O_2 is not necessary for maintenance of pH.
2. Sterile-filter under laminar flow hood with Millipore Stericup system.

8-4-14 ***2Ca80K***

Components	Conc. (mM)	1000 ml total
$CaCl_2$	2	20 ml of 0.1 M
NaCl	63	63 ml of 1.0 M
$MgCl_2$	1	10 ml of 0.1 M
KCl	80	80 ml of 1.0 M
HEPES	10	10 ml of 1.0 M
Glucose	10	1.8 g
pH (with NaOH)	7.4	3-4 ml of 1.0 M

8-4-14 ***2Ba80K5Na***

Components	Conc. (mM)	1000 ml total
$BaCl_2$	2	20 ml of 0.1 M
LiCl	63	63 ml of 1.0 M
$MgCl_2$	1	10 ml of 0.1 M
KCl	80	80 ml of 1.0 M
HEPES	10	10 ml of 1.0 M
Glucose	10	1.8 g
pH (with NaOH)	7.4	3-4 ml of 1.0 M

APPENDIX D

ORGAN CULTURE OF PIG CORONARY ARTERY RINGS TO INDUCE CALCIFICATION: 7-10 DAYS

Mikaela McKenney, Umut Ulge, 07/23/14

1. Euthanasia per standard protocol. With sterile gloves and sterile tools, remove heart with pericardial sac intact.

2. Lay heart on inside of paper from sterile glove pack and remove the pericardial sac with sterile tools.

3. Thoroughly rinse the heart with ice-cold sterile-filtered 2CaNa + 2% P/S.

4. Transfer rinsed, sterile heart to a sterilized metal stray for gross dissection of the coronary arteries.

5. Grossly dissect ("chunk" with surrounding myocardium) the coronary arteries and place in individual appropriately pre-labeled tubes of 2CaNa + 2% P/S. If possible, have a non-sterile partner to open and close the tubes and cooler. Tubes should be kept on ice at all times.

6. Transfer collected specimens pack to the lab on ice for dissection under the sterile laminar flow hood.

   (see *Cell culture etiquette v3-1.doc* for general guidelines for the use of cell culture facility)

7. Open the hood and turn off the U.V. first, then clean the surface with 70% EtOH. Perform this step first before you prepare other materials to allow for proper air flow and sterility of the hood.

8. Fine dissection of coronary rings can take time. Always keep tissue and solution on ice. To keep "sterile" technique, fill a large weigh boat with ice and wrap with cling plastic wrap, then generously spray with 70% EtOH before placing under the hood.

9. Thaw a frozen aliquot of 50 mL sterile-filtered Low Ca solution. Fine dissection should be performed in this solution within a 100x20 mm culture dish placed on top of ice weight boat.
   (Culture dish may be filled with Sylgard and to aid in dissection)
   *Roboz magnifying surgical loupes can be worn to aid in the fine dissection process.
   ****Tools must be sterile and gloves should be sprayed with 70% ethanol.**

10. After setup is complete, spray the surface of the hood with 70% EtOH again before exposing the sterile tissue.

11. Under the hood, remove grossly dissected artery from its designated 50 mL tube and place in the ice-cold Low Ca solution in the sterile culture dish. Finely dissect coronary artery from myocardium and adventitia carefully and gently. Try not to nick the artery, as this will influence changes to the vascular structure in culture. Blunt dissection technique can help avoid this.

    ****At this point, the cleaned artery can be cold-stored at 4°C in sterile-filtered EH solution for up to 5 days**

12. As the cleaned vessel rests in ice-cold Low Ca solution (this may be replaced as needed during the dissection process), prepare a 6-well plate with 4-5 mL of sterile phosphate-buffered saline (PBS) per well.

13. Cut the cleaned artery into 2-4 mm rings and place each artery in the first well (top left) of PBS in the 6-well plate.

14. Allow rings to sit in PBS for ~30 seconds then transfer to the next well (top middle). Transfer each ring separately and allow excess solution to drip off of the ring into the previous well before transfer. Continue to transfer clockwise until all rings have gone through the complete 6-well serial “sterilization”.

15. Prepare a 12-well plate for culture. (Depending on how the experiment is designed, one may need more than one plate.). Each well should be filled with 2 mL of culture media

CULTURE MEDIA FOR INDUCTION OF IN VITRO CORONARY ARTERY CALCIFICATION: Low-glucose DMEM + 3.8 mM NaPhos + 7.5 U/mL Alkaline Phosphatase: (40 mL total volume)

Ingredient	Stock Conc	Final Conc	Dilution	For 40 mL
Low-glucose Dulbecco's Modified Eagle's Medium (DMEM) + 1% PenStrep (P/S)	1X	1X	1:1	**39.5 mL**
Sodium Phosphate (NaPhos)	760 mM	3.8 mM	1:200	**200 uL**
Alkaline Phosphatase Enzyme (ALP)	1000 U/mL	7.5 U/mL	1:133	**300 uL**

DMEM + 1% P/S: add 50 µL P/S(100X) to 500 mL DMEM stock(Sigma).
*LABEL & DATE the DEMEstock bottle.
NaPhos solution: 17.3 g monobasic(NaH_2PO_4), 87.3 g dibasic(Na_2HPO_4), 1 mL ddH_20, then sterile syringe filtered
ALP: 1000 U/mL frozen stock (Promega)
****Do not keep a stock of calcification media for more than one day. (NaPhos and ALP should be prepared fresh each media change)**

16. Set aside the desired number of rings for Day 0/"Fresh" measures:
    Potential measures for OC time course:
    a. Histopathology: formalin fix
    b. Protein expression: flash freeze
    c. fura-2 Ca imaging: cold-store in EH until experiments
    d. isometric ring tension measures: cold-store in EH until experiments

17. Transfer a single coronary ring into a single well of the prepared 12-well plate.

18. Cover each plate and label appropriately with pig number, date, and culture media for particular rows or columns of wells.

19. Transfer plates to the 37°C incubator. Check that the CO_2 is set to 4.6% and that the tray at the bottom of the incubator is full of distilled water.

20. Media should be changed every 2-3 days. Note the color of the media daily as this is an indicator of pH. Media should appear pink-red. A shift towards acidity (closer to yellow) or alkalinity (closer to dark purple) would indicate the tissue is deprived of something. Acidity is more common and may be seen close to 3 days in the same media. This indicates cell metabolism and time to change media. RECORD DATE OF MEDIA CHANGE.

****Media should be changed under the hood using sterilized glass pipettes and vacuum system. Avoid catching the artery ring on the vacuum pipette tip as this will damage the arterial wall and affect the culture.**

21. For each time point, remove the necessary number of rings per measure. NOTE & DATE wells from which rings were removed.

22. Continue to change media every 2-3 days until culture is complete.

NOTES:

1. All solutions used should be sterile filtered with a 0.22 µm filter system: syringe filter
   (FisherBrand), Stericup, Steriflip (Millipore).
2. Larger coronary rings (domestic pigs) may need closer to 10-14 days in calcification media to
   induce *in vitro* coronary artery calcification.
3. "Low-glucose" DMEM is similar to physiologic blood glucose levels (1 g/L).
4. If freezing freshly dissected rings for protein or gene expression, always tend to those
   specimens first before starting the culture.

APPENDIX E

QUANTIFICATION OF MEDIAL AREA (IMAGEJ, NIH)

NKR 07/2013

1. Once you have set the focus and zoom on the camera, take a picture of the 1000-micron scale with the 2X lens and the 10X lens. (NOTE: once you have set the focus and zoom on the camera you cannot adjust it, as your scale will not reflect any adjustments made)

2. Open ImageJ

3. Then open the 2X scale image.

4. Click the line box in the menu: 

5. Draw a line from one end of the scale to the other, like this:

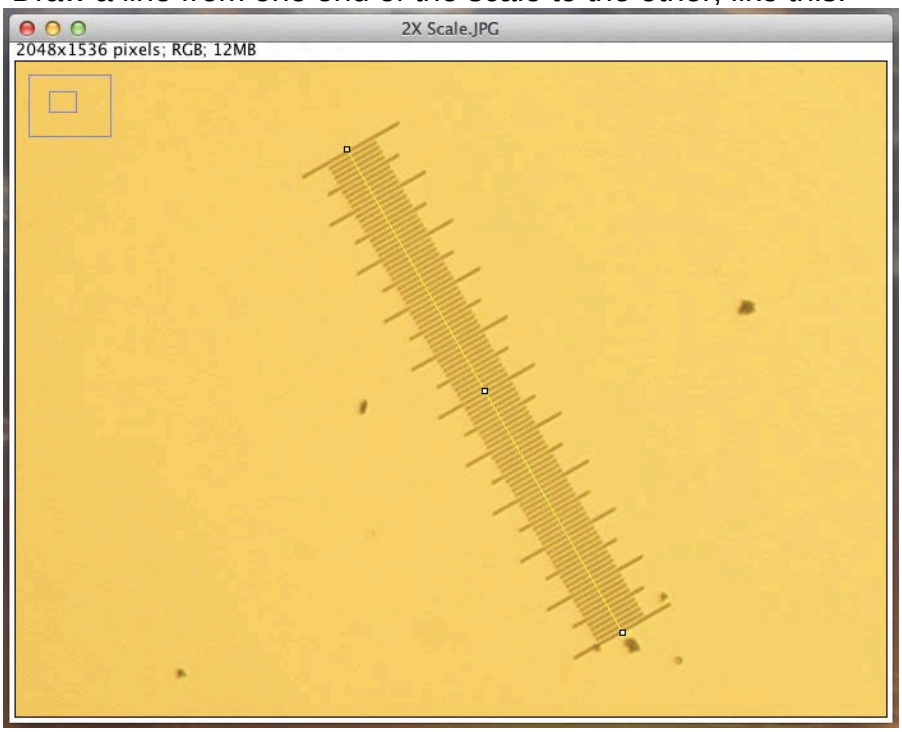

6. Then click set scale:

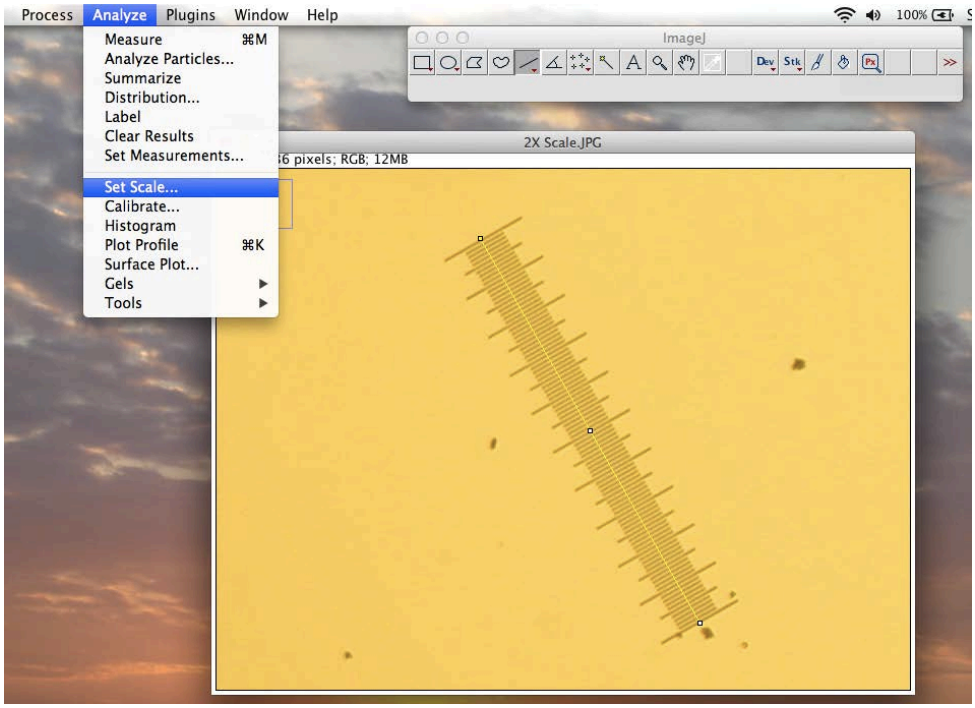

7. A box will pop-up, you should adjust your settings so they look like this (Note: the distance in pixels may differ, as long as you are close, the measurements will work):

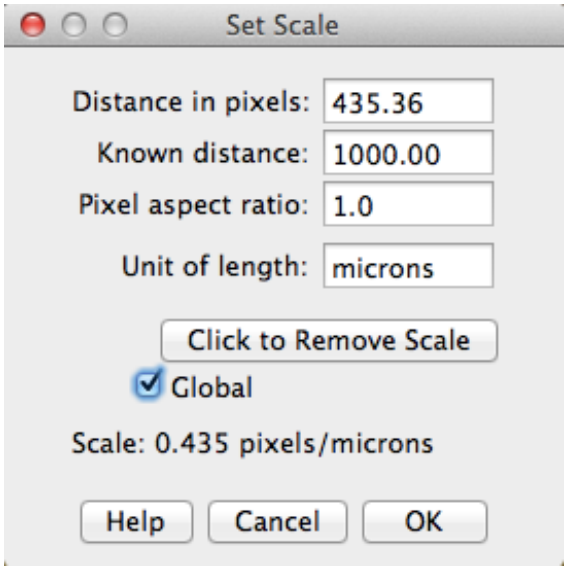

Click ok.

8. Open a coronary ring (2X image) that you would like to measure.

9. Zoom in as much as you like, but you must be able to view the whole ring.

10. Click Process, then click Sharpen:

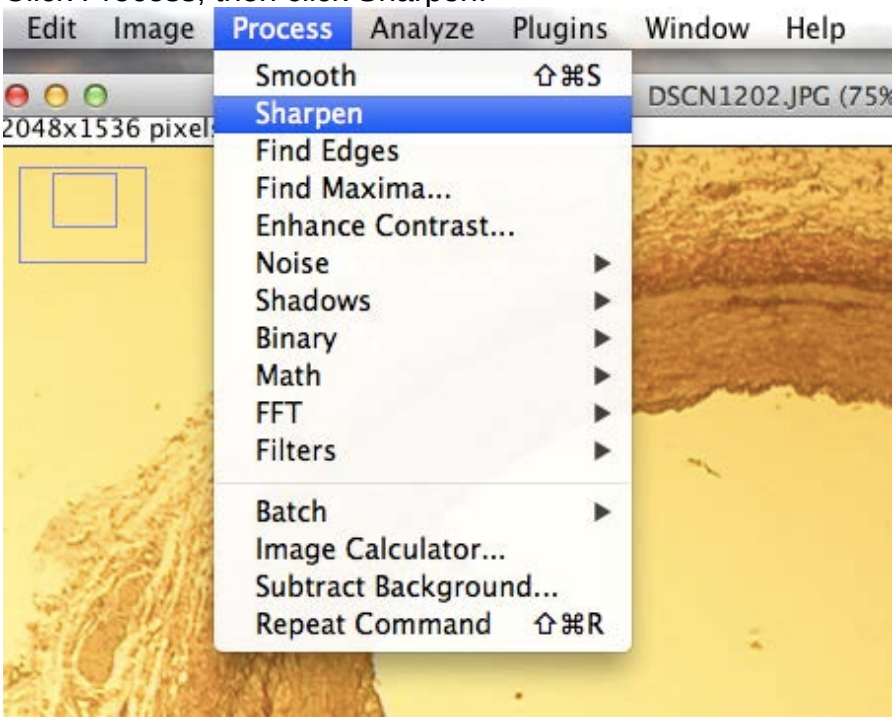

11. Click the Polygon selection tool : 

12. Trace the external elastic lamina (one-click to start the line, double-click to end):

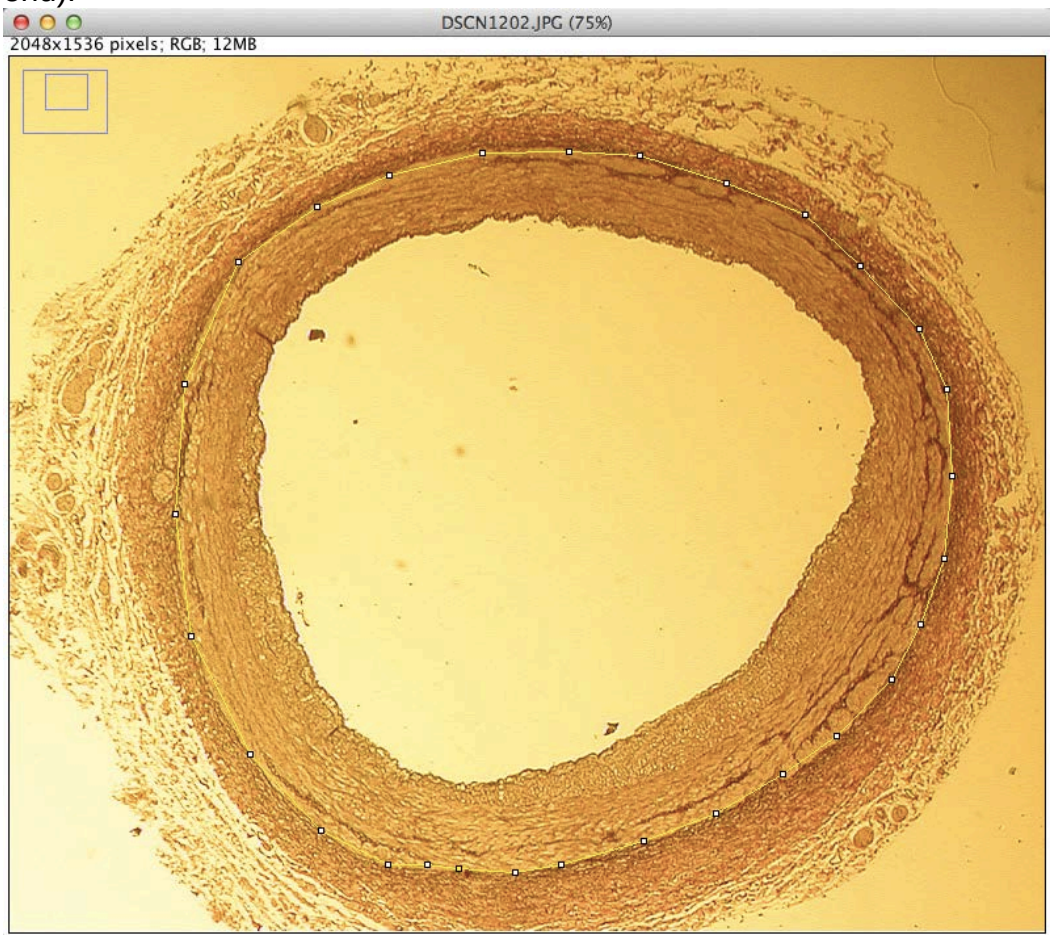

13. Click the letter “M” or ”Ctrl + M” on your keyboard, if it does not work, you can go to Analyze, then click measurement in the Menu bar.

14. A measurement box will pop-up and it will already have the area of the circle:

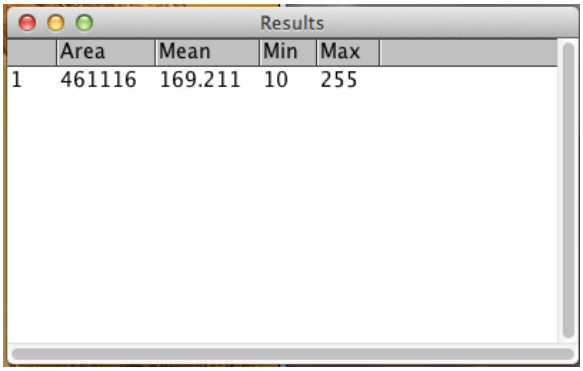

15. Click somewhere outside the selection area to reset the measuring tool, then trace the internal elastic lamina:

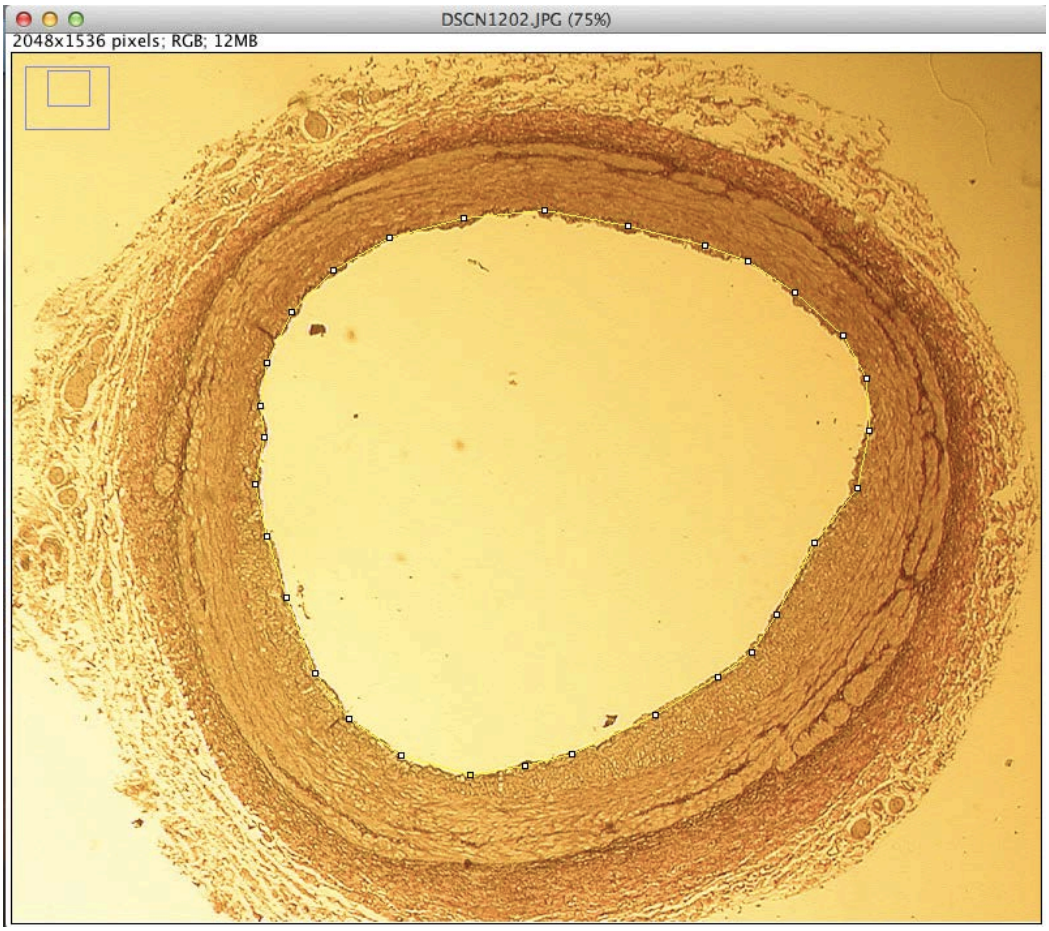

16. Click “M” to measure, now the measurement box should have two measurements:

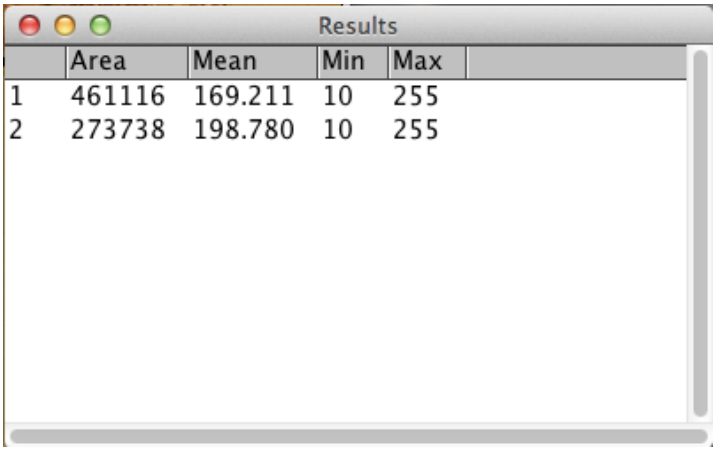

17. If you subtract the 1st number (area of Media + Lumen) minus 2nd number (Lumen), you will calculate the area of the medial layer.

QUANTIFICATION OF COLLAGEN AREA (IMAGEJ, NIH)

NKR 07/2013

1. Once you have set the focus and zoom on the camera, take a picture of the 1000-micron scale with the 2X lens and the 10X lens. (NOTE: once you have set the focus and zoom on the camera you cannot adjust it, as your scale will not reflect any adjustments made)

2. Open ImageJ

3. Then open the 2X scale image.

4. Click the line box in the menu: 

5. Draw a line from one end of the scale to the other, like this:

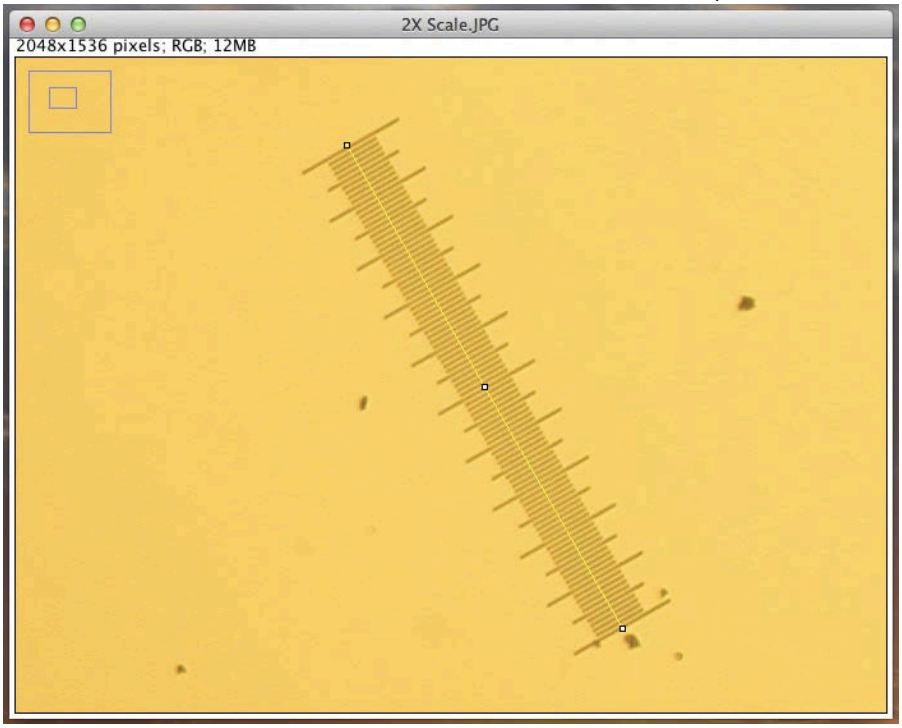

6. Then click set scale:

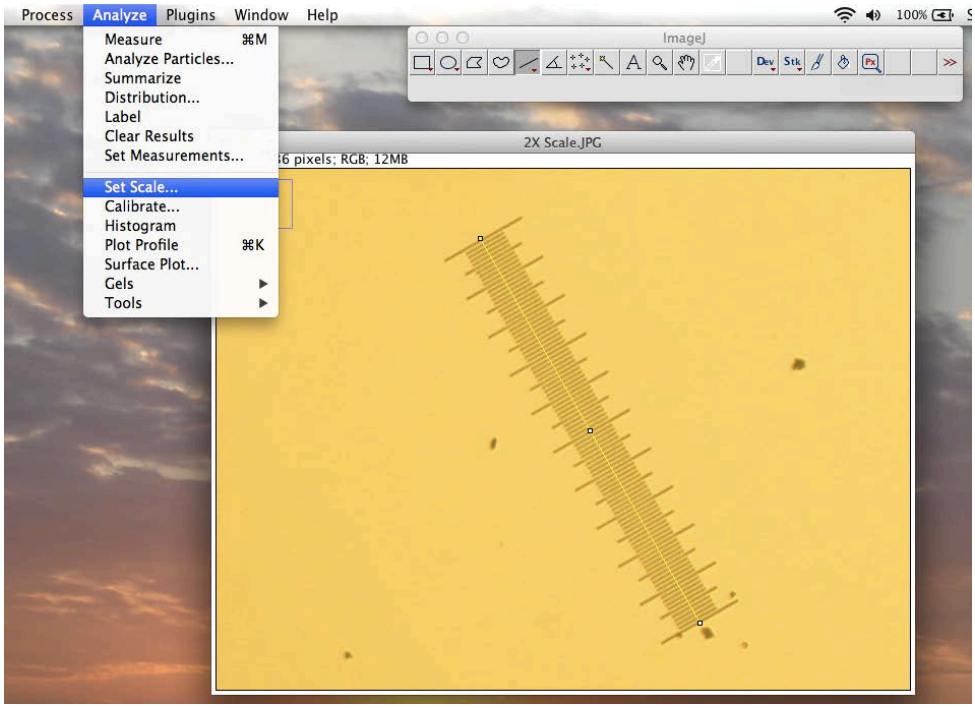

7. A box will pop-up, you should adjust your settings so they look like this (Note: the distance in pixels may differ, as long as you are close, the measurements will work):

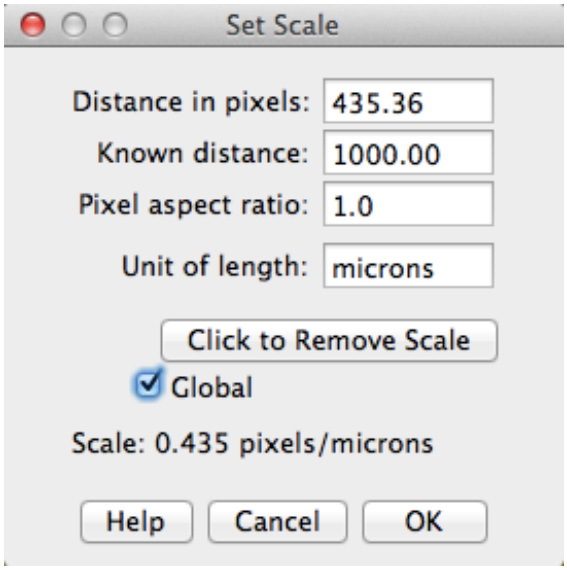

Click ok.

8. Open a coronary ring (2X image) that you would like to measure.

9. Zoom in as much as you like, but you must be able to view the whole ring.

10. Click Process, then click Sharpen:

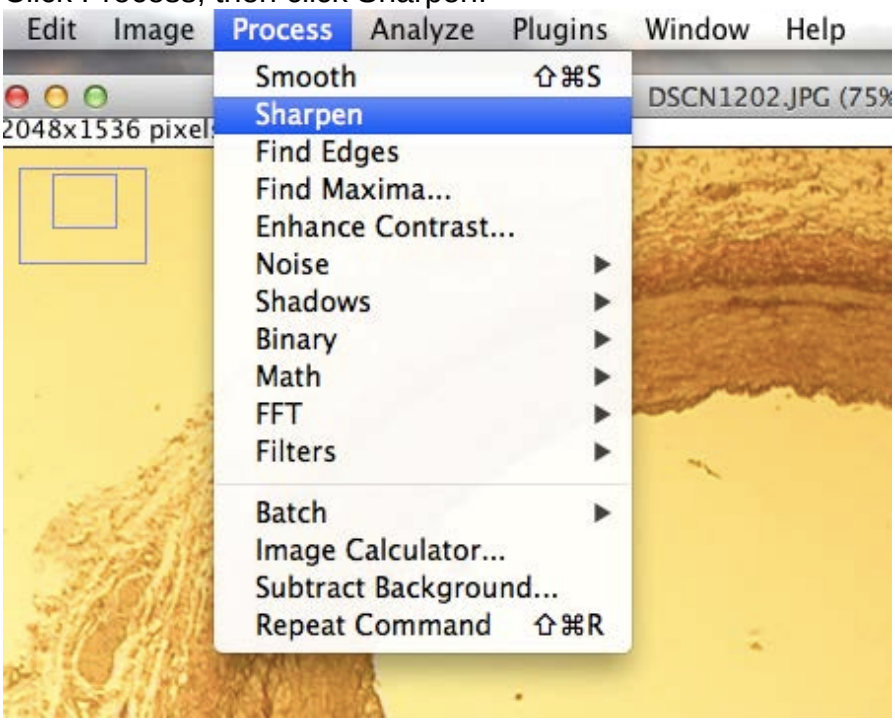

11. Then click Image, then Adjust, then Color Threshold:

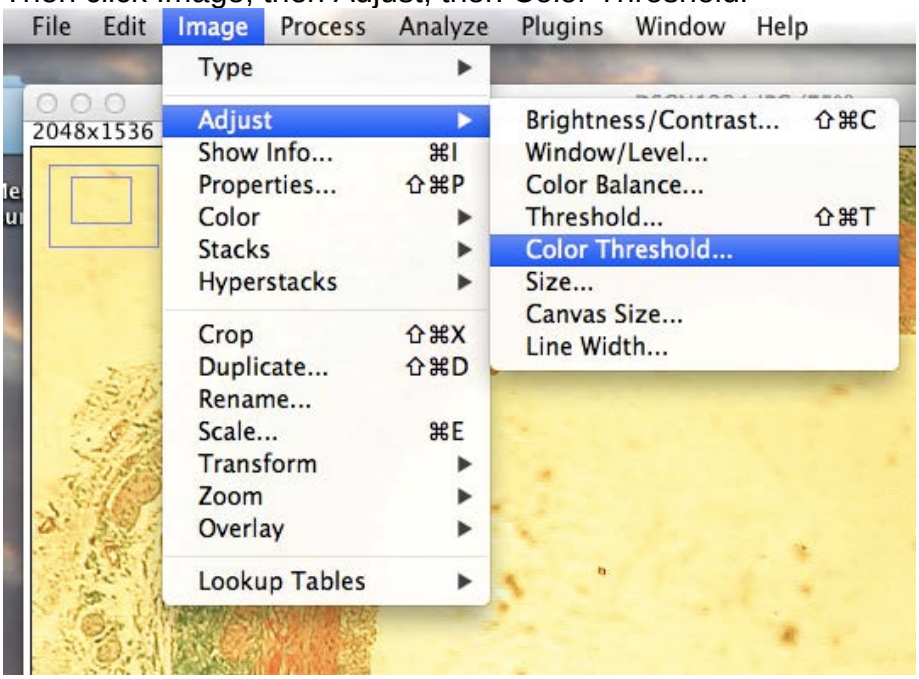

12. Set the color range from 0 to 62, this will exclude all of the red, yellow, and orange colors, thus leaving the collagen stained areas. Also make sure all three fields are “checked” Pass:

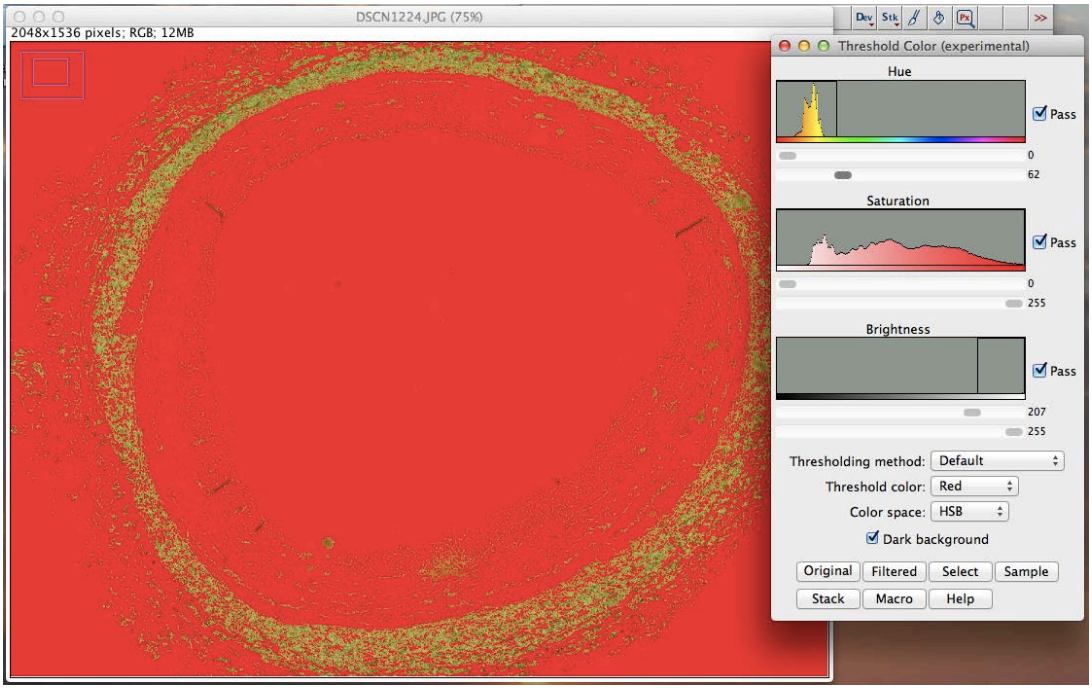

13. Then click Image, Type, then 8-bit:

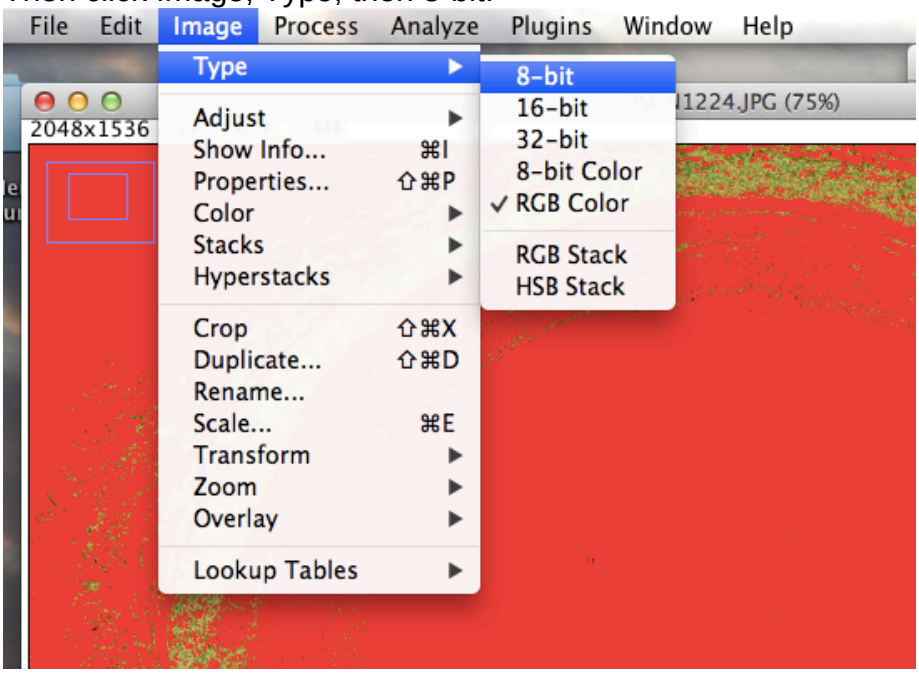

14. Then click Image, Adjust, then Threshold:

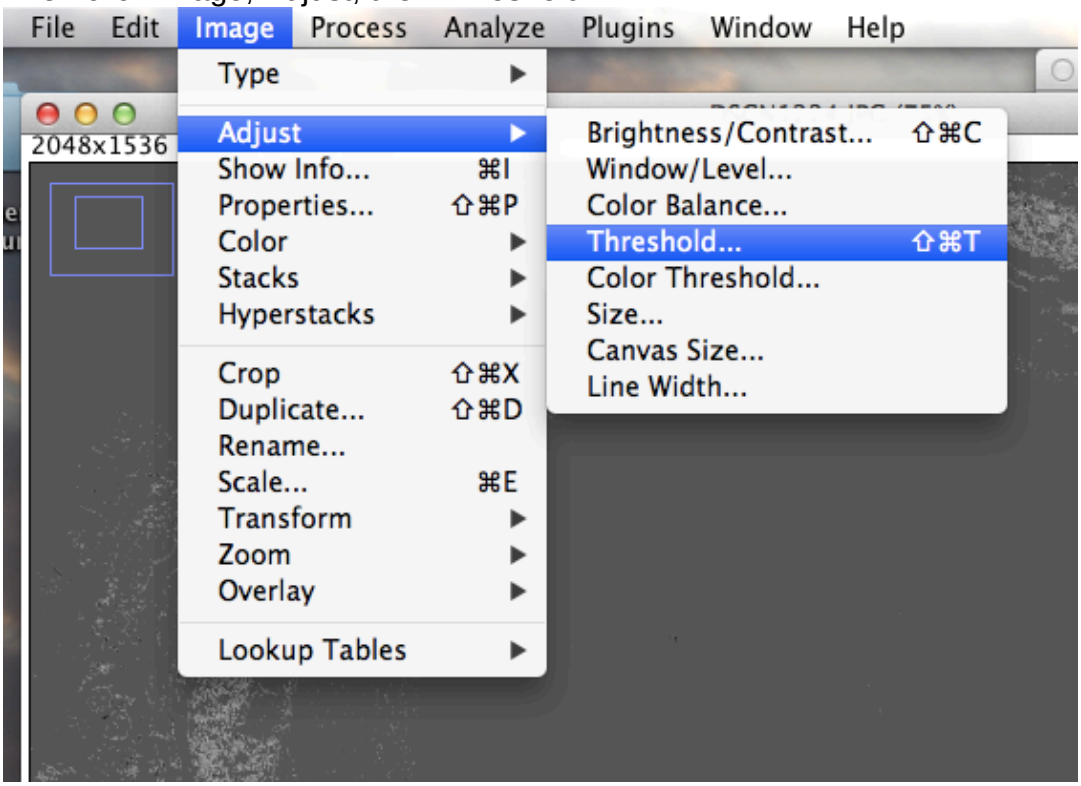

15. Slide both sliders until what you want to measure is colored red, this is what the program will analyze. Here is an example:

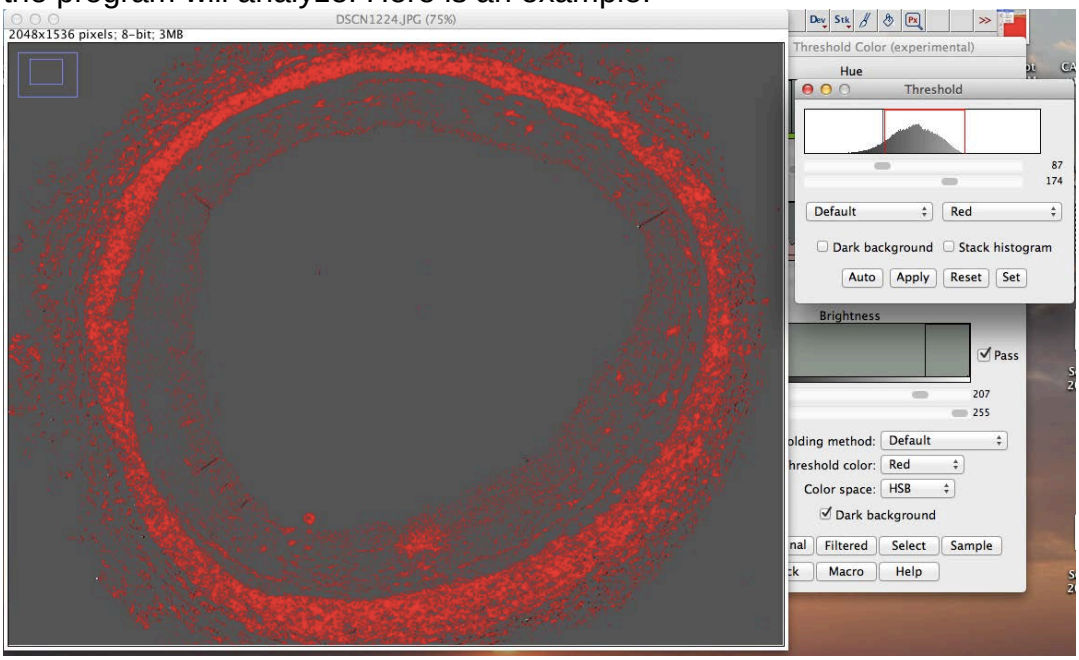

16. Click the Polygon selection tool : 

17. Since, we want medial collagen, trace the external elastic lamina (one-click to start the line, double-click to end):

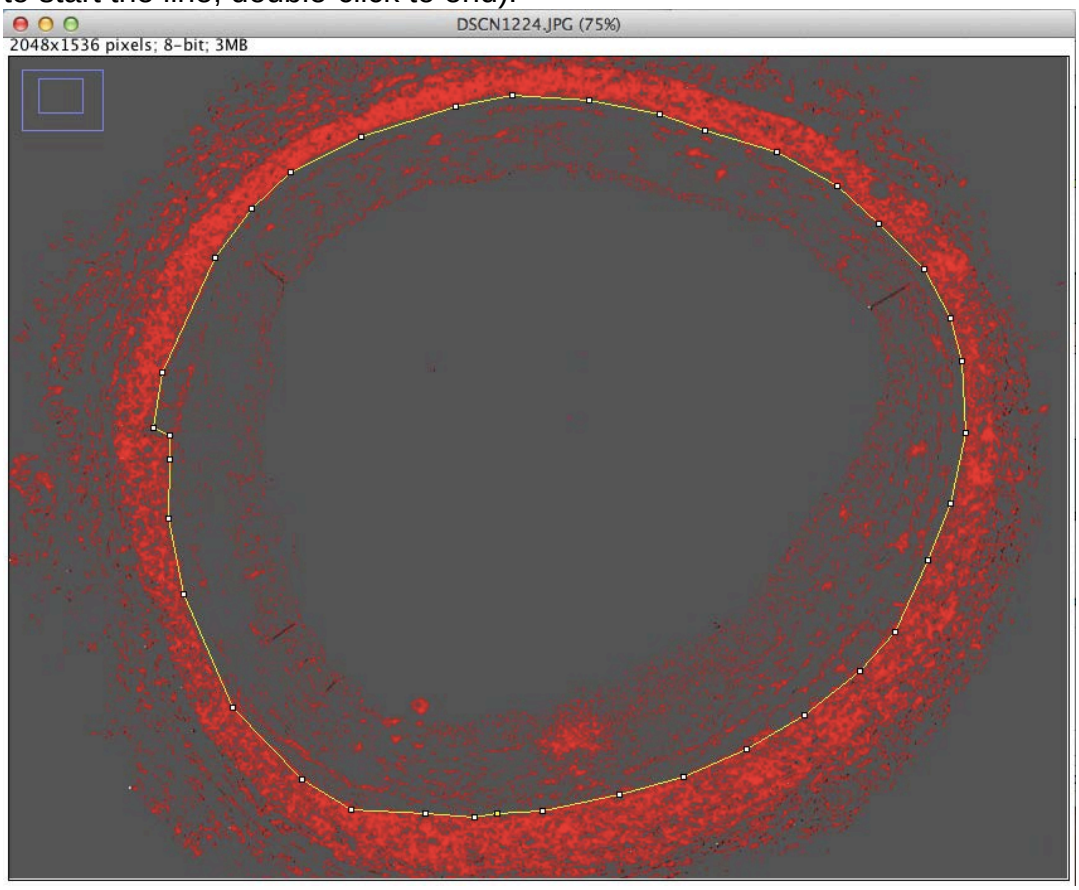

18. Click Analyze, then click Analyze Particles

19. A box will pop-up, use this criteria:

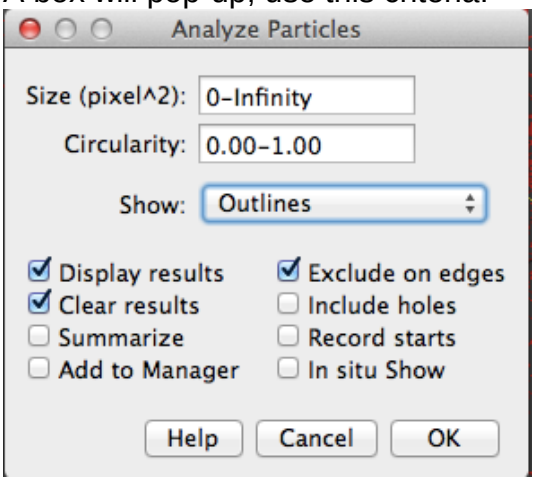

Click Ok.

20. Two windows will pop-up. One will have the area of all of the particles and one will show you which particles the program measured. I just check to make sure the program has not analyzed any random particles outside my region of interest.

21. Save the Results window by clicking on the Results sheet and then clicking File and Save As…

22. It should save as an Excel file. When you open the file, you can use a SUM equation to sum up all of the areas that ImageJ has calculated.

23. Repeat steps 16-22, except trace the internal elastic lamina, so the lumen is now the area of interest. This will pick up any random lumen collagen, which you can then subtract from the first measurement.

24. By subtracting the 1st number (Sum of area of Collagen in Media and Lumen) minus 2nd number (Sum of area of Collagen in Lumen), you will calculate the area of Collagen within the medial layer.

APPENDIX F

PROTOCOL FOR FLOW CYTOMETRY IDENTIFICATION OF CSM PHENOTYPES FROM FRESHLY DISPERSED PIG CORONARY ARTERIES:

Mikaela McKenney, Heather O'Leary, Ph.D.
08/02/2014

1. From freshly dissected coronary arteries or coronary rings from organ culture experiments.

2. Enzymatically isolate CSM from coronary artery/rings as described in CORSMC1_v2.doc.
    a. **NOTE**: keep ALL cell fractions from dispersion.
    b. Stop before fura-2 loading step.

3. Combine all cell fractions, spin down, and remove supernatant.

4. Resuspend in Cytofix/Cytoperm solution (BD, San Jose, CA). Triturate suspension several times.
   ****At this point, cells can be stored in fridge until time of flow experiments.**

The following Flow Cytometry methods are conducted in the Department of Microbiology and Immunology, Broxmeyer lab, contact: Heather O'Leary, Ph.D.:
haoleary@iupui.edu

5. Cell viability is determined by trypan blue exclusion and counting of cells on a hemacytometer.

6. Preps with an initial viability of 85% or above are subsequently fixed and permeabilized (BD Cytofix/Cytoperm, San Jose, CA).

7. Cells are washed from fixative and should remain in permwash for the remainder of the staining protocol. Markers of phenotypic smooth muscle group to determine phenotypic populations: Amount of antibody was titrated based on isotype controls but were within the manufacturers suggested guide lines. A common cocktail was made for all samples Containing matched isotype control or specific antibodies of interest.

    a. smooth muscle myosin heavy chain (SM-MHC)
        i. polyclonal rabbit anti-SM-MHC, Alex Fluor 488, Bioss, Woburn, MA)

    b. α-smooth muscle actin (SMA)
        i. (monoclonal mouse anti-human SMA. APC, R&D systems, Minneapolis, MN)

c. runt-related transcription factor 2 (RUNX2)
    i. (monoclonal mouse anti-RUNX2 antibody ab76956, abcam, Cambridge, MA
    ii. DyLight 405 ChromPure Rabbit IgG, Jackson ImmunoReseach Laboratories, West Grove, PA

8. Cells were stained for 30 minutes and washed in permwash followed by wash, and resusension, in PBS (~200UL).

9. Cells were run on an LSRII machine in the IU simon cancer center flow cytometry core running FACSDiva software. Gates were set up according to isotype controls

10. Analysis of samples was performed using FLOWJO software and gates/subgates were determined by isotype controls and were identical for all samples to ensure consistency.

List of References

(1) Ogden CL, Carroll MD, Kit BK, Flegal KM. Prevalence of childhood and adult obesity in the United States, 2011-2012. JAMA 2014;311(8):806-814.

(2) Neel JV. Diabetes mellitus: a "thrifty" genotype rendered detrimental by "progress"? Am J Hum Genet 1962;14:353-362.

(3) O'rourke RW. Metabolic thrift and the genetic basis of human obesity. Ann Surg 2014;259(4):642-648.

(4) Go AS, Mozaffarian D, Roger VL, Benjamin EJ, Berry JD, Borden WB et al. Heart disease and stroke statistics--2013 update: a report from the American Heart Association. Circulation 2013;127(1):e6-e245.

(5) Reaven GM. Banting Lecture 1988: Role of insulin resistance in human disease. Diabetes 1988;37:1595-1607.

(6) Sattar N, Gaw A, Scherbakova O, Ford I, O'Reilly DS, Haffner SM et al. Metabolic syndrome with and without C-reactive protein as a predictor of coronary heart disease and diabetes in the West of Scotland Coronary Prevention Study. Circulation 2003;108:414.

(7) Gami AS, Witt BJ, Howard DE, Erwin PJ, Gami LA, Somers VK et al. Metabolic syndrome and risk of incident cardiovascular events and death: a systematic review and meta-analysis of longitudinal studies. J Am Coll Cardiol 2007;49(4):403-414.

(8) Murphy SL, Xu J, Kochanek KD. Deaths: final data for 2010. Natl Vital Stat Rep 2013;61(4):1-117.

(9) Heidenreich PA, Trogdon JG, Khavjou OA, Butler J, Dracup K, Ezekowitz MD et al. Forecasting the future of cardiovascular disease in the United States: a policy statement from the American Heart Association. Circulation 2011;123(8):933-944.

(10) Virmani R, Burke AP, Kolodgie FD, Farb A. Vulnerable plaque: the pathology of unstable coronary lesions. J Interv Cardiol 2002;15(6):439-446.

(11) Roberts CK, Hevener AL, Barnard RJ. Metabolic Syndrome and Insulin Resistance: Underlying Causes and Modification by Exercise Training. Comprehensive Physiology. John Wiley & Sons, Inc.; 2013.

(12) Schlett CL, Massaro JM, Lehman SJ, Bamberg F, O'Donnell CJ, Fox CS et al. Novel measurements of periaortic adipose tissue in comparison to anthropometric measures of obesity, and abdominal adipose tissue. Int J Obes (Lond) 2009;33(2):226-232.

(13) Lehman SJ, Massaro JM, Schlett CL, O'Donnell CJ, Hoffmann U, Fox CS. Peri-aortic fat, cardiovascular disease risk factors, and aortic calcification: the Framingham Heart Study. Atherosclerosis 2010;210(2):656-661.

(14) Sarin S, Wenger C, Marwaha A, Qureshi A, Go BD, Woomert CA et al. Clinical significance of epicardial fat measured using cardiac multislice computed tomography. Am J Cardiol 2008;102(6):767-771.

(15) Greif M, Becker A, von Ziegler F, Lebherz C, Lehrke M, Broedl UC et al. Pericardial Adipose Tissue Determined by Dual Source CT Is a Risk Factor for Coronary Atherosclerosis. Arterioscler Thromb Vasc Biol 2009;29(5):781-786.

(16) Iacobellis G, Willens HJ. Echocardiographic epicardial fat: a review of research and clinical applications. J Am Soc Echocardiogr 2009;22(12):1311-1319.

(17) Dong DD, Wang K, Wang D, Zhang T, Tu YF, Shen BZ. Relationship between epicardial adipose tissue volume measured using coronary computed tomography angiography and atherosclerotic plaque characteristics in patients with severe coronary artery stenosis. J Int Med Res 2013;41(5):1520-1531.

(18) Sacks HS, Fain JN. Human epicardial adipose tissue: a review. Am Heart J 2007;153(6):907-917.

(19) Montani JP, Carroll JF, Dwyer TM, Antic V, Yang Z, Dulloo AG. Ectopic fat storage in heart, blood vessels and kidneys in the pathogenesis of cardiovascular diseases. Int J Obes Relat Metab Disord 2004;28 Suppl 4:S58-S65.

(20) Sacks HS, Fain JN, Cheema P, Bahouth SW, Garrett E, Wolf RY et al. Depot-specific overexpression of proinflammatory, redox, endothelial cell, and angiogenic genes in epicardial fat adjacent to severe stable coronary atherosclerosis. Metab Syndr Relat Disord 2011;(In press).

(21) McKenney ML, Schultz KA, Boyd JH, Byrd JP, Alloosh M, Teague SD et al. Epicardial adipose excision slows the progression of porcine coronary atherosclerosis. J Cardiothorac Surg 2014;9:2.

(22) de Vos AM, Prokop M, Roos CJ, Meijs MF, Van der Schouw YT, Rutten A et al. Peri-coronary epicardial adipose tissue is related to cardiovascular risk factors and coronary artery calcification in post-menopausal women. Eur Heart J 2008;29(6):777-783.

(23) Hughes-Austin JM, Wassel CL, Jimenez J, Criqui MH, Ix JH, Rasmussen-Torvik LJ et al. The relationship between adiposity-associated inflammation and coronary artery and abdominal aortic calcium differs by strata of central adiposity: The Multi-Ethnic Study of Atherosclerosis (MESA). Vasc Med 2014.

(24) Proudfoot D, Shanahan CM. Biology of calcification in vascular cells: intima versus media. Herz 2001;26(4):245-251.

(25) Kovacic JC, Moreno P, Nabel EG, Hachinski V, Fuster V. Cellular senescence, vascular disease, and aging: part 2 of a 2-part review: clinical vascular disease in the elderly. Circulation 2011;123(17):1900-1910.

(26) Stary HC. Natural history of calcium deposits in atherosclerosis progression and regression. Z Kardiol 2000;89 Suppl 2:28-35.

(27) Detrano R, Guerci AD, Carr JJ, Bild DE, Burke G, Folsom AR et al. Coronary calcium as a predictor of coronary events in four racial or ethnic groups. N Engl J Med 2008;358(13):1336-1345.

(28) Burke AP, Taylor A, Farb A, Malcom GT, Virmani R. Coronary calcification: insights from sudden coronary death victims. Z Kardiol 2000;89 Suppl 2:49-53.

(29) Ehara S, Kobayashi Y, Yoshiyama M, Shimada K, Shimada Y, Fukuda D et al. Spotty calcification typifies the culprit plaque in patients with acute myocardial infarction: an intravascular ultrasound study. Circulation 2004;110(22):3424-3429.

(30) Shanahan CM, Crouthamel MH, Kapustin A, Giachelli CM. Arterial Calcification in Chronic Kidney Disease: Key Roles for Calcium and Phosphate. Circ Res 2011;109(6):697-711.

(31) Agatston AS, Janowitz WR, Hildner FJ, Zusmer NR, Viamonte M, Jr., Detrano R. Quantification of coronary artery calcium using ultrafast computed tomography. J Am Coll Cardiol 1990;15(4):827-832.

(32) McEvoy JW, Blaha MJ, DeFilippis AP, Budoff MJ, Nasir K, Blumenthal RS et al. Coronary Artery Calcium Progression: An Important Clinical Measurement?: A Review of Published Reports. J Am Coll Cardiol 2010;56(20):1613-1622.

(33) Hawkins RA, Choi Y, Huang SC, Hoh CK, Dahlbom M, Schiepers C et al. Evaluation of the skeletal kinetics of fluorine-18-fluoride ion with PET. J Nucl Med 1992;33(5):633-642.

(34) Segall G, Delbeke D, Stabin MG, Even-Sapir E, Fair J, Sajdak R et al. SNM practice guideline for sodium 18F-fluoride PET/CT bone scans 1.0. J Nucl Med 2010;51(11):1813-1820.

(35) Czernin J, Satyamurthy N, Schiepers C. Molecular mechanisms of bone 18F-NaF deposition. J Nucl Med 2010;51(12):1826-1829.

(36) Beheshti M, Saboury B, Mehta NN, Torigian DA, Werner T, Mohler ER et al. Detection and global quantification of cardiovascular molecular calcification by fluoro-18-fluoride positron emission tomography/computed tomography-A novel concept. Hell J Nucl Med 2011;14:114-120.

(37) Basu S, Hilund-Carlsen P, Alavi A. Assessing global cardiovascular molecular calcification with F-fluoride PET/CT: will this become a clinical reality and a chayellenge to CT calcification scoring? European Journal of Nuclear Medicine and Molecular Imaging 2010;1-5.

(38) Joshi NV, Vesey AT, Williams MC, Shah ASV, Calvert PA, Craighead FHM et al. 18F-fluoride positron emission tomography for identification of ruptured and high-risk coronary atherosclerotic plaques: a prospective clinical trial. The Lancet 2014;383(9918):705-713.

(39) Dyson M, Alloosh M, Vuchetich JP, Mokelke EA, Sturek M. Components of metabolic syndrome and coronary artery disease in female Ossabaw swine fed excess atherogenic diet. Comp Med 2006;56:35-45.

(40) Sturek M, Alloosh M, Wenzel J, Byrd JP, Edwards JM, Lloyd PG et al. Ossabaw Island miniature swine: cardiometabolic syndrome assessment. In: Swindle MM, editor. Swine in the Laboratory: Surgery, Anesthesia, Imaging, and Experimental Techniques. 2nd Edition ed. Boca Raton: CRC Press; 2007. p. 397-402.

(41) Lee L, Alloosh M, Saxena R, Van Alstine W, Watkins BA, Klaunig JE et al. Nutritional model of steatohepatitis and metabolic syndrome in the Ossabaw miniature swine. Hepatology 2009;50:56-67.

(42) Neeb ZP, Edwards JM, Alloosh MA, Long X, Mokelke EA, Sturek M. Metabolic syndrome and coronary artery disease in Ossabaw compared with Yucatan swine. Comp Med 2010;60:300-315.

(43) Wang H-W, Langohr IM, Sturek M, Cheng J-X. Imaging and quantitative analysis of atherosclerotic lesions by CARS-based multimodal nonlinear optical microscopy. Arterioscler Thromb Vasc Biol 2009;29:1342-1348.

(44) Edwards JM, Neeb ZP, Alloosh MA, Long X, Bratz IN, Peller CR et al. Exercise training decreases store-operated Ca^{2+} entry associated with metabolic syndrome and coronary atherosclerosis. Cardiovasc Res 2010;85:631-640.

(45) Kreutz RP, Alloosh M, Mansour K, Neeb ZP, Kreutz Y, Flockhart DA et al. Morbid obesity and metabolic syndrome in Ossabaw miniature swine are associated with increased platelet reactivity. Diabetes Metab Syndr Obes 2011;4:99-105.

(46) Sturek M. Ca^{2+} regulatory mechanisms of exercise protection against coronary artery disease in metabolic syndrome and diabetes. J Appl Physiol 2011;111:573-586.

(47) Crick SJ, Sheppard MN, Ho SY, Gebstein L, Anderson RH. Anatomy of the pig heart: comparisons with normal human cardiac structure. J Anat 1998;193 (Pt 1):105-119.

(48) Libby P, Ridker PM, Hansson GK. Progress and challenges in translating the biology of atherosclerosis. Nature 2011;473(7347):317-325.

(49) Rader DJ, Daugherty A. Translating molecular discoveries into new therapies for atherosclerosis. Nature 2008;451(7181):904-913.

(50) Owens GK. Regulation of differentiation of vascular smooth muscle cells. Physiol Rev 1995;75:487-517.

(51) Speer MY, Yang HY, Brabb T, Leaf E, Look A, Lin WL et al. Smooth Muscle Cells Give Rise to Osteochondrogenic Precursors and Chondrocytes in Calcifying Arteries. Circ Res 2009;104(6):733-741.

(52) Witczak CA, Sturek M. Exercise prevents diabetes-induced impairment in superficial buffer barrier in porcine coronary smooth muscle. J Appl Physiol 2004;96:1069-1079.

(53) Witczak CA, Wamhoff BR, Sturek M. Exercise training prevents Ca^{2+} dysregulation in coronary smooth muscle from diabetic dyslipidemic Yucatan swine. J Appl Physiol 2006;101:752-762.

(54) Adachi T, Matsui R, Xu S, Kirber M, Lazar HL, Sharov VS et al. Antioxidant improves smooth muscle sarco/endoplasmic reticulum Ca(2+)- ATPase function and lowers tyrosine nitration in hypercholesterolemia and improves nitric oxide-induced relaxation. Circ Res 2002;90(10):1114-1121.

(55) Bowles DK, Heaps CL, Turk JR, Maddali KK, Price EM. Hypercholesterolemia inhibits L-type calcium current in coronary macro-, not microcirculation. J Appl Physiol 2004;96:2240-2248.

(56) Berwick ZC, Dick GM, O'Leary HA, Bender SB, Goodwill AG, Moberley SP et al. Contribution of Kv and Cav1.2 electromechanical coupling in coronary dysfunction in metabolic syndrome. FASEB Journal . 2012.

(57) Kumar B, Dreja K, Shah SS, Cheong A, Xu SZ, Sukumar P et al. Upregulated TRPC1 channel in vascular injury in vivo and its role in human neointimal hyperplasia. Circ Res 2006;98(4):557-563.

(58) Behavioral Risk Factor Surveillance System CfDCaP. Obesity Trends Among U.S. Adults. 4-24-2013. Centers for Disease Control and Prevention, Behavioral Risk Factor Surveillance System.

(59) Payne GA, Borbouse L, Kumar S, Neeb Z, Alloosh M, Sturek M et al. Epicardial perivascular adipose-derived leptin exacerbates coronary endothelial dysfunction in metabolic syndrome via a protein kinase C-â pathway. Arterioscler Thromb Vasc Biol 2010;30:1711-1717.

(60) Posner AS. The mineral of bone. Clin Orthop Relat Res 1985;(200):87-99.

(61) Ouwens DM, Sell H, Greulich S, Eckel J. The role of epicardial and perivascular adipose tissue in the pathophysiology of cardiovascular disease. Journal of Cellular and Molecular Medicine 2010;14(9):2223-2234.

(62) Verhagen SN, Visseren FLJ. Perivascular adipose tissue as a cause of atherosclerosis. Atherosclerosis 2011;214(1):3-10.

(63) Iozzo P. Myocardial, Perivascular, and Epicardial Fat. Diabetes Care 2011;34(Supplement 2):S371-S379.

(64) Ding J, Hsu FC, Harris TB, Liu Y, Kritchevsky SB, Szklo M et al. The association of pericardial fat with incident coronary heart disease: the Multi-Ethnic Study of Atherosclerosis (MESA). Am J Clin Nutr 2009;90(3):499-504.

(65) Tamarappoo B, Dey D, Shmilovich H, Nakazato R, Gransar H, Cheng VY et al. Increased Pericardial Fat Volume Measured From Noncontrast CT Predicts Myocardial Ischemia by SPECT. J Am Coll Cardiol Img 2010;3(11):1104-1112.

(66) Cheng VY, Dey D, Tamarappoo B, Nakazato R, Gransar H, Miranda-Peats R et al. Pericardial Fat Burden on ECG-Gated Noncontrast CT in Asymptomatic Patients Who Subsequently Experience Adverse Cardiovascular Events. J Am Coll Cardiol Img 2010;3(4):352-360.

(67) Mazurek T, Zhang L, Zalewski A, Mannion JD, Diehl JT, Arafat H et al. Human Epicardial Adipose Tissue Is a Source of Inflammatory Mediators. Circulation 2003;108(20):2460-2466.

(68) Sacks HS, Fain JN. Human epicardial fat: what is new and what is missing? Clinical and Experimental Pharmacology and Physiology 2011;38(12):879-887.

(69) Institute for Laboratory Animal Research. Guide for the care and use of laboratory animals. 8th ed. Washington, D.C.: National Academy Press; 2010.

(70) AVMA Panel on Euthanasia.American Veterinary Medical Association. 2000 Report of the AVMA panel on euthanasia. JAVMA 2001;218:669-696.

(71) Arce-Esquivel AA, Kreutzer KV, Rush JW, Turk JR, Laughlin MH. Exercise does not attenuate early CAD progression in a pig model. Med Sci Sports Exerc 2012;44(1):27-38.

(72) Bustin SA. Absolute quantification of mRNA using real-time reverse transcription polymerase chain reaction assays. J Mol Endocrinol 2000;25:169-193.

(73) Sacks HS, Fain JN. Human epicardial adipose tissue: A review. Am Heart J 2007;153(6):907-917.

(74) Horton JD, Cohen JC, Hobbs HH. PCSK9: a convertase that coordinates LDL catabolism. J Lipid Res 2008;R800091-RJLR200.

(75) Owen MK, Witzmann FA, McKenney ML, Lai X, Berwick ZC, Moberly SP et al. Perivascular adipose tissue potentiates contraction of coronary vascular smooth muscle: influence of obesity. Circulation 2013;128:9-18.

(76) Philippova M, Suter Y, Toggweiler S, Schoenenberger AW, Joshi MB, Kyriakakis E et al. T-cadherin is present on endothelial microparticles and is elevated in plasma in early atherosclerosis. Eur Heart J 2011;32(6):760-771.

(77) Takeuchi T, Adachi Y, Ohtsuki Y, Furihata M. Adiponectin receptors, with special focus on the role of the third receptor, T-cadherin, in vascular disease. Med Mol Morphol 2007;40(3):115-120.

(78) Kodama T, Freeman M, Rohrer L, Zabrecky J, Matsudaira P, Krieger M. Type I macrophage scavenger receptor contains alpha-helical and collagen-like coiled coils. Nature 1990;343(6258):531-535.

(79) Matsumoto A, Naito M, Itakura H, Ikemoto S, Asaoka H, Hayakawa I et al. Human macrophage scavenger receptors: primary structure, expression, and localization in atherosclerotic lesions. Proc Natl Acad Sci U S A 1990;87(23):9133-9137.

(80) Zhu XY, Bentley MD, Chade AR, Ritman EL, Lerman A, Lerman LO. Early changes in coronary artery wall structure detected by microcomputed tomography in experimental hypercholesterolemia. Am J Physiol Heart Circ Physiol 2007;293(3):H1997-H2003.

(81) Damas JK, Smith C, Oie E, Fevang B, Halvorsen B, Waehre T et al. Enhanced expression of the homeostatic chemokines CCL19 and CCL21 in clinical and experimental atherosclerosis: possible pathogenic role in plaque destabilization. Arterioscler Thromb Vasc Biol 2007;27(3):614-620.

(82) Tanaka R, Miwa Y, Mou K, Tomikawa M, Eguchi N, Urade Y et al. Knockout of the l-pgds gene aggravates obesity and atherosclerosis in mice. Biochem Biophys Res Commun 2009;378(4):851-856.

(83) Iacobellis G, Singh N, Wharton S, Sharma AM. Substantial changes in epicardial fat thickness after weight loss in severely obese subjects. Obesity (Silver Spring) 2008;16(7):1693-1697.

(84) Nadra I, Mason JC, Philippidis P, Florey O, Smythe CD, McCarthy GM et al. Proinflammatory activation of macrophages by basic calcium phosphate crystals via protein kinase C and MAP kinase pathways: a vicious cycle of inflammation and arterial calcification? Circ Res 2005;96(12):1248-1256.

(85) Bostrom K. Proinflammatory vascular calcification. Circ Res 2005;96(12):1219-1220.

(86) Aikawa E, Nahrendorf M, Figueiredo JL, Swirski FK, Shtatland T, Kohler RH et al. Osteogenesis associates with inflammation in early-stage atherosclerosis evaluated by molecular imaging in vivo. Circulation 2007;116(24):2841-2850.

(87) Shanahan CM. Inflammation ushers in calcification: a cycle of damage and protection? Circulation 2007;116(24):2782-2785.

(88) Stary HC, Chandler AB, Dinsmore RE, Fuster V, Glagov S, Insull W, Jr. et al. A definition of advanced types of atherosclerotic lesions and a histological classification of atherosclerosis. A report from the Committee on Vascular Lesions of the Council on Arteriosclerosis, American Heart Association. Circulation 1995;92(5):1355-1374.

(89) Huang H, Virmani R, Younis H, Burke AP, Kamm RD, Lee RT. The impact of calcification on the biomechanical stability of atherosclerotic plaques. Circulation 2001;103(8):1051-1056.

(90) Vengrenyuk Y, Carlier S, Xanthos S, Cardoso L, Ganatos P, Virmani R et al. A hypothesis for vulnerable plaque rupture due to stress-induced debonding around cellular microcalcifications in thin fibrous caps. Proc Natl Acad Sci U S A 2006;103(40):14678-14683.

(91) Vengrenyuk Y, Cardoso L, Weinbaum S. Micro-CT based analysis of a new paradigm for vulnerable plaque rupture: cellular microcalcifications in fibrous caps. Mol Cell Biomech 2008;5(1):37-47.

(92) Maldonado N, Kelly-Arnold A, Vengrenyuk Y, Laudier D, Fallon JT, Virmani R et al. A mechanistic analysis of the role of microcalcifications in atherosclerotic plaque stability: potential implications for plaque rupture. Am J Physiol Heart Circ Physiol 2012;303(5):H619-H628.

(93) Kataoka Y, Wolski K, Uno K, Puri R, Tuzcu EM, Nissen SE et al. Spotty calcification as a marker of accelerated progression of coronary atherosclerosis: insights from serial intravascular ultrasound. J Am Coll Cardiol 2012;59(18):1592-1597.

(94) Doherty TM, Asotra K, Fitzpatrick LA, Qiao JH, Wilkin DJ, Detrano RC et al. Calcification in atherosclerosis: bone biology and chronic inflammation at the arterial crossroads. Proc Natl Acad Sci U S A 2003;100(20):11201-11206.

(95) Budoff MJ, Gul KM. Expert review on coronary calcium. Vasc Health Risk Manag 2008;4(2):315-324.

(96) Rambhia SH, Liang X, Xenos M, Alemu Y, Maldonado N, Kelly A et al. Microcalcifications increase coronary vulnerable plaque rupture potential: a patient-based micro-CT fluid-structure interaction study. Ann Biomed Eng 2012;40(7):1443-1454.

(97) Liang X, Xenos M, Alemu Y, Rambhia SH, Lavi I, Kornowski R et al. Biomechanical factors in coronary vulnerable plaque risk of rupture: intravascular ultrasound-based patient-specific fluid-structure interaction studies. Coron Artery Dis 2013;24(2):75-87.

(98) Srinivasan A, Ramaswamy V, Kuruvilla S, Sehgal P, Balakrishnan K. Calcified atherosclerotic plaque - where exactly is the calcium and what does it contain? Indian J Thorac Cardiovasc Surg 12 A.D.;28(1):6-14.

(99) Dweck MR, Jones C, Joshi NV, Fletcher AM, Richardson H, White A et al. Assessment of Valvular Calcification and Inflammation by Positron Emission Tomography in Patients With Aortic Stenosis. Circulation 2012;125(1):76-86.

(100) Dweck MR, Khaw HJ, Sng GKZ, Luo ELC, Baird A, Williams MC et al. Aortic stenosis, atherosclerosis, and skeletal bone: is there a common link with calcification and inflammation? Eur Heart J 2013;34(21):1567-1574.

(101) Li Y, Berenji GR, Shaba WF, Tafti B, Yevdayev E, Dadparvar S. Association of vascular fluoride uptake with vascular calcification and coronary artery disease. Nucl Med Commun 2012;33:14-20.

(102) Janssen T, Bannas P, Herrmann J, Veldhoen S, Busch JD, Treszl A et al. Association of linear (1)(8)F-sodium fluoride accumulation in femoral arteries as a measure of diffuse calcification with cardiovascular risk factors: a PET/CT study. J Nucl Cardiol 2013;20(4):569-577.

(103) Dweck MR, Jenkins WSA, Vesey AT, Pringle MAH, Chin CWL, Malley TS et al. 18F-Sodium Fluoride Uptake Is a Marker of Active Calcification and Disease Progression in Patients With Aortic Stenosis. Circ Cardiovasc Imaging 2014;7(2):371-378.

(104) Studholme C, Hawkes D, Hill D. A normalised entropy measure for multi-modality image alignment. Proc SPIE Medical Imaging 1998;3338:132-143.

(105) Chen NX, O'Neill KD, Chen X, Kiattisunthorn K, Gattone VH, Moe SM. Activation of arterial matrix metalloproteinases leads to vascular calcification in chronic kidney disease. Am J Nephrol 2011;34(3):211-219.

(106) Detrano RC, Wong ND, Doherty TM, Shavelle RM, Tang WY, Ginzton LE et al. Coronary calcium does not accurately predict near-term future coronary events in high-risk adults. Circulation 1999;99(20):2633-2638.

(107) Johnson RC, Leopold JA, Loscalzo J. Vascular calcification: pathobiological mechanisms and clinical implications. Circ Res 2006;99(10):1044-1059.

(108) Cocker MS, Mc AB, Spence JD, Lum C, Hammond RR, Ongaro DC et al. Imaging atherosclerosis with hybrid [18F]fluorodeoxyglucose positron emission tomography/computed tomography imaging: what Leonardo da Vinci could not see. J Nucl Cardiol 2012;19(6):1211-1225.

(109) Rudd JH, Warburton EA, Fryer TD, Jones HA, Clark JC, Antoun N et al. Imaging atherosclerotic plaque inflammation with [18F]-fluorodeoxyglucose positron emission tomography. Circulation 2002;105(23):2708-2711.

(110) Rogers IS, Nasir K, Figueroa AL, Cury RC, Hoffmann U, Vermylen DA et al. Feasibility of FDG imaging of the coronary arteries: comparison between acute coronary syndrome and stable angina. JACC Cardiovasc Imaging 2010;3(4):388-397.

(111) Wykrzykowska J, Lehman S, Williams G, Parker JA, Palmer MR, Varkey S et al. Imaging of inflamed and vulnerable plaque in coronary arteries with 18F-FDG PET/CT in patients with suppression of myocardial uptake using a low-carbohydrate, high-fat preparation. J Nucl Med 2009;50(4):563-568.

(112) Cheng VY, Slomka PJ, Le ML, Tamarappoo BK, Nakazato R, Dey D et al. Coronary arterial 18F-FDG uptake by fusion of PET and coronary CT angiography at sites of percutaneous stenting for acute myocardial infarction and stable coronary artery disease. J Nucl Med 2012;53(4):575-583.

(113) Kapustin AN, Davies JD, Reynolds JL, McNair R, Jones GT, Sidibe A et al. Calcium regulates key components of vascular smooth muscle cell-derived matrix vesicles to enhance mineralization. Circ Res 2011;109(1):e1-12.

(114) New SE, Goettsch C, Aikawa M, Marchini JF, Shibasaki M, Yabusaki K et al. Macrophage-derived matrix vesicles: an alternative novel mechanism for microcalcification in atherosclerotic plaques. Circ Res 2013;113(1):72-77.

(115) Sturek M, Mokelke EA, Sindermann JR, Adam LP, March KL. Molecular and cellular physiology of differentiated vascular smooth muscle. In: Willerson JT, Cohn JN, Wellens HJJ, Holmes DR, editors. Cardiovascular Medicine. Third Edition ed. London: Springer-Verlag; 2006. p. 1511-1523.

(116) Bobryshev YV, Killingsworth MC, Orekhov AN. Increased shedding of microvesicles from intimal smooth muscle cells in athero-prone areas of the human aorta: implications for understanding of the predisease stage. Pathobiology 2013;80(1):24-31.

(117) Bobryshev YV, Killingsworth MC, Lord RS, Grabs AJ. Matrix vesicles in the fibrous cap of atherosclerotic plaque: possible contribution to plaque rupture. J Cell Mol Med 2008;12(5B):2073-2082.

(118) Wastney M, Lee W, Jackson G, Alloosh M, Sturek M, Lachick P et al. Soft tissue calcification in the Ossabaw miniature pig: experimental and kinetic modeling studies (abstract). FASEB J 2012;26:34.3.

(119) Grundy SM, Brewer HB, Cleeman JI, Smith SC, Jr., Lenfant C. Definition of the metabolic syndrome. Circulation 2004;109:433-438.

(120) Gomez D, Owens GK. Smooth muscle cell phenotypic switching in atherosclerosis. Cardiovasc Res 2012;95(2):156-164.

(121) Kapustin AN, Davies JD, Reynolds JL, McNair R, Jones GT, Sidibe A et al. Calcium Regulates Key Components of Vascular Smooth Muscle Cell-derived Matrix Vesicles to Enhance Mineralization / Novelty and Significance. Circ Res 2011;109(1):e1-e12.

(122) Stary HC. Natural History and Histological Classification of Atherosclerotic Lesions : An Update. Arterioscler Thromb Vasc Biol 2000;20(5):1177-1178.

(123) Payne GA, Borbouse L, Bratz IN, Roell WC, Bohlen HG, Dick GM et al. Endogenous adipose-derived factors diminish coronary endothelial function via inhibition of nitric oxide synthase. Microcirculation 2008;15(5):417-426.

(124) Heaps CL, Sturek M, Price EM, Laughlin MH, Parker JL. Sarcoplasmic reticulum Ca^{2+}-ATPase uptake is impaired in coronary smooth muscle distal to chronic occlusion. Am J Physiol : Heart Circ Physiol 2001;281:H223-H231.

(125) Heaps CL, Bowles DK, Sturek M, Laughlin MH, Parker JL. Enhanced L-type Ca^{2+} channel current density in coronary smooth muscle of exercise trained swine is compensated to limit myoplasmic net Ca^{2+} accumulation. J Physiol (Lond) 2000;528(3):435-445.

(126) Schilling WP, Rajan L, Strobl-Jager E. Characterization of the bradykinin-stimulated calcium influx pathway of cultured vascular endothelial cells. Saturability, selectivity, and kinetics. J Biol Chem 1989;264:12838-12848.

(127) Chen NX, Kircelli F, O'Neill KD, Chen X, Moe SM. Verapamil inhibits calcification and matrix vesicle activity of bovine vascular smooth muscle cells. Kidney Int 2010;77(5):436-442.

(128) Dixon JL, Shen S, Vuchetich JP, Wysocka E, Sun G, Sturek M. Increased atherosclerosis in diabetic dyslipidemic swine: protection by atorvastatin involves decreased VLDL triglycerides but minimal effects on the lipoprotein profile. J Lipid Res 2002;43:1618-1629.

(129) Hill BJF, Price EM, Dixon JL, Sturek M. Increased calcium buffering in coronary smooth muscle cells from diabetic dyslipidemic pigs. Atherosclerosis 2003;167:15-23.

(130) Lipskaia L, Hadri L, Le PP, Esposito B, Atassi F, Liang L et al. SERCA2a gene transfer prevents intimal proliferation in an organ culture of human internal mammary artery. Gene Ther 2012.

(131) Lipskaia L, del MF, Capiod T, Yacoubi S, Hadri L, Hours M et al. Sarco/endoplasmic reticulum Ca2+-ATPase gene transfer reduces vascular smooth muscle cell proliferation and neointima formation in the rat. Circ Res 2005;97(5):488-495.

(132) Sen L, Bialecki RA, Smith E, Smith TW, Colucci WS. Cholesterol increases the L-type voltage-sensitive calcium channel current in arterial smooth muscle cells. Circ Res 1992;71:1008-1014.

(133) Schroder F, Handrock R, Beuckelmann DJ, Hirt S, Hullin R, Priebe L et al. Increased availability and open probability of single L-type calcium channels from failing compared with nonfailing human ventricle. Circulation 1998;98(10):969-976.

(134) Kaimoto T, Yasuda O, Ohishi M, Mogi M, Takemura Y, Suhara T et al. Nifedipine inhibits vascular smooth muscle cell dedifferentiation via downregulation of Akt signaling. Hypertension 2010;56(2):247-252.

(135) Neeb ZP, Alloosh M, Edwards JM, Bratz IN, Sturek M. Store-operated Ca^{2+} influx predicts coronary artery disease and is induced by dyslipidemia in metabolic syndrome and type 2 diabetes (abstract). FASEB Journal 24, 978.4. 2010.

(136) Berwick Z, Dick G, O'Leary H, Bender S, Goodwill A, Moberly S et al. Contribution of electromechanical coupling between KV and CaV1.2 channels to coronary dysfunction in obesity. Basic Res Cardiol 2013;108(5):370.

(137) Matchkov VV, Kudryavtseva O, Aalkjaer C. Intracellular Ca(2)(+) signalling and phenotype of vascular smooth muscle cells. Basic Clin Pharmacol Toxicol 2012;110(1):42-48.

(138) Wamhoff BR, Bowles DK, McDonald OG, Sinha S, Somlyo AP, Owens GK. L-type voltage-gated Ca2+ channels modulate expression of smooth muscle differentiation marker genes via a Rho kinase/myocardin/SRF-dependent mechanism. Circ Res 2004;95:406-414.

(139) Fleckenstein-Grun G, Thimm F, Czirfuzs A, Matyas S, Frey M. Experimental vasoprotection by calcium antagonists against calcium-mediated arteriosclerotic alterations. J Cardiovasc Pharmacol 1994;24 Suppl 2:S75-S84.

(140) Motro M, Shemesh J. Calcium channel blocker nifedipine slows down progression of coronary calcification in hypertensive patients compared with diuretics. Hypertension 2001;37(6):1410-1413.

(141) Kaplan NM. The deadly quartet. Upper-body obesity, glucose intolerance, hypertriglyceridemia, and hypertension. Arch Intern Med 1989;149(7):1514-1520.

(142) Foster DW. Insulin resistance--a secret killer? N Engl J Med 1989;320(11):733-734.

(143) Ford ES, Giles WH, Mokdad AH. Increasing prevalence of the metabolic syndrome amoung U.S. adults. Diabetes Care 2004;27:2444-2449.

(144) Ford ES. Prevalence of the metabolic syndrome defined by the International Diabetes Federation among adults in the U.S. Diabetes Care 2005;28(11):2745-2749.

(145) Galassi A, Reynolds K, He J. Metabolic syndrome and risk of cardiovascular disease: a meta-analysis. Am J Med 2006;119(10):812-819.

(146) Alexopoulos N, McLean DS, Janik M, Arepalli CD, Stillman AE, Raggi P. Epicardial adipose tissue and coronary artery plaque characteristics. Atherosclerosis 2010;210(1):150-154.

(147) María J.Fernández Muñoz, Lourdes Basurto Acevedo, Nydia Córdova Pérez, Ana Laura Vázquez Martínez, Nayive Tepach Gutiérrez, Sara Vega García et al. Epicardial Adipose Tissue Is Associated With Visceral Fat, Metabolic Syndrome, and Insulin Resistance in Menopausal Women. Revista Española de Cardiología 2014;67(8):593-680.

(148) Djaberi R, Schuijf JD, van Werkhoven JM, Nucifora G, Jukema JW, Bax JJ. Relation of epicardial adipose tissue to coronary atherosclerosis. Am J Cardiol 2008;102(12):1602-1607.

(149) Eroglu S, Sade LE, Yildirir A, Bal U, Ozbicer S, Ozgul AS et al. Epicardial adipose tissue thickness by echocardiography is a marker for the presence and severity of coronary artery disease. Nutr Metab Cardiovasc Dis 2009;19(3):211-217.

(150) Wu FZ, Huang YL, Wang YC, Lin HS, Chen CS, Ju YJ et al. Impact of location of epicardial adipose tissue, measured by coronary artery calcium-scoring computed tomography on obstructive coronary artery disease. Am J Cardiol 2013;112(7):943-949.

(151) Wu FZ, Chou KJ, Huang YL, Wu MT. The relation of location-specific epicardial adipose tissue thickness and obstructive coronary artery disease: systemic review and meta-analysis of observational studies. BMC Cardiovasc Disord 2014;14:62.

(152) Mahabadi AA, Berg MH, Lehmann N, Kalsch H, Bauer M, Kara K et al. Association of epicardial fat with cardiovascular risk factors and incident myocardial infarction in the general population: the Heinz Nixdorf Recall Study. J Am Coll Cardiol 2013;61(13):1388-1395.

(153) Wykrzykowska JJ, Mintz GS, Garcia-Garcia HM, Maehara A, Fahy M, Xu K et al. Longitudinal distribution of plaque burden and necrotic core-rich plaques in nonculprit lesions of patients presenting with acute coronary syndromes. JACC Cardiovasc Imaging 2012;5(3 Suppl):S10-S18.

(154) De Araujo GP, Garcia-Garcia HM, Carvalho MS, Dores H, Sousa PJ, Marques H et al. Diabetes as an independent predictor of high atherosclerotic burden assessed by coronary computed tomography angiography: the coronary artery disease equivalent revisited. Int J Cardiovasc Imaging 2013;29(5):1105-1114.

(155) Neeb ZP, Edwards JM, Alloosh MA, Long X, Mokelke EA, Sturek M. Metabolic syndrome and coronary artery disease in Ossabaw compared with Yucatan swine. Comp Med 2010;60:300-315.

(156) Rosito GA, Massaro JM, Hoffmann U, Ruberg FL, Mahabadi AA, Vasan RS et al. Pericardial fat, visceral abdominal fat, cardiovascular disease risk factors, and vascular calcification in a community-based sample: the Framingham Heart Study. Circulation 2008;117(5):605-613.

(157) Nakanishi R, Rajani R, Cheng VY, Gransar H, Nakazato R, Shmilovich H et al. Increase in epicardial fat volume is associated with greater coronary artery calcification progression in subjects at intermediate risk by coronary calcium score: a serial study using non-contrast cardiac CT. Atherosclerosis 2011;218(2):363-368.

(158) Tintut Y, Patel J, Parhami F, Demer LL. Tumor necrosis factor-alpha promotes in vitro calcification of vascular cells via the cAMP pathway. Circulation 2000;102(21):2636-2642.

(159) Shioi A, Katagi M, Okuno Y, Mori K, Jono S, Koyama H et al. Induction of bone-type alkaline phosphatase in human vascular smooth muscle cells: roles of tumor necrosis factor-alpha and oncostatin M derived from macrophages. Circ Res 2002;91(1):9-16.

(160) Dweck MR, Chow MWL, Joshi NV, Williams MC, Jones C, Fletcher AM et al. Coronary Arterial 18F-Sodium Fluoride Uptake: A Novel Marker of Plaque Biology. J Am Coll Cardiol 2012;59(17):1539-1548.

(161) House SJ, Potier M, Bisaillon J, Singer HA, Trebak M. The non-excitable smooth muscle: calcium signaling and phenotypic switching during vascular disease. Pflugers Arch 2008;456(5):769-785.

(162) Beech DJ. Orai1 calcium channels in the vasculature. Pflugers Arch 2012;463(5):635-647.

(163) Edwards JM, Neeb ZP, Alloosh MA, Long X, Bratz IN, Peller CR et al. Exercise training decreases store-operated Ca^{2+} entry associated with metabolic syndrome and coronary atherosclerosis. Cardiovasc Res 2010;85:631-640.

(164) Fleckenstein-Grun G, Frey M, Thimm F, Hofgartner W, Fleckenstein A. Calcium overload--an important cellular mechanism in hypertension and arteriosclerosis. Drugs 1992;44 Suppl 1:23-30.

(165) Reynolds JL, Joannides AJ, Skepper JN, McNair R, Schurgers LJ, Proudfoot D et al. Human vascular smooth muscle cells undergo vesicle-mediated calcification in response to changes in extracellular calcium and phosphate concentrations: a potential mechanism for accelerated vascular calcification in ESRD. J Am Soc Nephrol 2004;15(11):2857-2867.

(166) Anderson HC. The role of matrix vesicles in physiological and pathological calcification. Curr Opin Orthop 2007;18(5):428-433.

CURRICULUM VITAE

Mikaela Lee McKenney

EDUCATION/ACCOMPLISHMENTS

2010, B.S. Molecular Biology ,
Florida Institute of Technology,
College of Science,
Melbourne, FL

2011, M.S. Physiology,
Indiana University School of Medicine,
Department of Cellular & Integrative Physiology,
Indianapolis, IN

2012, Certificate in the Business of Life Sciences,
Indiana University,
Kelley School of Business,
Indianapolis, IN

2014, Ph.D. Physiology, Minor: Cardiovascular Science,
Indiana University School of Medicine,
Department of Cellular & Integrative Physiology,
Indianapolis, IN

Doctoral dissertation
Coronary artery disease progression and calcification in metabolic syndrome

Advisory Committee
Michael S. Sturek, Ph.D**.** - Professor and Department Chair, Indiana University,
Department of Cellular & Integrative Physiology

Sharon Moe, M.D. - Professor and Director, Division of Nephrology,
Indiana University, Department of Medicine

Johnathan Tune, Ph.D. - Associate Professor, Indiana University,
Department of Cellular &Integrative Physiology

Carmella Evans-Molina, M.D., Ph.D. - Assistant Professor of Medicine,
Indiana University, Department of Medicine

Awards

2011 - Moenkhaus Physiology Graduate Fellowship for Academic Excellence, Indiana University School of Medicine Department of Cellular & Integrative Physiology

2012 - Society for Experimental Biology and Medicine Young Investigator Award

2012 - Indiana Clinical and Translational Sciences Institute Predoctoral Training Fellowship,TL1 Program

2012 - Indiana Clinical and Translational Sciences Institute Annual Meeting, Outstanding Poster Presentation

2012 - Society of General Physiologists Symposium Award

2012 - Society of General Physiologists Poster Competition Award

2013 - Indiana Physiological Society selected student speaker at the Annual chapter meeting

2013 - Indiana Clinical and Translational Sciences Institute Predoctoral Training Fellowship Renewal, TL1 Program

2014 - Association for Clinical and Translational Science & American Federation for Medical Research selected TL1 Predoctoral speaker at the Annual Translational Science meeting

Grant Support

NIH/NCATS- Indiana Clinical and Translational Sciences Institute- TL1 Program 07/01/2012-06/30/2014. TL1 TR000162 (A. Shekhar, PI)

TEACHING/MENTORSHIP EXPERIENCE

Lectures

Fall 2012, Indiana University, F503 Human Physiology
- Cardiac & Smooth Muscle
- Cardiovascular System Design
- Electrocardiogram and the Cardiac Cycle
- Cardiac Output

Fall 2013, Indiana University, F503 Human Physiology
- Same as above

Service/Outreach

APS Physiology Understanding week events (PhUn week)
Fall 2012 St. Malachy 6th grade science
Spring 2013 St. Simon 7th grade science

Student Mentoring

IBMG rotation student, Fall 2011 - fura-2 calcium imaging

IBMG rotation student, Spring 2012 - fura-2 calcium imaging

M.S. student, Fall 2012-Summer 2013 - fura-2 calcium imaging

IBMG rotation student, Spring 2013 - fura-2 calcium imaging

IBMG rotation student, Spring 2013 - fura-2 calcium imaging

M.D. student, Summer 2013 - coronary ring organ culture

M.D./Ph.D. student, Summer 2013 - coronary ring organ culture

Ph.D. student, Spring 2013-Summer 2014 - fura-2 calcium imaging and all other lab procedures

PROFESSIONAL ORGANIZATIONS

Memberships

2011-present	American Physiological Society
2011-present	Indiana Physiological Society
2011-present	Society for Experimental Biology and Medicine
2012-present	Society of General Physiologists

PUBLICATIONS

Manuscripts

1. **McKenney ML*,** Schultz KA*, Boyd J, Byrd JP, Alloosh M, Teague SD, Arce-Esquivel AA, Fain JN, Sacks HS, and Sturek M. Surgical excision of coronary epicardial adipose tissue provides evidence for its role in progression of coronary artery disease. *Journal of Cardiothoracic Surgery* 9:2, 2014. PMID 24387639.

2. Owen MK, Witzmann FA, **McKenney ML,** Lai X, Berwick ZC, Moberly SP, Alloosh M, Sturek M, Tune JD. Perivascular adipose tissue potentiates contraction of coronary vascular smooth muscle: Influence of obesity. *Circulation.* Epub: 128:9-18, 2013. PMID 23685742.

3. **(under review)** Phillips A, **McKenney ML,** Bahls M, Newcomer S, Radcliffe JS, Wastney M, Van Alstine W, Martin B, Sturek M, and Weaver C. High calcium intake from dairy or calcium carbonate does not alter cardiovascular function, coronary artery disease burden, or coronary artery calcium deposition in Ossabaw miniature swine fed atherogenic diet. *ATVB.*

4. **(under review) McKenney ML.**, Territo PR, Salavati A, Houshmand S, Persohn S, Liang Y, Alloosh M, Moe SM, Weaver CM, Alavi A, Sturek M. Assessment of 18F-NaF positron emission tomography imaging as a diagnostic tool for early coronary artery calcification. *Circulation: CV Imaging.*

5. **(under review) McKenney ML**, Territo PR, Salavati A, Houshmand S, Persohn S, Liang Y, Sturek JM, Alloosh M, Moe SM, Weaver CM, Alavi A, Sturek M. Assessment of 18F-NaF positron emission tomography imaging of early coronary artery calcification. *JACC: CV Imaging.*

6. **(in prep) McKenney ML**, Owen MK, Noblet JN, Schultz KA, Dineen SL, Alloosh M, Tune JD, Sturek M. Transient increase in L-type Ca channel activity in early stage coronary artery disease followed by a loss of function in coronary smooth muscle cells from Ossabaw miniature swine with metabolic syndrome.

7. **(in prep)** Dineen SL, **McKenney ML,** Schultz KA, Alloosh M, and Sturek M. GLP-1 analogs enhance intracellular coronary smooth muscle Ca2+ handling and attenuate progression of metabolic syndrome in Ossabaw swine.

8. **(in prep)** Chawla AR, Dineen SL, Bolduan AJ, **McKenney ML,** Alloosh M, Mather KJ, and Sturek M. AMP Kinase mutation exacerbates electrocardiographic ST segment elevation in Ossabaw miniature swine during acute myocardial ischemia.

Published Abstracts

1. **McKenney ML,** Kohr MC, Alloosh M, Schultz KA, Tune JD, Bell LN and Sturek M. Dysfunction of coronary smooth muscle Ca^{2+} regulation in the progression of metabolic syndrome and coronary artery disease in Ossabaw miniature swine. *FASEB J*: 2012 and *JGP*: July 2012.

2. Chawla AR, Spencer SM, **McKenney ML**, Schultz KA, Byrd JP, Alloosh M, Mather K, and Sturek M. Ossabaw miniature swine models with mutant vs. non-mutant AMP kinase alleles for study of electrocardiographic properties during myocardial ischemia. *FASEB J*: 2012.

3. Schultz KA, Boyd J, Byrd JP, **McKenney ML**, Chawla AR, Alloosh M, Teague S, Sacks HS, and Sturek M. Surgical excision of coronary epicardial adipose tissue provides evidence for its role in coronary artery disease. *FASEB J*: 2012.

4. **McKenney ML**, Alloosh M, Schultz KA, Bell LN, Chalasani N, Sturek M. Effects of GLP-1 Receptor Agonist on Ca^{2+} handling of coronary smooth muscle cells from metabolic syndrome Ossabaw swine with coronary artery disease. *Diabetes*: June 2012 and *JGP*: July 2012.

5. **McKenney ML**, Suh D, Martin JR, Alloosh M, Schultz KA, Sturek M. Effects of GLP-1 receptor agonist on Ca^{2+} handling in coronary smooth muscle cells from lean and metabolic syndrome Ossabaw swine with coronary artery disease. *FASEB J:* 2013.

6. Martin JR, **McKenney ML**, Weaver CM, Sturek M. Effect of dietary calcium supplementation on store-operated calcium entry in coronary smooth muscle cells from Ossabaw miniature swine with coronary artery disease. *FASEB J:* 2013.

7. Dineen SL, **McKenney ML**, Sturek M. An in vitro model of coronary artery disease and the changes in intracellular calcium regulation during its progression. *FASEB J:* 2013.

8. **McKenney ML,** Dineen SL, Noblet JN, Tune JD, Sturek M. Increased Ca^{2+}-activated Ca^{2+} influx and impaired Ca^{2+} buffering in coronary smooth muscle from metabolic syndrome Ossabaw swine. *FASEB J:* 2014.

9. Dineen SL, **McKenney ML**, Sturek M. Glucagon-like peptide-1 (GLP-1) receptor agonist, exenatide, enhances Ca^{2+} buffering by SERCA in coronary smooth muscle cells from lean, healthy Ossabaw swine. *FASEB J:* 2014.

10. Salavati A, **McKenney ML,** Alloosh M, Territo PR, Chen N, Moe SM, Weaver CM, Sturek M, Alavi A. Discrepancy between in vivo cardiac uptake imaging of ^{18}F-NaF, atherosclerotic plaque, and biochemical assessment of calcification. *Journal of Nuclear Medicine* (submitted).

11. **McKenney ML,** Salavati A, Alloosh M, Territo PR, Chen N, Moe SM, Weaver CM, Alavi A, Sturek M. Atherosclerotic plaque quantification, biochemical cardiac calcification assessment, and ^{18}F-NaF cardiac uptake imaging in Ossabaw swine. *Clinical and Translational Science* (submitted).

Presentations

1. **McKenney ML,** Chawla AR, Spencer SM, Byrd JP, and Sturek M. Store-operated Ca^{2+} entry in coronary smooth muscle of Ossabaw miniature swine with coronary artery disease. **Poster presentation**, 1st Annual Meeting of the Indiana Physiological Society, Feb 2011, Indianapolis, IN.

2. **McKenney ML,** Chawla AR, Spencer SM, Byrd JP, and Sturek M. Store-operated Ca^{2+} Entry in Coronary Smooth Muscle of the AMP Kinase genotypes of Ossabaw Miniature Swine. **Poster presentation**, Swine in Biomedical Research, July 2011, Chicago, IL.

3. **McKenney ML**, Kohr MC, Alloosh M, Schultz KA, Tune JD, Bell LN and Sturek M. Dysfunction of coronary smooth muscle Ca^{2+} regulation in the progression of metabolic syndrome and coronary artery disease in Ossabaw miniature swine. **Poster presentation**: 2nd Annual Meeting of the Indiana Physiological Society, "Peak performance: mice to men", Feb 2012, Muncie, IN**. Poster presentation**: Experimental Biology, April 2012, San Diego, CA. **Poster presentation**: 4th Annual Indiana Clinical and Translational Sciences Institute Meeting, August 2012, Indianapolis, IN. **Poster presentation**: 66th Annual Meeting and Symposium of the Society of General Physiologists, "Integrative Membrane Physiology in the Post-Genome Era", September 2012, Woods Hole, MA.

4. **McKenney ML**, Alloosh M, Schultz KA, Bell LN, Chalasani N, Sturek M. Effects of GLP-1 Receptor Agonist on Ca^{2+} handling of coronary smooth muscle cells from metabolic syndrome Ossabaw swine with coronary artery disease. **ePoster**: American Diabetes Association 72nd Scientific Sessions, June 2012 Philadelphia, PA. **Poster presentation:** 66th Annual Meeting and Symposium of the Society of General Physiologists, "Integrative Membrane Physiology in the Post-Genome Era", September 2012, Woods Hole, MA.

5. **McKenney ML**, Suh D, Martin JR, Alloosh M, Schultz KA, Sturek M. Effects of GLP-1 receptor agonist on Ca^{2+} handling in coronary smooth muscle cells from lean and metabolic syndrome Ossabaw swine with coronary artery disease. **Poster presentation**: Indiana Physiological Society, Feb 2013, Indianapolis, IN. **Poster presentation:** Experimental Biology, April 2013, Boston, MA.

6. **McKenney ML**. Dysfunction of coronary smooth muscle Ca^{2+} regulation in the progression of metabolic syndrome and coronary artery disease in Ossabaw miniature swine. **Oral presentation:** Indiana Physiological Society, Feb 2013, Indianapolis, IN.

7. **McKenney ML**, Dineen SL, Noblet JN, Tune JD, Sturek M. Increased Ca2+-activated Ca2+ influx and impaired Ca2+ buffering in coronary smooth muscle from metabolic syndrome Ossabaw swine. **Poster presentation:** Indiana Physiological Society Annual meeting, Feb 2014, Evansville, IN. **Poster presentation:** Experimental Biology, April 2014, San Diego, CA.

8. **McKenney ML,** Salavati A, Alloosh M, Territo PR, Chen N, Moe SM, Weaver CM, Alavi A, Sturek M. Imaging for the Early Diagnosis of Vascular Calcification. **Oral presentation:** Translational Science, April 2014, Washington D.C.